Doctoral Thesis

Locomotion Study of Passive-Spine Multi-Legged Robot

September 2019

Doctoral Program in Advanced Mechanical Engineering and Robotics

Graduate School of Science and Engineering

Ritsumeikan University

TANG Yongchen

Doctoral Thesis Reviewed
By Ritsumeikan University

Locomotion Study of Passive-Spine Multi-Legged Robot
(受動体節構造を有する多脚ロボットの歩行研究)

September 2019
2019 年 9 月

Doctoral Program in Advanced Mechanical
Engineering and Robotics
Graduate School of Science and Engineering
Ritsumeikan University
立命館大学大学院理工学研究科
機械システム専攻博士課程後期課程

TANG Yongchen
タン ヨンチェン

Supervisor：Professor MA Shugen
研究指導教員：馬 書根 教授

Abstract

Locomotion Study of Passive-Spine Multi-Legged Robot

by

Yongchen TANG

Doctor of Philosophy in the Department of Robotics

Ritsumeikan University, Biwako-Kusatsu Campus

Professor Shugen MA, Chair

In complex natural environments, multi-legged animals, such as centipedes, can adapt to different environments. Multi-legged animals typically move in varied environments, such as on soft land or rough terrain, with strong adaptability, fault tolerance, and high mobility. The trajectory of a multi-legged robot constitutes a series of discrete footprints, while wheeled and crawler robots are a series of continuous tracks. Rough terrains often contain obstacles, such as rocks, mud, sand, and even cliffs and steep slopes, which means that wheeled and crawler robots are no longer suitable for this type of terrain. While legged robots only need discrete points to touch the ground, they possess strong adaptability to this kind of terrain. Consequently, legged robots tend cause less damage to the environment. Although multi-legged robots have many advantages, numerous disadvantages remain. For example, in order to make the legs coordinate with each other and stabilize movement, the mechanical structural design and the control system are more complicated than those of other types of robots. As a result, compared with natural arthropods, the performance of bionic leg robots needs to be improved.

In order to overcome these challenges, a new methodology for designing a multi-legged robot with a simple structure and a small number of actuators has been proposed. A traditional multi-legged robot with $2n$-legs requires three motors per leg and necessitates a total of $6n$ actuators. In this thesis, we have proposed a legged robot with only one actuator per leg that controls the lateral swing of the legs to achieve leg lifting and landing.

Such a $2n$-legged robot requires just $2n$ actuators, and thus not only the number of the actuators, but also body weight, are greatly reduced compared to the conventional design. This multi-legged robot comprises n body segments and $n-1$ passive body segment joints between the body segments.

Determination of precisely how to design this robot, which can abduct and adduct its legs with the same motion ability as a traditional legged-robot, constitutes the focus and challenge of our research. To model the mobility of this kind of robot with a simple design, the candidate configurations are first selected by a mobility analysis based on screw theory. By analyzing these configurations, omni-directional locomotive performance which is generated by a different order of configuration transitions has been deduced.

Our research also needs to solve the problem of how to better combine motion of the active leg joints with the passive body segment joints to form the motion of the entire robot. Considering the results of the mobility analysis, we have obtained the locomotion principle of omni-directional motion based on a geometric analysis. The contribution of the duration of the supporting phase of various configurations to the direction of rotation between configuration transitions has been determined. These different gaits and gait transitions have been also achieved to complete an obstacle avoidance task.

Our research also provides a method to design multi-legged robots based on the internal motion mechanism of centipedes. Indeed, the movement method of passive-spine can be extended to a $2n$-legged robot to perform undulatory motion by abducting and adducting in the frontal plane of their active legs.

We have utilized the Open Dynamics Engine (ODE) environment to obtain the simulation results of the robot design, mobility and the different gait patterns, which verified the correctness of our robot model and the above analysis. Finally, the results of the analysis that are demonstrated in this thesis have been confirmed by experiments of a six-legged and a 10-legged robot. The experimental results show that the proposed design and analysis methodology effectively decrease the numbers of actuators installed on the multi-legged robot.

Table of Contents

List of Figures

List of Tables

Acknowledgements

I would like to express my deep gratitude to Prof. Shugen Ma, my research supervisor, a Professor in the Department of Robotics at Ritsumeikan University, for his patient guidance, enthusiastic encouragement, useful critiques of this research work, and especially his advice and assistance in keeping my progress on schedule.

Furthermore, I am grateful to all of my lab mates in the Biomimetic Intelligent Mechatronics Laboratory, and especially to Dr. Xiaodong Wu and Dr. Yi Sun, who gave me great assistance at the beginning of my doctoral course and continuously supported my researches after their graduation from Ritsumeikan University; to Dr. Atsushi Kakogawa, Dr. Yang Tian and Dr. Guoteng Zhang, for their kind advice during the doctoral seminar and their invaluable comments in proofreading of my journal and conference papers; and to Ms. Nitto Aiko and Mr. Sawabe Taishi, for their critical assistance and support in fabricating and testing of the prototype robot. Studying with them together in Ritsumeikan University lead me to experience such a colorful and productive campus life that I will always treasure.

My great appreciation also goes to all of the fellows and officers in the Department of Robotics and the Office of the Graduate School of Science and Engineering of Ritsumeikan University for guiding me so well during my life in Japan. My sincere gratitude is also extended to the staff at the workshop of Ritsumeikan University for their kind help in fabricating the prototype in this thesis.

Finally, I wish to thank my family members for their strong support and unrelenting encouragement throughout my study. I am deeply grateful for my husband, Mr. Dingxin Ge, who studies in the same laboratory as I do. Thank you so much for your company and support. I would not have been successful in this work without you. My special love and gratitude are given to my two lovely children who have always inspired me. I love you all! Thank you!

Curriculum Vitæ

Yongchen TANG

Education

1991-1997	Air Force Engineering Academy Primary School (Xi'an, Shanxi Province, China) Elementary School Student
1997-2000	Air Force Engineering Academy Junior High School (Xi'an, Shanxi Province, China) Junior School Student
2000-2003	Air Force Engineering Academy High School (Xi'an, Shanxi Province, China) High School Student
2003-2007	Xi'an University of Technology (Xi'an, Shanxi Province, China) Bachelor Degree of Industrial Engineering
2007-2010	Hebei University of Technology (Tianjin, China) Master Degree of Mechanical Engineering
2011-2019	Ritsumeikan University, BKC (Kusatsu, Shiga, Japan) Doctoral Candidate, Robotics

Personal

Born	Nov. 25, 1985, Shanxi, China
Research Interests	Robotic Locomotion, Biomimetic Systems, Legged Robots.

Chapter 1

Research Background

1.1 Legged Robots

Legged robots have been extensively developed in recent years [1, 2, 3, 4, 5, 6, 7, 8, 9, 10]. They are currently able to traverse unstructured terrains, provide superior mobility in complex environments [11, 12], and possess fault-tolerant capability when any problem occurs on one leg or foot [13].

Some researchers are designing quadruped robots [14, 15], hexapod robots [11, 16, 17, 12], and octopod robots [18] which can perform different types of tasks for detection, inspection, and even missions in hazardous and unknown environments that cannot be performed by other types of robots.

However, conventional walking robots require three DOFs (degree of freedom) for each leg. Therefore, a $2n$-legged robot needs a minimum of $6n$ actuated joints, where n is the number of leg pairs. This means that 18 DOFs and 24 DOFs are required for a general type of six-legged and eight-legged robot, respectively. Obviously, such a design will markedly increase the energy consumption and weight of the robot, as well as complicate gait planning and control [19, 20, 21].

The main challenges are the high weight and complicated control method, especially

in a situation in which one or more motors encounter a failure, which will definitely affect the movement of the entire robot. Reducing the number of actuated joints decreases, in concert, the probability of failure. Therefore, in this paper, our proposed locomotion method of passive-spine multi-legged robots with under-actuated design can be utilized as a behavior compensation for the damage of ordinary multi-legged robots, and improve the adaptation of the robot in cases in which the leg is damaged, broken, or missing [22]. This new methodology will enable more robust, effective, autonomous robots, and may advance our understanding of how animals adapt to injury.

1.2 Biological Inspiration for Legged Locomotion

1.2.1 Multi-Legged Robot with Decreased Active DOF

In order to decrease the number of actuators and energy consumption, reduce the difficulty of control algorithms, and achieve higher efficiency, many researchers proposed robot design to decrease the number of actuated joints in multi-legged robots, as body propulsion in the horizontal plane and transition between the swinging and the supporting phases in the vertical plane still necessitate two actuators for each leg [23, 24, 19].

Torigs et al. proposed a six-segment walking robot with four motors of each segment to control two legs [2]. In this design, a $2n$-legged robot needs $4n$ actuated joints. Inagaki et al. designed multi-segment joints to swing the body in a snake-like motion [25]. Their robot walks by coordinating its body segments and legs to achieve movement. Jimenez introduced a decreased DOF multi-legged robot with one actuated DOF per leg and active joints between the body segments [26]. Matthey et al. analyzed the locomotion of a centipede robot with eight segments, in which each segment has two DOFs, and an extra DOF is introduced through the intersegmental joints [27]. However, such a $2n$-legged robot still requires $3n$-1 actuated joints. These robots mainly use actuated joints installed between adjacent segments, which necessitates additional energy to rotate the body segments. Saranil et al. proposed a six-legged robot with six actuated DOFs, named the RHex robot

[28]. The authors adopted a C-shaped structure for the leg design. Chou et al. developed RHex-based robots to produce gaits on different terrains. These robots were characterized by their simple designs, but impressive locomotion versatility and energetic efficiency. The propulsive forces for locomotion are directly provided by spring-like legs which are mounted on a rigid robot body, and a careful tuning of the magnitudes and directions of the resultant propulsive forces are necessary for controlling a RHex-based robot [29]. Yoneda et al. proposed a four-DOF four-legged robot [8]. The robot body is separated into a front part and a rear part, which is connected by an active joint that can rotate about the horizontal direction. This twisting motion generates alternating up-and-down motions of legs in the same segment. However, this design is difficult to implement in multi-legged robots, especially in robots with more than six legs, because the legs are fixed to the body.

Leg mechanisms with a limited number of DOF are widely adopted in multi-legged robots to reduce the number of active actuators and simplify gait planning. Inspired by the movements of living organisms, which tend to be highly adapted to their natural environments, increasing researches on bio-inspired robots need to be developed.

1.2.2 Bio-inspiration Robot Design with Decreased Active DOF

In order to optimize the design and control method of robots, increasing numbers of studies are combining the motion characteristics of animals in nature with mechanical designs to develop bio-inspired robots, because animals or insects have very special leg or limb structures which are suitable for motion and adaptable to different environments. For example, Grzelczyk proposed a prototype of a hexapod robot designed based on the inspiration of insects [30]. The control system was based on a central pattern generator model, and the characteristics of the proposed robot compared with animals were verified by simulations and experiments.

Inspired by insects, such as cockroaches, robotics researchers have attempted to mimic insect-like behaviour in legged robots for developing hexapod robots [31, 32]. In addition, Liang et al. proposed a tripod walking robot inspired by the tripod gaits of kangaroos with

its tail [33]. Moreover, Kinugasa et al. developed a light, simple, and adaptive myriapod robot named i-CentiPot P. However, i-CentiPot P can roughly just follow a straight line only on a horizontal surface [34]. Aoi presented a centipede-like multi-legged robot composed of six body segments and 12 legs, in which each leg had two active joints. The body segments were passively connected through yaw joints with torsional springs. The robot walked in a straight line and exhibited a quick turning motion [35]. Koh developed a centipede robot inspired by the motion of centipedes when they traverse uneven terrains [36]. Ijspeert developed a salamander robot to realize aquatic and terrestrial gaits by a central pattern generator control system [37].

However, these studies essentially focus on the bionics of structure or observed laws of motion without mimicking the internal motion mechanisms of the organism. Therefore, if we can design robots based on the internal motion mechanism of the centipede, we can not only be inspired by the laws of natural biological evolution, but also explore some biological movements from the perspective of mechanical design.

Anderson et al. utilized electromyograms (EMGs) to record the lateral flexor muscles of centipedes running on a treadmill. The EMGs showed muscle activity synchronization with posteriorly propagated waves caused by bending. It is found that the lateral flexor muscles of centipedes are actively promoted body undulations [38].

In order to verify and investigate the effects of lateral motion on centipede movement, and to elucidate the undulatory motion of multi-legged creatures, we begin to consider the use of lateral motion of legs to promote the undulatory motion of body segments. Then, we propose a new design which used a single actuated DOF in each leg and a single passive body-segment joint between each pair of body segments. In this design, the active leg joints are responsible for abducting and adducting in the frontal plane of the body segment. This design not only enables less actuation and multi-legged motion, but also provides a way to study adduction motion by introducing a passive spine for multi-segment robots.

Multi-legged robots can also be utilized as a platform for swarm robotics on smaller scales. For example, Hoffman et al. proposed a centipede micro-robot with repeated two-

legged, two-DOF segments which are connected by passive joints [39]. This micro-robot realized forward locomotion on flat surfaces.

For multi-legged robots, not only do the number of actuators increase with the number of legs, but so does the difficulty of cooperation between legs, or leg and body joints. Therefore, determination of precisely how to coordinate the relationships between body and legs has also become the focus of designing multi-legged robots.

1.3 Motivation and Outline of this Thesis

Although many researchers have developed multi-legged robots with decreased active DOF, decreasing the number of actuated joints of multi-legged robots remains an unsolved problem. Furthermore, the methodology to effectively analyze the mobility and gait patterns of decreased active DOF robots needs to be developed. This motivated us to attain similar working abilities with fewer actuators by reducing the number of actuated joints.

The purpose of this research is to solve the fundamental mobility problem of the legged robot with decreased active DOF by proposing a passive-spine multi-legged robot. A new method is presented for achieving omni-directional locomotion with a robot that has only one actuated degree of freedom (DOF) in each leg and one passive body segment joint between each pair of body segments. The methodology of mobility and gait analysis could be applicable to a wider class of decreased active DOF robots.

The contents of this thesis are organized as follows.

Chapter 2 first discusses the functions of multiple DOFs in conventional legged robots. Next, the design of the multi-legged robot with decreased active DOF is proposed. In this design, each leg has only one actuator, which rotates about the joint axis parallel to the roll axis to swing the leg up and down. The methodology of this kind of design is to introduce passive joints on body segments of the multi-legged robot. Then, the concept, including definitions, locomotion principle, and prototype design of the passive-spine multi-legged robot is introduced.

Chapter 3 analyzes the locomotion generated by different gait configurations. The locomotion principle of our proposed design differs from that of other legged robots. The candidate gait configurations are selected by performing a mobility analysis of the robot. The mobilities of different gait configurations of the robot are analyzed by using a geometrical method. Based on the mobility analysis of gait configuration transitions, the kinematic model is analyzed to obtain the forward propulsive contribution, and the geometrical model is analyzed for the rotating motion ability of the passive body segment joint.

Chapter 4 proposes a method to design the gait patterns for realizing omni-directional motion. The gait transition is achieved by switching between the existing gaits for a multi-legged robot. Straight line motion is obtained by the selected gait configuration transition. The turning motion and rotating motion are attained by modifying the duration time of transition. Sideways motion is also achieved by geometric analysis. The omni-directional motion is verified in a simulation environment. The design can be utilized as a behavior compensation for the multi-legged robot in some unexpected cases.

Chapter 5 introduces FSM (Finite State Machine) to expand the locomotion principle to $2n$-legged passive-spine robots. The undulatory gait for achieving straight line motion, as well as turning motion, is obtained for a 10-legged robot in a simulation environment.

Chapter 6 verifies the prototype design of our multi-legged robot. Experiments on our robot are used to confirm the proposed concepts of the legged locomotion with fewer actuated joints. The capability of the omni-directional locomotion of our configuration of multi-legged robot is tested. Finally, the methodology, including mobility analysis and gait planning methods, is tested successfully.

Chapter 7 summarizes the obtained results and discusses directions for future work.

Chapter 2

Principle and Prototype of the Passive-Spine Legged Robot

Through combining the characteristics of conventional multi-legged robots, such as robots in [40, 41], we can find that multiple DOFs serve two main functions: 1) actuation in the horizontal direction, which propels the body segment across the ground or swings a leg through the air; and 2) actuation in the vertical direction, which transits the leg between the supporting phase and the swinging phase. Such vertical leg movement is requisite when traversing uneven terrain.

Therefore, the critical issues that need to be discussed and solved are precisely how to use simple leg-lifting action, not only to complete the supporting and swinging phase switching, but also to use the lifting leg movement to push the body forward, or to bring the body to swing to ensure that the swinging phase of the legs are completed in the air.

Fukuhara et al. designed a quadruped robot to study the minimal model with a spine and four legs [42]. A rotary actuator is implemented in the spine to drive the spine in the yaw direction at the segment joint in the horizontal plane. A linear actuator is implemented in each leg to realize the leg locomotion in the vertical direction. In addition, two torsion springs are installed in the pitch and yaw directions. With a control scheme designed by

coordination of the legs and the body, the quadruped robot realized forward movement in a simulation environment. In order to apply a methodology to a wider class of legged robots, coordination of the spine and the spine, and the spine and the legs, of a multi-legged robot will introduce great difficulty.

In this chapter, the concept of the passive-spine legged robot is introduced. Finally, the prototype of this mechanism is designed to confirm the proposed conception.

2.1 Concept of the Passive-Spine Legged Robot

The passive-spine legged robot is characterized by its segmented body (each of which is called a body segment) and the passive *body segment joints* between adjacent body segments, which are shown in Fig. 2.1(a). This design uses a single actuated DOF in each leg and a single passive body segment joint between each pair of body segments. Each body segment has two legs, which are actuated by two active leg joints individually for abducting and adducting in the frontal plane of the body segment.

The body segments are connected by body segment joints which have no actuators or springs. The passive body segment joints allow the body segments to rotate about joint axes freely. In order to reduce the friction of the body joints, bearings are used in the passive joints in the prototype, as shown in Fig. 2.1(b). Angles formed by the sagittal planes of the two adjacent body segments are called body-angles and denoted by θ_{Bi}, where i represents the i-th body segment from the head of the robot; and $\theta_{Bi} = 0$ when the two sagittal planes are coincident.

Two legs are carried on each body segment, and individually actuated by two active leg joints to realize abduction and adduction in the frontal plane of the body segment. Angular positions of the two leg joints are called leg-angles and denoted by θ_{Li} and θ_{Ri}, respectively, for the left and the right legs of the i-th body segment.

Since the pose of the i-th body segment can be represented by its body-angle and leg-angles, the pose vector is defined as $\vec{\theta}_i = [\theta_{Bi}, \theta_{Li}, \theta_{Ri}]^T$. Therefore, the posture of

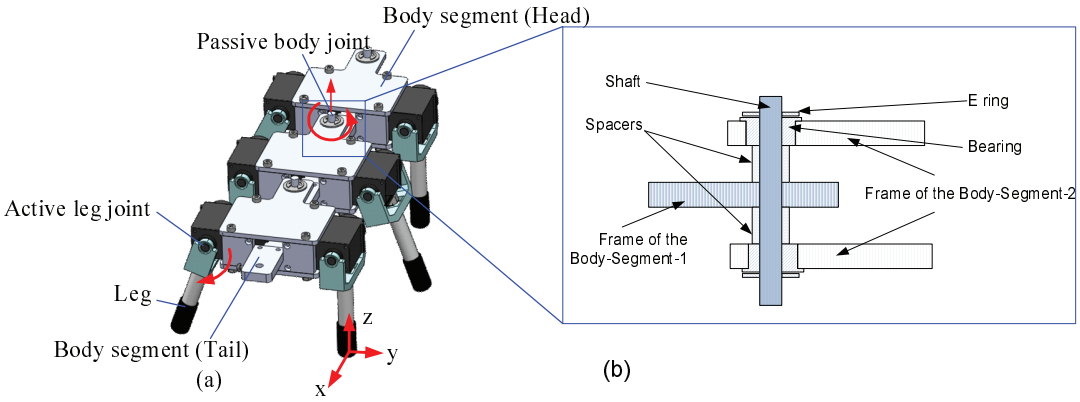

Figure 2.1. Design of the passive-spine legged robot. (a) CAD model of the passive-spine six-legged robot. (b) Implementation of the passive body segment joints.

the robot consists of n body segments, which can be represented by the posture vector $\vec{\Theta} = [\vec{\theta}_1, \vec{\theta}_2, ..., \vec{\theta}_n]^T$.

A schematic drawing of the robot is shown in Fig. 2.2(a), where the body segments, the passive body segment joints, and the active leg joints are represented by polygons, green cylinders, and orange cylinders, respectively. Note that, although a six-legged robot example is shown in Fig. 2.1 and Fig. 2.2, a centipede robot possessing n body segments and $2n$ actuators can be easily assembled with the same modules.

2.1.1 Definitions

The situation terms of legs of the passive-spine multi-legged robot are firstly defined.

The leg of the robot can be either in stance phase, where the leg is in contact with the ground, or in swing phase, where the leg is lifted above the ground. The legs in the stance phase are supporting legs, whereas other legs are swinging legs. Contact between their foot-tips and the ground can be treated as spherical joints, which can freely rotate about the supporting points on the ground or footprints. A schematic diagram, as shown in Fig. 2.2(b), is used to graphically illustrate phases of the legs, in which solid circles and open circles indicate the footprints of the supporting legs and the swinging legs, respectively.

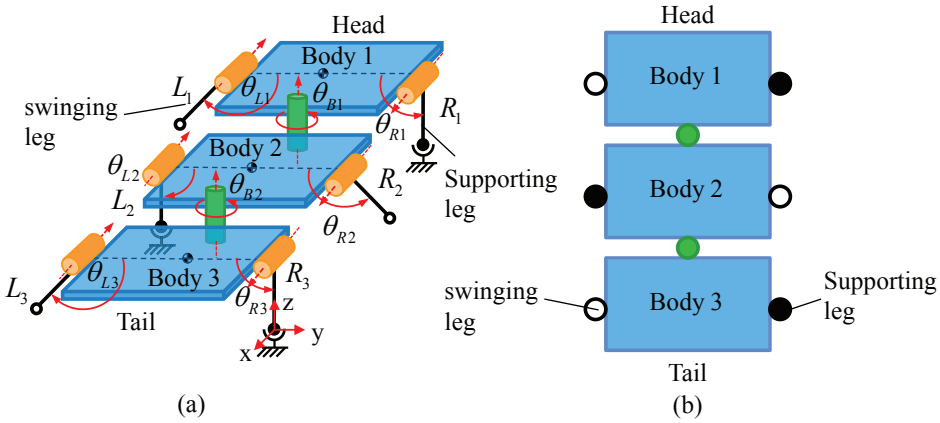

Figure 2.2. Concept of the passive-spine legged robot. (a) Schematic diagram of the passive-spine six-legged robot. The labels "L_1","L_2", and "L_3" represent the left legs 1, 2, and 3, respectively. The labels "R_1","R_2", and "R_3" represent the right legs 1, 2, and 3, respectively. (b) Schematic diagram of the configuration of the passive-spine six-legged robot, in which solid and open circles indicate footprints of the supporting and the swinging cases, respectively.

Since each body segment has two legs, the contact mode of each body segment can be classified into the following four conditions:

1. **Non-contact**: Both the left and the right legs are in the swinging phase.

2. **Left-contact**: Only the left leg is in contact with the ground.

3. **Right-contact**: Only the right leg is in contact with the ground.

4. **Full-contact**: Both the left and the right legs are in the stance phase.

Consquently, according to the contact mode, each body segment can be labeled by "0", "L", "R", or "2". The configuration of the robot is defined by the contact modes of all of its body segments and labeled by a configuration string, each character of which represents the contact condition of a body segment. The first character in the configuration string indicates the contact condition of the head segment of the robot. For example, the configuration string of a six-legged robot shown in Fig. 2.1(a) is "RLR", where the head and the tail segments are in the right-contact condition, and the second segment is in the left-contact condition.

For a passive-spine multi-legged robot consisting of n body segments, a number of 4^n configurations are geometrically possible. However, to firmly support the weight of the robot, the projected point of the center of mass (CoM) of the robot on the ground should always be located inside of the supporting polygon formed by footprints. Therefore, only the configurations that have at least three supporting legs and all of the supporting legs are not on the same side of the robot are standing configurations that could result in a static stable standing of the robot. All of the standing configurations of the passive-spine six-legged robot are summarized in Fig. 2.3, in which M_r represents the mobility of the robot that will be discussed in Chapter 3.

2.1.2 Locomotion Principle

In the presence of passive body joints, the passive-spine legged robot is capable of walking with a unique locomotion principle that differs from static crawling or dynamic walking of other legged robots.

The principle of the proposed passive-spine legged walking is shown in Fig. 2.4, in which several crucial steps are illustrated.

As shown in Fig. 2.4(a), the six-legged robot standing at an initial configuration "RLR" starts the locomotion by simultaneously abducting leg R_1 and adducting leg L_1. During the short period of time before the leg R_1 lifts up, horizontal reaction forces are generated at tips of all of the supporting legs, as shown in Fig. 2.4(b), which are denoted by f_{R1}, f_{L2}, and f_{R3}, respectively. Although these horizontal reaction forces result in a zero net horizontal force, they trigger the body segments to rotate about the axes of the body joints to a new posture, as shown in Fig. 2.4(c). Consequently, along with the rotating body segments, the swinging legs are swung to their new positions, as well. Once the adduction of leg L_1 is completed, the robot enters the configuration "LLR". The process in which the robot changes from one configuration to another one is called the configuration transition. Due to rotations of the body segments during the configuration transition, the CoM of the robot moves to a new position.

Supporting state	Configuration	Example	M_r
3 supporting legs	LRL RLR LLR RLL RRL LRR 20R 20L L02 R02	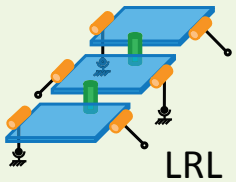 LRL	2
	2L0 0L2 0R2 02L 2R0 02R L20 R20	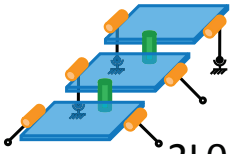 2L0	1
4 supporting legs	202 220 022 2RL 2RR 2LR 2RL R2R R2L L2R L2L LL2 RR2 RL2 LR2	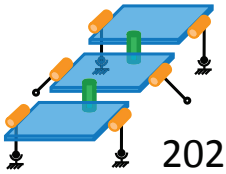 202	1
5 supporting legs	2L2 2R2 22R 22L R22 L22	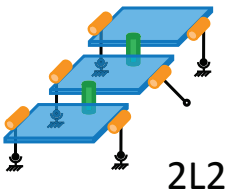 2L2	1
6 supporting legs	222	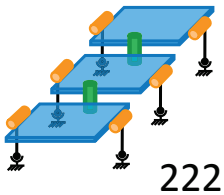 222	1

Figure 2.3. Standing configurations which can form a static stable standing of the passive-spine six-legged robot shown in Fig. 2.1 (a).

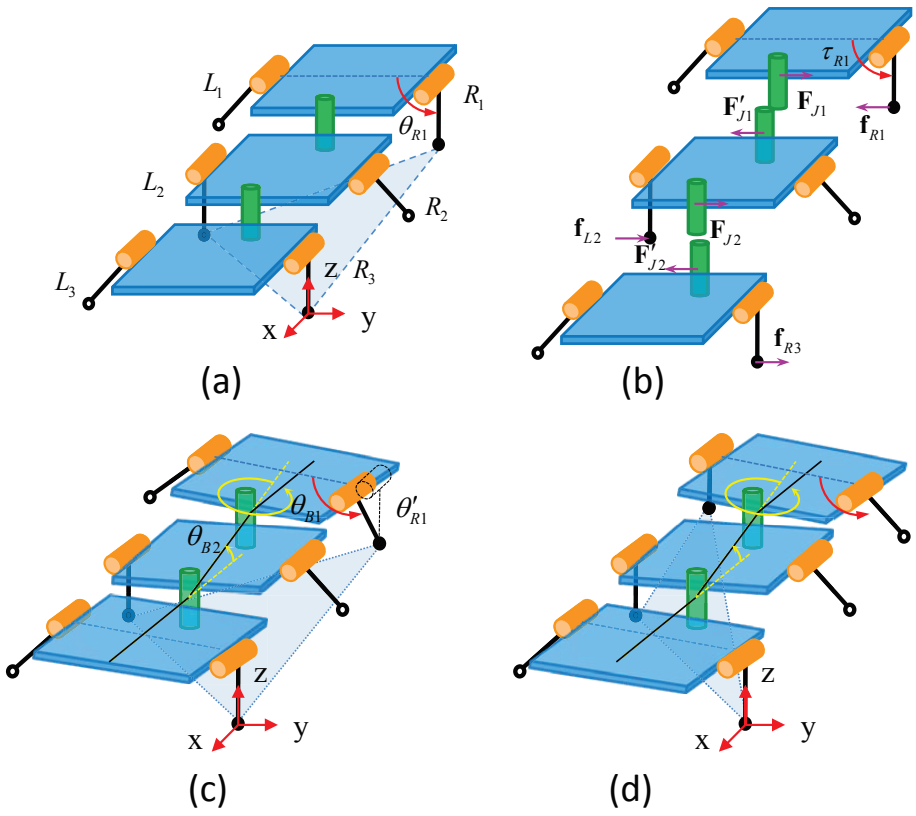

Figure 2.4. Walking principle of the passive-spine legged robot. (a) The six-legged robot starts at an initial configuration "RLR" by abducting leg R_1 and adducting leg L_1 simultaneously. (b) Horizontal reaction forces on footprints of the supporting legs are generated during the short period of time before the abducting of leg R_1. (c) These horizontal reaction forces result in rotating of the body segments and swinging of the swinging legs. (d) When leg L_1 touches the ground, the robot becomes configuration "LLR". During the transition from configuration "RLR" to "LLR", the CoM of the robot moves by rotating the body segments.

The most unique feature of the proposed locomotion principle is that the legs of the robot use a kind of "kicking" movement to provide an impulsive force to rotate body segments. By sequentially conducting a series of configuration transitions, a passive-spine legged gait is obtained. It should be noted that transitions may not exist between two configurations, and not every configuration transition can result in legged locomotion. Analysis of feasible configuration transitions and the method to find a passive-spine legged gait will be discussed in the next chapter.

2.2 Prototype Design of the Passive-Spine Legged Robot

2.2.1 Mechanism Design of the Passive-Spine Legged Robot

The model specifications are given in Table 2.1. The six-legged robot has three modules, which are connected by a passive body joint between adjacent body segments. The legs are made of plastic resin, and the foot-tips are covered by rubber caps in order to increase friction to avoid slippage.

A prototype of the six-legged robot is shown in Fig. 2.5. The robot weighs approximately 1.07$[kg]$. Since stable forward and backward locomotion of the robot largely depend on mass distribution of its parts, the mass of the robot is symmetrically distributed in the x and y directions.

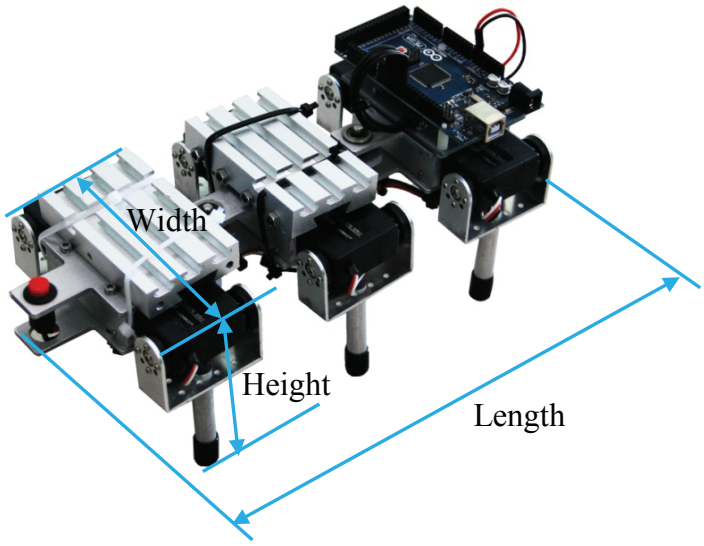

Figure 2.5. The six-legged robot prototype.

2.2.2 Control System Design of the Passive-Spine Legged Robot

The servomotors in the six-legged robot prototype module are controlled by an Arduino controller in Fig. 2.6. The control schematic of this controller is shown in Fig. 2.7. In

Table 2.1. Specifications of the six-legged robot.

Items	Specification
Size [m]	Height 0.096 × Width 0.12× Length 0.27
Weight [kg]	1.07 (with three batteries)
Servomotors	LDX-227 (10.0 [kg·cm], 0.14 [s/60°])
On-board controller	Arduino MEGA 2560
Battery	TR18650 3.7 [V], 9800 [mAh]

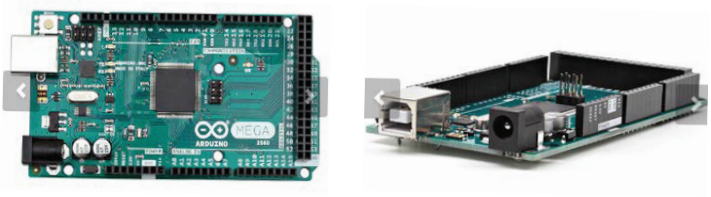

Figure 2.6. Control board for controlling the servomotors of legs.

the six-legged robot, each leg is controlled by a servomotor to realize the abduction and adduction of the leg, which is shown in Fig. 2.6.

2.3 Summary

In this chapter, the concept of a novel legged locomotion mechanism, called the passive-spine multi-legged robot, has been presented. The proposed multi-legged robot provides a new and simple locomotion method to achieve planar locomotion. The principle and the features of this design have been introduced.

To fully understand the characteristics of the proposed passive-spine multi-legged robot, the mechanism and the control system design have been introduced. The mobility of the proposed design will be analyzed in Chapter 3 based on the locomotion principle.

The prototype of the proposed multi-legged robot has been designed and fabricated for verifying the presented idea of the passive-spine mechanism.

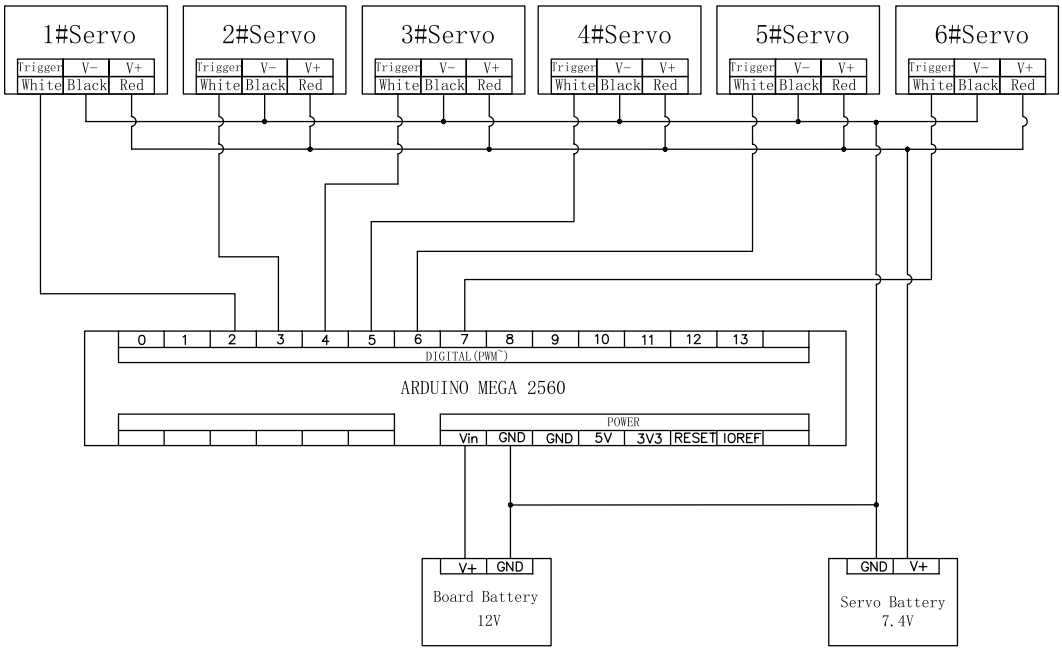

Figure 2.7. Control schematic of the six-legged robot.

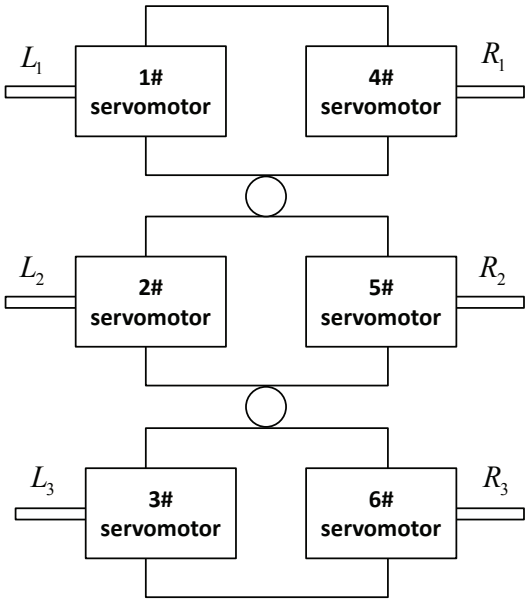

Figure 2.8. Control diagram of the six-legged robot.

Chapter 3

Locomotion Analysis of Passive-Spine Legged Robots

3.1 Mobility Analysis

3.1.1 Mobility of the Robot

As introduced in Chapter 2, the crucial step of passive-spine legged walking is the rotation of the body segments under constraints formed by supporting legs at their footprints. To identify the feasible configurations that can be used to form configuration transitions to realize gait planning, the mobility of the robot at each of the configurations should be firstly analyzed. In our study, mobility of the robot M_r is specified by the maximum DoFs of the body segments, namely:

$$M_r = \max\{M_i\}, \tag{3.1}$$

where M_i is the mobility of the i-th body segment.

The six-legged robot adopting the given configuration can be represented by a parallel mechanism consisting of several chains. The number of the chains is equal to the number of supporting legs. For example, the six-legged robot, as shown in Fig. 2.2(a), is the

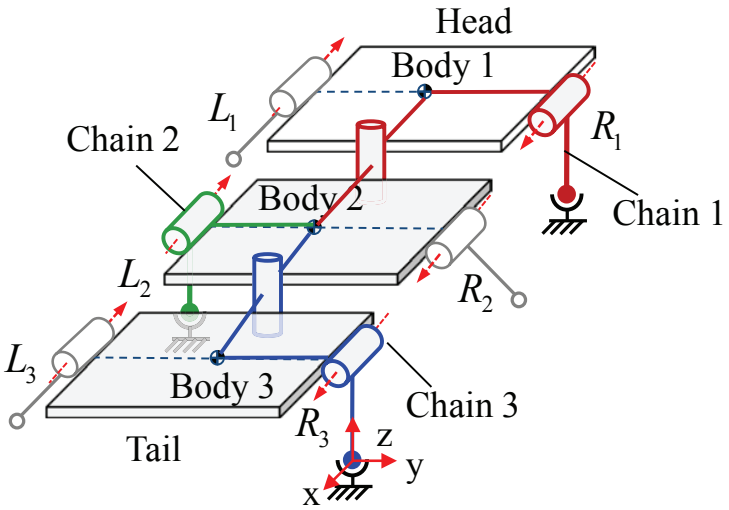

Figure 3.1. The passive-spine six-legged robot in configuration "RLR".

configuration "RLR", which can be viewed as a parallel mechanism consisting of the three chains shown in Fig. 3.1.

3.1.2 DOFs of the Body Segments

In the presence of parallel chains, the DoFs of the body segments are calculated by the modified Grübler and Kutzbach mobility criterion [43]:

$$M_i = \mathrm{d}(n_l - g - 1) + \sum_{i=1}^{g} f_i + \nu - \xi, \tag{3.2}$$

where n_l is the number of links; g is the number of joints; f_i is the DOF of joint-i; ξ is the number of passive DOFs; and d is the order of the mechanism, which is given by:

$$d = 6 - \lambda. \tag{3.3}$$

Here, λ and ν define the number of common and redundant constraints, respectively. ν is given by:

$$\nu = \sum_{j=1}^{p} q_j - \lambda p - c, \tag{3.4}$$

where p is the number of legs; q_j is the number of constraints imposed by the j-th leg; and c is the number of linearly-independent constraints in the linear space of the constraints

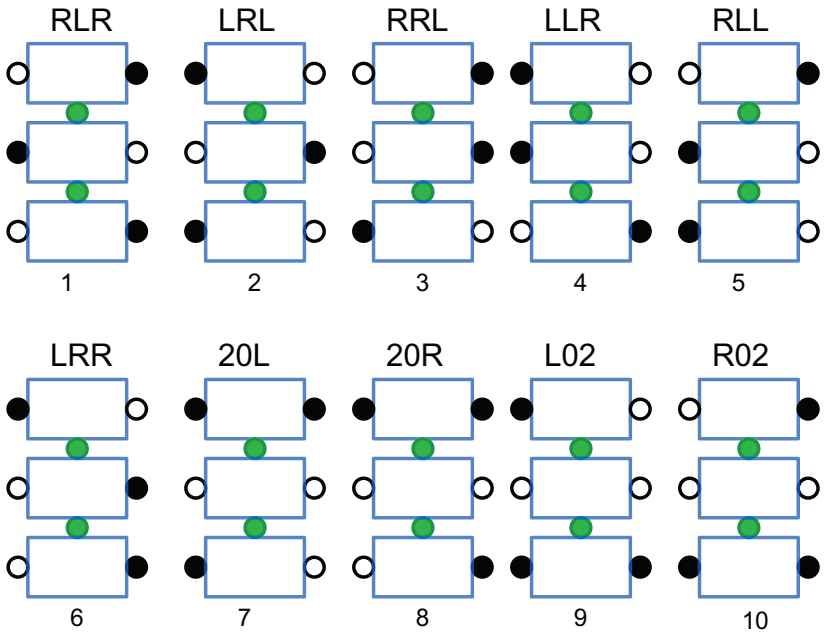

Figure 3.2. Ten candidate configurations of the passive-spine six-legged robot.

imposed by all legs [44]. The common constraints of the mechanism are analyzed by the screw theory, which is discussed in Appendix A.

Calculated mobilities of the passive-spine six-legged robot at all of the standing configurations are summarized in Fig. 2.3.

With the screw theory presented in Appendix A, it can be found that configurations having a mobility of $M_r = 1$, as shown in Fig. 2.3, can only allow the robot to perform translational movement along the y-axis. To perform planar locomotion, the robot should use those configurations that have mobilities $M_r > 1$. According to the analysis in Appendix A, the feasible motion of those configurations processes a translation along the y-axis, and a rotation about the axis that is parallel to the z-axis. Such configurations are indicated in Fig. 3.2, and called candidate configurations. Fig. 2.3 summarizes all of the candidate configurations, in which the candidate configurations are labeled by unique numbers.

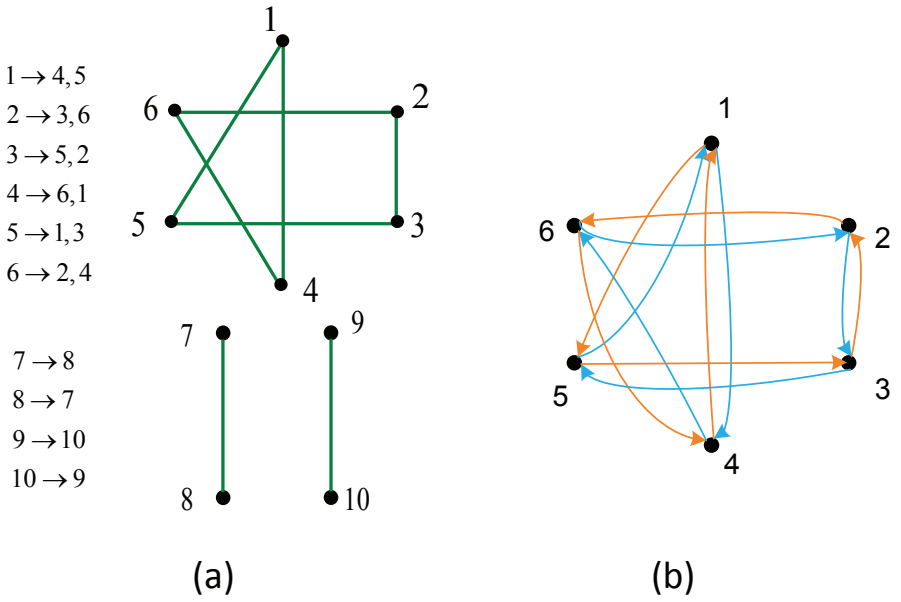

Figure 3.3. Graph of the possible transitions among candidate configurations of the six-legged robot.

3.1.3 Possible Configuration Transitions

As introduced in Chapter 2, passive-spine legged walking is achieved by sequentially conducting transitions among configurations. For the sake of simplicity and the stability of the robot during motion, we specify that at any time only one of the body segments can change its contact modes.

Under this rule, the possible configuration transitions are identified and represented by a graph $G = (V, E)$ [45], as shown in Fig. 3.3, where V is the set of candidate configurations; and E is the set of configuration transitions.

A passive-spine legged gait is therefore defined as a sequence of configuration transitions starting from and ending at a candidate configuration. The length of the gait is defined as the number of transitions in the gait, which is denoted by k.

For a six-legged robot, since every leg should be in contact with the ground at least one time, the length of the gait satisfies that $6 \leq k$. On the other hand, to avoid forming infinite

Table 3.1. Possible transition of the candidate configurations.

Length	Number	Generated sequences	Sign of each transition	Total value	Velocity $[m/s]$	Locomotion direction
k=6	1	$1 \to 4 \to 6 \to 2 \to 3 \to 5 \to 1$	++++++	+6	0.05	Forward
	2	$1 \to 5 \to 3 \to 2 \to 6 \to 4 \to 1$	- - - - - -	-6	-0.05	Backward
	3	$1 \to 4 \to 6 \to 2 \to 6 \to 4 \to 1$	+++ - - -	0	0.004	Unclear
	4	$1 \to 5 \to 3 \to 2 \to 3 \to 5 \to 1$	- - - +++	0	-0.004	Unclear
k=8	5	$1 \to 4 \to 6 \to 2 \to 3 \to 2 \to 3 \to 5 \to 1$	++++ - +++	+6	0.03	Forward
	6	$1 \to 4 \to 6 \to 2 \to 3 \to 2 \to 6 \to 4 \to 1$	++++ - - - -	0	0.005	Unclear
	7	$1 \to 4 \to 6 \to 2 \to 3 \to 5 \to 3 \to 5 \to 1$	+++++ - ++	+6	0.039	Forward
	8	$1 \to 4 \to 6 \to 2 \to 6 \to 2 \to 3 \to 5 \to 1$	+++ - ++++	+6	0.035	Forward
	9	$1 \to 4 \to 6 \to 4 \to 6 \to 2 \to 3 \to 5 \to 1$	++ - +++++	+6	0.035	Forward
	10	$1 \to 5 \to 3 \to 2 \to 3 \to 2 \to 6 \to 4 \to 1$	- - - + - - - -	-6	-0.037	Backward
	11	$1 \to 5 \to 3 \to 2 \to 6 \to 2 \to 3 \to 5 \to 1$	- - - - ++++	0	-0.003	Unclear
	12	$1 \to 5 \to 3 \to 2 \to 6 \to 2 \to 6 \to 4 \to 1$	- - - - + - - -	-6	-0.041	Backward
	13	$1 \to 5 \to 3 \to 2 \to 6 \to 4 \to 6 \to 4 \to 1$	- - - - - + - -	-6	-0.042	Backward
	14	$1 \to 5 \to 3 \to 5 \to 3 \to 2 \to 6 \to 4 \to 1$	- - + - - - - -	-6	-0.032	Backward
k=10	15	$1 \to 4 \to 6 \to 2 \to 3 \to 5 \to 3 \to 2 \to 6 \to 4 \to 1$	+++++ - - - - -	0	0.005	Unclear
	16	$1 \to 4 \to 6 \to 2 \to 6 \to 2 \to 3 \to 5 \to 3 \to 5 \to 1$	+++ - +++ - ++	+6	0.039	Forward
	17	$1 \to 4 \to 6 \to 4 \to 6 \to 2 \to 3 \to 2 \to 3 \to 5 \to 1$	++ - +++ - +++	+6	0.020	Forward
	18	$1 \to 4 \to 6 \to 4 \to 6 \to 2 \to 3 \to 5 \to 3 \to 5 \to 1$	++ - ++++ - ++	+6	0.035	Forward
	19	$1 \to 5 \to 3 \to 2 \to 3 \to 2 \to 6 \to 4 \to 6 \to 4 \to 1$	- - - + - - - + - -	-6	-0.031	Backward
	20	$1 \to 5 \to 3 \to 2 \to 6 \to 4 \to 6 \to 2 \to 3 \to 5 \to 1$	- - - - - +++++	0	-0.029	Unclear
	21	$1 \to 5 \to 3 \to 5 \to 3 \to 2 \to 6 \to 2 \to 6 \to 4 \to 1$	- - + - - - + - - -	-6	-0.035	Backward
	22	$1 \to 5 \to 3 \to 5 \to 3 \to 2 \to 6 \to 4 \to 6 \to 4 \to 1$	- - + - - - - + - -	-6	-0.038	Backward

loops in the gait, the length of the gait should also satisfy that $k \leq 10$. If the robot starts at candidate configuration 1, a number of 22 gaits can be found, as shown in Table 3.1.

3.2 Locomotion Method

3.2.1 Kinematic Model of the Body Segment

During the configuration transition, the robot's center of mass (CoM) moves due to rotations of body segments. The projected position of the robot's CoM on the ground is calculated in this section.

Taking the configuration transition "1 $\to$ 4" shown in Fig. 3.4 as an example, with

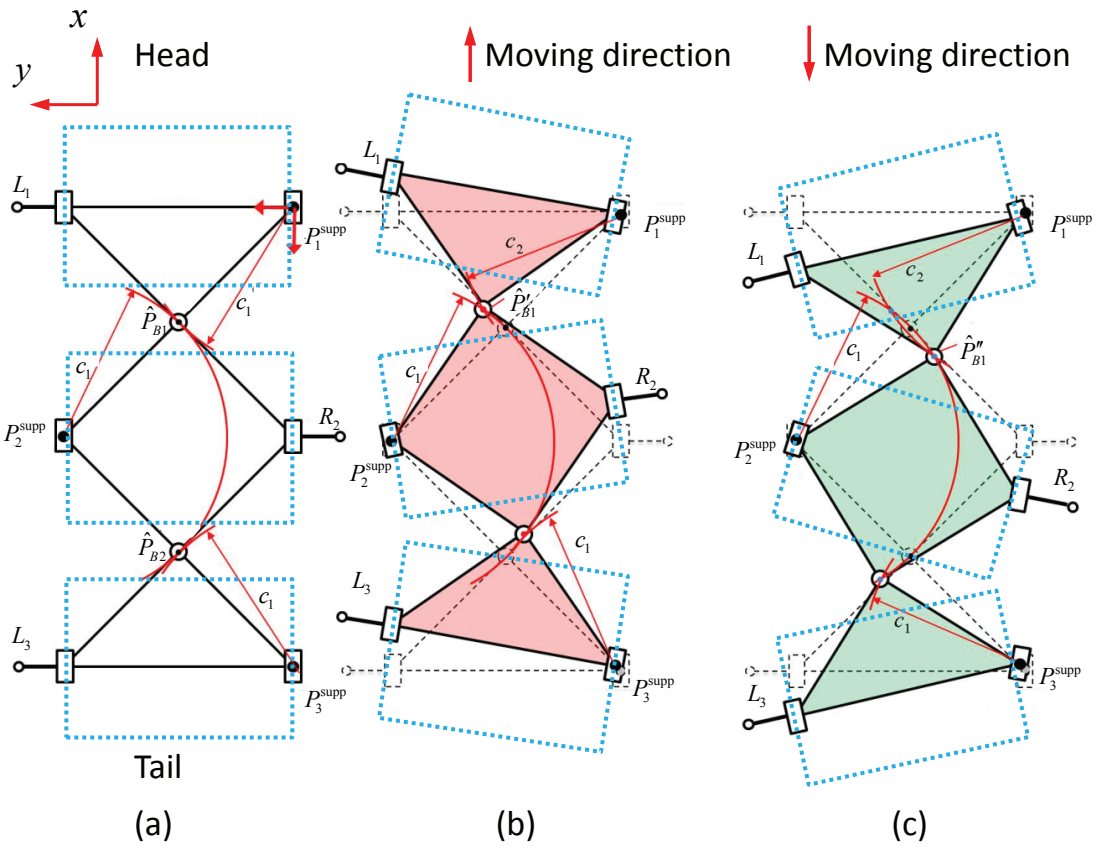

Figure 3.4. (a) Schematic diagram of the configuration "RLR". (b) and (c) Possible movements of the body segments which are brought by the configuration transition "RLR" to "LLR".

the posture as shown in Fig. 3.4(a), the robot stands on the ground at three footprints, respectively, denoted by $\vec{P}_1^{supp}$, $\vec{P}_2^{supp}$, and $\vec{P}_3^{supp}$. A global coordinate $\{\vec{O}\}$ is defined in such a way that its origin locates at $\vec{P}_1^{supp}$, its y-axis is parallel to the sagittal plane of the robot towards the head of the robot, and its z-axis is upwards from the ground. For the sake of simplicity, joint angles of the supporting legs are identically equal to $\pi/2$, and therefore coordinates of the footprints are expressed by $\vec{P}_1^{supp} = [0, 0, 0]^T$, $\vec{P}_2^{supp} = [2l_2, 2l_3, 0]^T$, and $\vec{P}_3^{supp} = [0, 4l_3, 0]^T$, respectively.

During the configuration transition "$1 \rightarrow 4$", abduction of leg R_1 and adduction of leg L_1 will firstly result in rotation of body-segment 1 about the axis of body-joint-1.

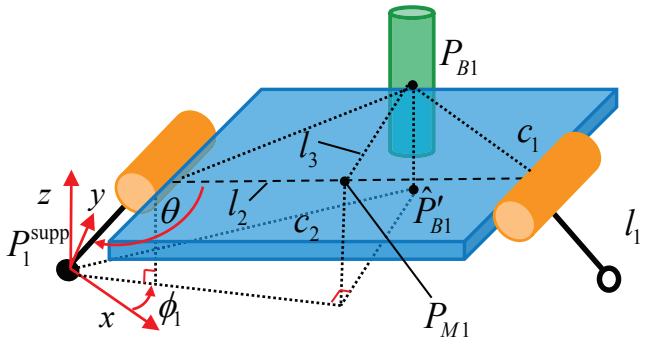

Figure 3.5. Geometric relationship between the posture of the body segment and leg angle.

As shown in Fig. 3.5, once the leg R_1 abducts to a new posture $\theta_{R1} = \theta$, projected point of the body-joint-1 will locate at a new position, $\vec{\hat{P}}'_{B1}$, that is the intersection of two circles that have radii of $c_1 = \sqrt{l_2^2 + l_3^2}$ and $c_2 = \sqrt{(l_2 - l_1 \cos\theta)^2 + l_3^2}$, respectively. In other words, coordinates of the center of the body-joint-1, $\vec{P}'_{B1} = [x, y, l_1]^T$, satisfy the following equations:

$$\begin{cases} x^2 + y^2 = c_2^2 \\ (x - 2l_2)^2 + (y - 2l_3)^2 = c_1^2, \end{cases} \tag{3.5}$$

where l_1 is the length of the leg; and l_2 and l_3 are the half-width and half-length of the body segment, respectively.

Note that two solutions are feasible for (3.5), as respectively shown in Fig. 3.4(b) and

Fig. 3.4(c), which can be expressed by:

$$\begin{cases} x = c_2 \cos(\gamma - \beta) \\ y = c_2 \sin(\gamma - \beta) \end{cases} \tag{3.6}$$

and

$$\begin{cases} x = c_2 \cos(\gamma + \beta) \\ y = c_2 \sin(\gamma + \beta), \end{cases} \tag{3.7}$$

where $\gamma = \text{atan2}(2l_3, 2l_2)$; and $\beta = \arccos((3c_1^2 + c_2^2)/(4c_1c_2))$.

These two solutions imply that body-segment 1 is capable of rotating in two different directions from a kinematic perspective. The two possible angular positions of body-joint-1 can be expressed as:

$$\phi_1 = \text{atan2}(y, x) - \text{atan2}(l_3, l_2 - l_1 \cos\theta). \tag{3.8}$$

This means that only one of them is the resultant rotation direction when reaction forces between the ground and the supporting legs are taken into account.

Because of body-joint 2, rotation of body-segment 2 will result in rotation of body-segment 3. As a consequence, all of the body segments rotate during the configuration transition. It is worth noting that rotation of body-segment 3 will result in a small amount of slippage between supporting leg R_3 and the ground. However, such slippage is experimentally verified to be small, and is therefore ignored in this study. In our future study, slippage at the footprints will be eliminated by allowing two body segments to alter their contact modes simultaneously.

As shown in Fig. 3.5, the point $\vec{P}_{M1} = [x_{M1}, y_{M1}, z_{M1}]^T$ denotes the position of the CoM of the body segment, which is located at:

$$\begin{cases} x_{M1} = (l_2 - l_1 \cos\theta) \cos\phi_1 \\ y_{M1} = (l_2 - l_1 \cos\theta) \sin\phi_1 \\ z_{M1} = l_1 \sin\theta \end{cases} \tag{3.9}$$

From (3.9), it can be found that the position of the CoM of the body segment is a function of abduction angle θ of the supporting leg.

3.2.2 Forward Propulsion Possibility of Configuration Transitions

For our robot, the weight of the body segment concentrates at its geometric center. Therefore, the body segment can be treated as a point mass attached to a massless rod. Only the masses of the robot are considered in the force analysis. In our analysis, the pitch and roll angle of the body segments were less than 2° in the simulation environment and experiments in Chapters 4, 5, and 6. In the following discussions, the projection of the rotation direction of the supporting legs on the horizontal xy plane is analyzed. In the following text, the rotation direction on the horizontal xy plane is analyzed at this instant.

Based on the obtained rotation direction of each body segment, the configuration is projected onto the horizontal xy plane in Fig. 3.6 (b). Here, the points $\mathbf{P^{supp}_{j,i}} = [x^{supp}_{j,i}, y^{supp}_{j,i}]^T$ and $\mathbf{P^{b}_{j,i}} = [x^{b}_{j,i}, y^{b}_{j,i}]^T$ are the positions of the supporting leg and CoM, respectively, of body segment j at the ith step; $\phi_{j,i}$ represents the rotation angle of the body segment about the supporting leg; and $\theta_{j,i}$ represents the deflection angle of the jth supporting leg at the ith step. The CoM of the jth body segment is then given by:

$$\begin{aligned} x^{b}_{j,i} &= x^{supp}_{j,i-1} + (l_2 - l_1 \cos\theta_{j,i}) \cos\phi_{j,i} \\ y^{b}_{j,i} &= y^{supp}_{j,i-1} + f_i (l_2 - l_1 \cos\theta_{j,i}) \sin\phi_{j,i} \end{aligned} \tag{3.10}$$

where f_i is a constant equal to $+1$ and -1 when the right and left legs contact the ground, respectively.

The velocity of the jth body segment is given by:

$$\begin{aligned} \dot{x}^{b}_{j,i} =& \dot{x}^{supp}_{j,i-1} + l_1 \sin\theta_{j,i} \cos\phi_{j,i} \dot{\theta}_{j,i} - (l_2 - l_1 \cos\theta_{j,i}) \sin\phi_{j,i} \dot{\phi}_{j,i} \\ \dot{y}^{b}_{j,i} =& \dot{y}^{supp}_{j,i-1} + f_i l_1 \sin\theta_{j,i} \sin\phi_{j,i} \dot{\theta}_{j,i} + f_i (l_2 - l_1 \cos\theta_{j,i}) \cos\phi_{j,i} \dot{\phi}_{j,i} \end{aligned} \tag{3.11}$$

where $\dot{x}^{supp}_{j,i-1}$ and $\dot{y}^{supp}_{j,i-1}$ are the velocity of the supporting leg along x-axis and y-axis, respectively. Since we have assumed that slippage between the supporting legs and the ground does not occur, it yields $\dot{x}^{supp}_{j,i-1} = 0$ and $\dot{y}^{supp}_{j,i-1} = 0$.

The acceleration of the jth body segment is then given by:

$$\begin{aligned} \ddot{x}^{b}_{j,i} &= P_{j,i} + Q_{j,i} \\ \ddot{y}^{b}_{j,i} &= f_i (U_{j,i} + V_{j,i}) \end{aligned} \tag{3.12}$$

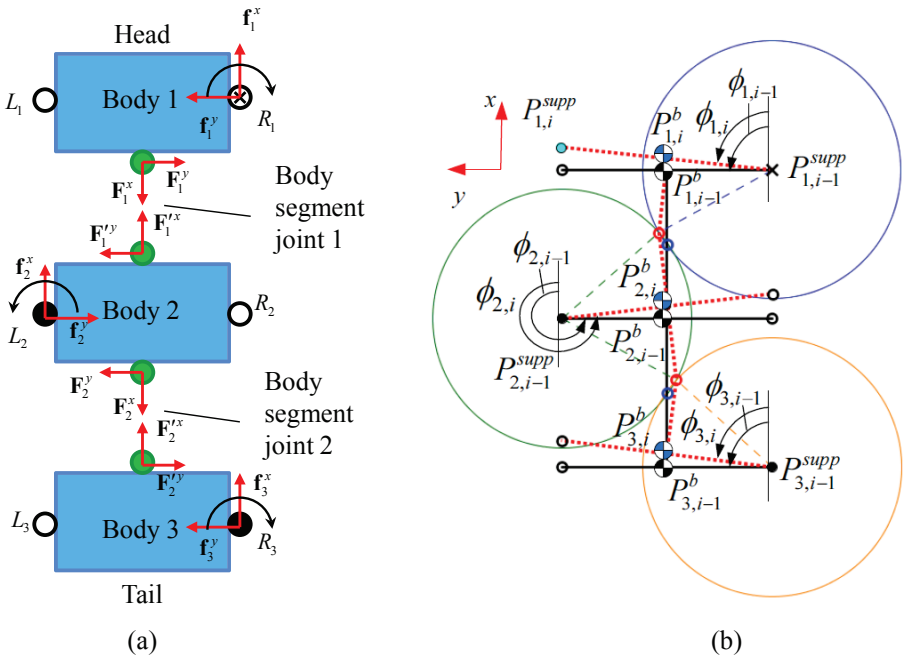

Figure 3.6. (a) Forces acting on the six-legged robot during configuration transition $1 \rightarrow 4$. Solid and open circles represent supporting and swinging legs, respectively. Legs that will abduct are marked by crosses. Body-segments-1 and 2, and body-segments-2 and 3, are connected by body-segment-joint-1 and 2, respectively. (b) Projection of the passive-spine six-legged robot on the horizontal xy plane.

where

$$\begin{aligned}
P_{j,i} =& l_1 \cos\theta_{j,i} \cos\phi_{j,i} \dot{\theta}_{j,i}^2 - 2l_1 \sin\theta_{j,i} \sin\phi_{j,i} \dot{\theta}_{j,i} \dot{\phi}_{j,i} - (l_2 - l_1 \cos\theta_{j,i}) \cos\phi_{j,i} \dot{\phi}_{j,i}^2 \\
Q_{j,i} =& l_1 \sin\theta_{j,i} \cos\phi_{j,i} \ddot{\theta}_{j,i} - (l_2 - l_1 \cos\theta_{j,i}) \sin\phi_{j,i} \ddot{\phi}_{j,i} \\
U_{j,i} =& l_1 \cos\theta_{j,i} \sin\phi_{j,i} \dot{\theta}_{j,i}^2 + 2l_1 \sin\theta_{j,i} \cos\phi_{j,i} \dot{\theta}_{j,i} \dot{\phi}_{j,i} - (l_2 - l_1 \cos\theta_{j,i}) \sin\phi_{j,i} \dot{\phi}_{j,i}^2 \\
V_{j,i} =& l_1 \sin\theta_{j,i} \sin\phi_{j,i} \ddot{\theta}_{j,i} + (l_2 - l_1 \cos\theta_{j,i}) \cos\phi_{j,i} \ddot{\phi}_{j,i}
\end{aligned} \tag{3.13}$$

From (3.12), it can be noted that the direction of the resultant acceleration of the robot's body is given by the sign of $\ddot{x}_{j,i}^b$, which depends on the sign of $P_{j,i}$ and $Q_{j,i}$.

Taking the transition $1 \rightarrow 4$ shown in Fig. 3.4 as an example again, the direction of the robot's motion can be determined by the following analysis. At the initial moment, the body segment and legs are stationary and their velocities are zero, yielding $P_j = 0$ according to (3.13), where $j = 1, 2, 3$. Therefore, the acceleration directions of the robot's body segments are solely determined by Q_j according to (3.12). Since only leg R_1 swings up with a deflection angular acceleration of $\ddot{\theta}_1 > 0$ and the other legs remain stationary during the transition, Q_j in (3.13) can be simplified as:

$$\begin{aligned}
Q_1 &= l_1 \sin\theta_1 \cos\phi_1 \ddot{\theta}_1 - (l_2 - l_1 \cos\theta_1) \sin\phi_1 \ddot{\phi}_1 \\
Q_2 &= -(l_2 - l_1 \cos\theta_2) \sin\phi_2 \ddot{\phi}_2 \\
Q_3 &= -(l_2 - l_1 \cos\theta_3) \sin\phi_3 \ddot{\phi}_3
\end{aligned} \tag{3.14}$$

Considering the initial posture of the robot, where $\phi_1 = \pi/2$, $\phi_2 = 3\pi/2$, and $\phi_3 = \pi/2$, (3.14) can be further simplified as:

$$\begin{aligned}
Q_1 &= l_1 \sin\theta_1 \cos\phi_1 \ddot{\theta}_1 \\
Q_2 &= Q_3 = 0.
\end{aligned} \tag{3.15}$$

Since $\ddot{\theta}_1 > 0$, Q_1 in (3.15) is positive, which means that the first body segment of the robot will have a positive acceleration in the direction along the x-axis, according to (3.12). Such acceleration will result in a forward motion of the robot, as shown in Fig. 3.4(b).

The directions of the body segment rotations in the next configuration transitions are shown in Fig. 3.7. The body segments are found to be affected by the resultant force along

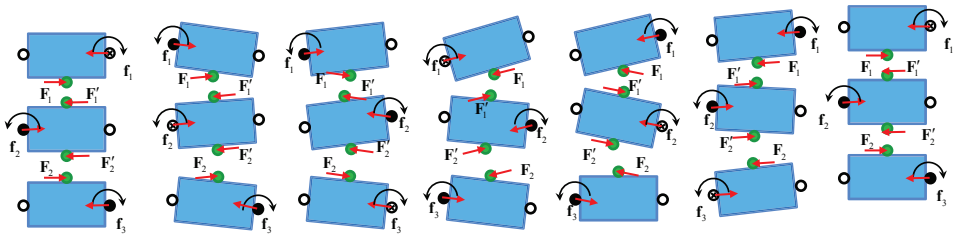

Figure 3.7. Rotation directions of configuration transitions $1 \rightarrow 4 \rightarrow 6 \rightarrow 2 \rightarrow 3 \rightarrow 5 \rightarrow 1$. The rotation direction of each body segment is indicated by curved arrows.

Table 3.2. Locomotion possibilities of configuration transitions.

Configuration						
Transitions	$1 \rightarrow 4$	$4 \rightarrow 6$	$6 \rightarrow 2$	$2 \rightarrow 3$	$3 \rightarrow 5$	$5 \rightarrow 1$
Sign	+	+	+	+	+	+
Configuration						
Transitions	$1 \rightarrow 5$	$5 \rightarrow 3$	$3 \rightarrow 2$	$2 \rightarrow 6$	$6 \rightarrow 4$	$4 \rightarrow 1$
Sign	-	-	-	-	-	-

the positive direction of the x axis, which generates forward locomotion. This implies that the analyzed configuration transitions enable forward movement of the robot.

In this thesis, such configuration transitions that propel the robot forward are called positive transitions and are labeled "+," while transitions yielding backward motion are called negative transitions and labeled "−." By the same method, the transitions $1 \rightarrow 5 \rightarrow 3 \rightarrow 2 \rightarrow 6 \rightarrow 4 \rightarrow 1$ were confirmed to drive the robot backward. In the result, the locomotion possibilities of both configurations are summarized in Table 3.2.

3.2.3 Rotation Ability of Passive Body Joints

Although we discussed the mobility analysis of passive-spine legged robots, and obtained a forward and backward straight gait sequence by analyzing its motion possibilities in the previous section, the effect of each step configuration transition on the body segments has not yet been deeply analyzed. We can analyze the influence of the configuration transition

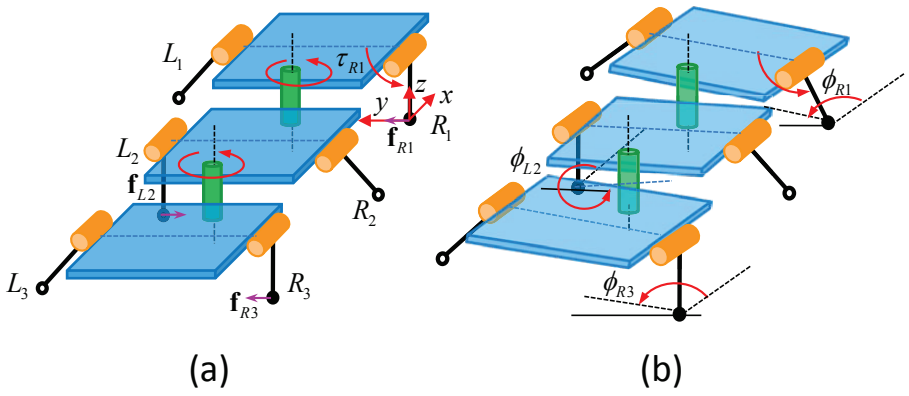

Figure 3.8. Changes in the RLR model before lifting leg R_1. (a) Horizontal force distribution on footprints of supporting legs. (b) The schematic diagram of changes of rotation angles and deflection angle.

of each step in the obtained motion on the rotation of the body segment, and then determine the corresponding rotation principle. Here, we take the first step of the forward-locomotion configuration sequence $1 \rightarrow 4 \rightarrow 6 \rightarrow 2 \rightarrow 3 \rightarrow 5 \rightarrow 1$ as an example to analyze the rotation directions of body segments.

In the step of RLR to LLR (configuration transition $1 \rightarrow 4$), the robot starts changing the configuration from RLR by abducting leg R_1 and adducting leg L_1 simultaneously. The whole process can be expressed in the schematic diagram in Fig. 3.8. Since the configuration RLR is ready to lift R_1, the robot is in the condition that is only supported by three legs R_1, L_2, and R_3. At this moment, R_1 cannot quickly leave the ground. The friction between the leg and the ground gives the body a force in the positive direction of the y-axis before R_1 leaves the ground. During this process, a deflection angle θ_{R1} occurs between the leg and the body segment.

Based on the analysis of force distribution during the process of the configuration transitions, the geometric method is continuously utilized to analyze the changes of the rotation angle of the supporting legs.

Fig. 3.9 presents a schematic diagram that graphically illustrates the leg phases, in which the solid and open circles indicate the footprints of the supporting and swinging legs,

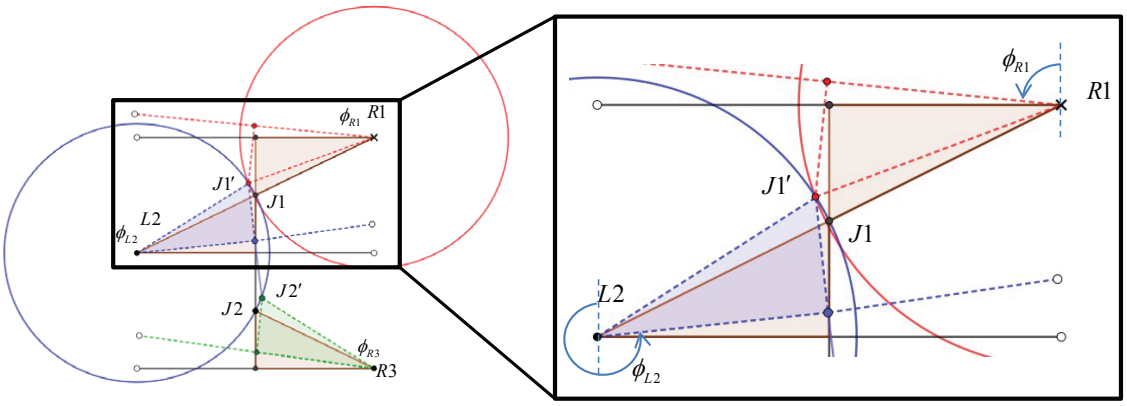

Figure 3.9. Geometric relationship of configuration transitions RLR to LLR.

respectively. The gray circle indicates the segment body joint. In Fig. 3.9, the geometric relationship of the body segments and legs can be calculated.

In $\triangle R_1 J_1 J_1'$,

$$2\left|R_1J_1'\right|\left|R_1J_1\right|\cos\angle J_1R_1J_1' = \left|R_1J_1'\right|^2 + \left|R_1J_1\right|^2 - \left|J_1J_1'\right|^2. \tag{3.16}$$

in $\triangle L_2 J_1' J_1$,

$$2\left|L_2J_1'\right|\left|L_2J_1\right|\cos\angle J_1'L_2J_1 = \left|L_2J_1'\right|^2 + \left|L_2J_1\right|^2 - \left|J_1J_1'\right|^2, \tag{3.17}$$

and in $\triangle R_1 J_1' L_2$,

$$2\left|R_1J_1'\right|\left|R_1L_2\right|\cos\angle J_1R_1J_1' = \left|R_1J_1'\right|^2 + \left|R_1L_2\right|^2 - \left|L_2J_1'\right|^2. \tag{3.18}$$

where

$$\begin{aligned} \left|R_1J_1\right| = \left|L_2J_1\right| = \left|L_2J_1'\right| &= \sqrt{(l_2 - l_1\cos\theta_{R1})^2 + l_3^2} = R, \\ \left|R_1J_1'\right| &= \sqrt{l_2^2 + l_3^2} = R'. \end{aligned} \tag{3.19}$$

Then, the relationship between deflection angle θ_{R1} and rotation angle of supporting leg $R1$ and $L2$ can be given as:

$$\begin{aligned} \phi_{R1} &= \frac{\pi}{2} - \angle J_1R_1J_1', \\ \phi_{L2} &= \frac{3\pi}{2} + \angle J_1'L_2J_1, \end{aligned} \tag{3.20}$$

where

$$\begin{aligned} \angle J_1R_1J_1' &= \arccos\frac{R'^2}{4RR'}, \\ \angle J_1'L_2J_1 &= \arccos\frac{2RR'\cos\angle J_1R_1J_1' - R'^2 + R^2}{2R^2}. \end{aligned} \tag{3.21}$$

In this way, we can obtain the expression of the rotation angles of the two supporting legs and the deflection angle of leg R_1 that will lift up. These solutions indicate the rotation angle of the supporting legs during the configuration transition 1 to 4.

Because we aim to determine the direction of rotation of the supporting legs at the initial time in the lifting motion, the rotation angle that is analyzed can be calculated by a given deflection angle, θ_R, which is determined by the function $\theta_{R1} = 0.3 \sin \pi t$. The required parameters are $l_1 = 0.082m$, $l_2 = 0.05m$, and $l_3 = 0.046m$.

Based on these given values, the rotation angles ϕ_{R1} changed with respect to θ_R are calculated in a same period of time (see Fig. 3.10). The decrease of rotation angle ϕ_{R1}

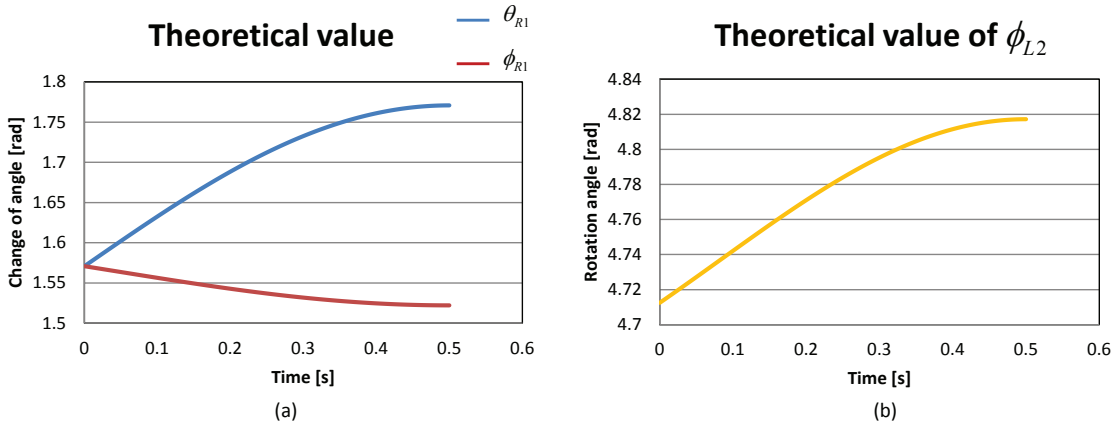

Figure 3.10. Change of rotation angles during the transition RLR to LLR when deflection angle θ_{R1} changes within 0.5 [s]. (a) Change of θ_{R1} and ϕ_{R1}. (b) Change of ϕ_{L2}.

reveals that supporting leg R_1 rotate in the clockwise direction. The increase of rotation angle ϕ_{L2} reveals that supporting leg L_2 rotate in the counterclockwise direction.

The trend of the change in Fig. 3.10 implies that the position of the leg to be lifted and the direction of the deflection angle of this leg has affected the direction of rotation. The rotation angle of the supporting leg is mainly determined by the length of time of the rotation in the supporting phase before it swings up, i.e., the longer is the duration of the rotation, the larger is the angle of the rotation. In a later study, we can use this feature to design the turning gait of the robot.

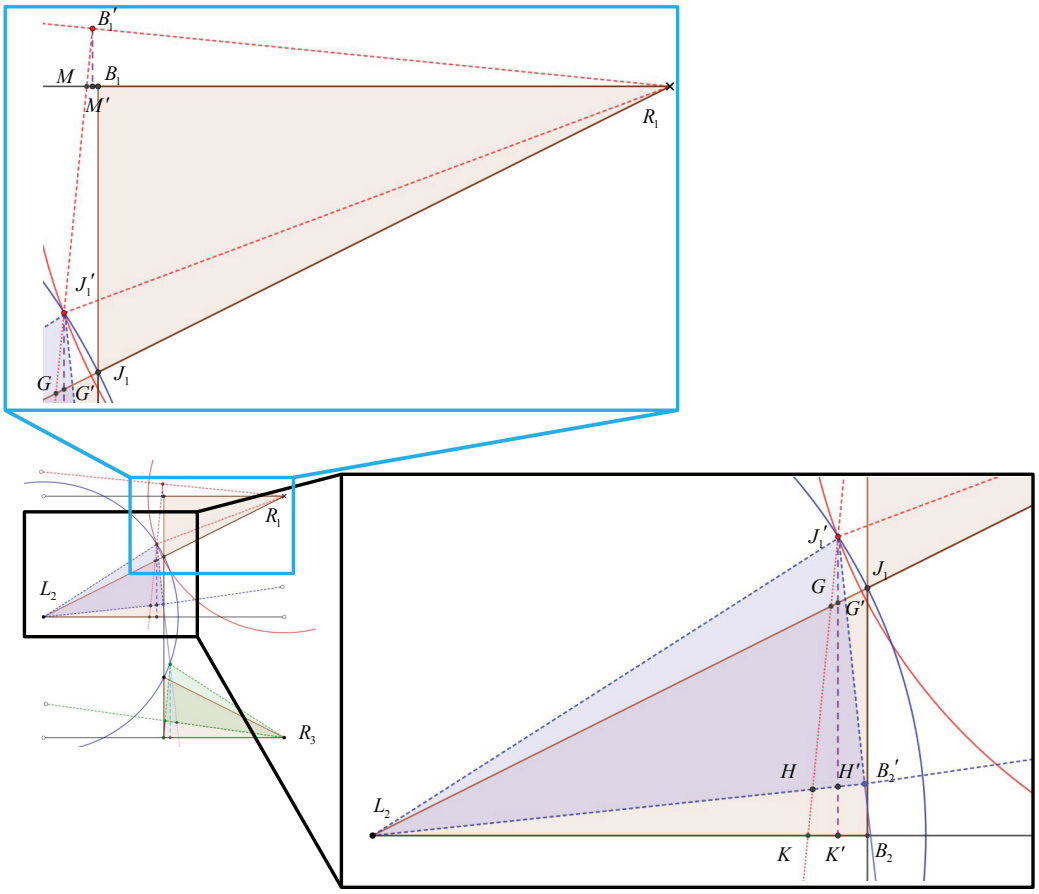

Figure 3.11. Geometric relationship of body segment joint J_1.

Based on the analysis of the supporting leg, according to the geometric model, the relationship between supporting legs and passive body segment can be calculated.

In Fig. 3.11, guidelines passed point J_1' and B_1' that paralleled line J_1B_2 and B_1J_1 are made firstly. Points G', H', and K' are the cross points of line $J_1'K'$ with lines L_2J_1, L_2B_2', and L_2B_2, respectively.

In $\triangle MB_1'M'$ and $\triangle MB_1'R_1$, we can obtain:

$$\begin{aligned} \angle GJ_1'G' = \angle MB_1'M' &= \angle B_1'R_1B_1 \\ &= \angle B_1'R_1J_1' - \angle B_1R_1J_1' \\ &= \angle B_1'R_1J_1' - (\angle B_1R_1J_1 - \angle J_1'R_1J_1'). \end{aligned} \tag{3.22}$$

Then, in $\triangle J_1' H' B_2'$ and $\triangle L_2 H' K'$, we can find:

$$\angle H' J_1' B_2' = \angle H' L_2 K. \tag{3.23}$$

The angles in Equation (3.22) and (3.23) can be obtained by calculating the rotation angles of the supporting legs based on the previous analysis.

For $\triangle L_2 J_1' G'$, the exterior angle can be given as:

$$\angle L_2 G' K' = \angle J_1' L_2 G + \angle L_2 J_1' G + \angle G J_1' G', \tag{3.24}$$

that is,

$$\angle L_2 J_1' G = \angle L_2 G' K' - \angle J_1' L_2 G - \angle G J_1' G', \tag{3.25}$$

where

$$\angle L_2 G' K' = \arctan \frac{l_2}{l_3}. \tag{3.26}$$

Therefore, in $\triangle J_1' L_2 B_2'$, the change of the angle of body segment J_1 can be given as:

$$\angle H J_1' B_2' = \frac{\pi}{2} - \angle J_1' L_2 B_2' - \angle L_2 J_1' G \tag{3.27}$$

Here, the angle of $\angle J_1' L_2 B_2'$ can be known by the structural parameters of the robot.

According to the calculations, the rotation direction trend and rotation angles of body segment joint $J1$ changed with respect to θ_R that is represented in a same period of time can be obtained (see Fig. 3.12). The solid orange line represents the calculated theoretical value, and the decrease in the angle of rotation means that the body joint rotates clockwise around the body segment joint, which is consistent with the direction of rotations of supporting legs R_1 and R_2, as well as the geometric relationship between them.

Through the analysis of the above geometric model, we can know that these rotation directions and angles of the supporting legs and the body segment joints can be analyzed and predicted by giving the change of the angle of the leg to be lifted. In the next section, a rotation principle for this design will be discussed.

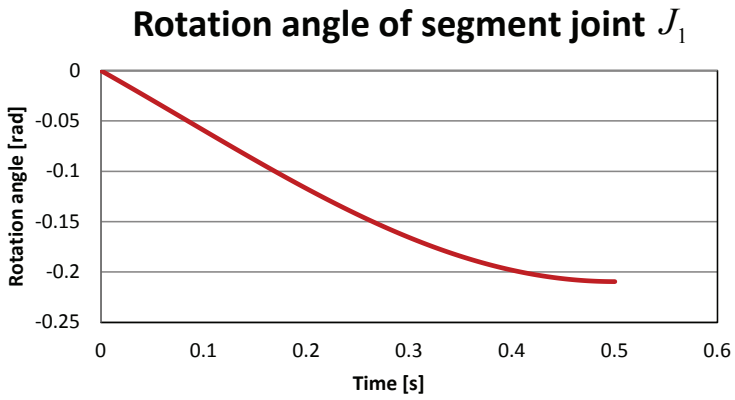

Figure 3.12. Comparison of theoretical and simulation value of rotation angles ϕ_{R1} during the transition RL to LL when deflection angle θ changes within 0.5 [s].

3.2.4 Rotation Principle of Body Segment Joint

According to the analysis of the first step, the other steps of the configuration transitions are analyzed in the same manner. The rotation principles of the geometric model of configurations $1-6$ are easily summarized. As shown in Fig. 3.13, the same analysis gives the rotation direction about the supporting legs. Fig. 3.13 contains these six configurations and six common transitions between these configurations. Here, the upward arrow indicates the leg to swing up, the circle represents the swinging leg in the air, and the clockwise and counterclockwise arrows represent the rotational direction of the supporting leg in contact with the ground. The last row in Fig. 3.13 indicates the configuration transition when the leg swings up and the swinging leg fails to complete the transition. For example, in the second column, when leg R_2 is lifted, then legs R_1, R_2, and L_3 rotate, and when leg L_2 contacts the ground, then transition 3 to 5 is completed, which means that the system transitions from RRL to RLL.

If the right leg is about to swing up, its body segment will rotate clockwise, and the legs on the same body side will rotate in the same direction as the given leg. On the opposite side of the given leg, the leg rotates in the direction opposite that to the given leg. Moreover, in this process, the longer the duration of the supporting rotation on the ground before the leg leaves the ground, the greater the change of the rotation angle. By symmetry, the same conclusion is also obtained for the left side. In addition, the principle

Supporting leg	Rotation direction					
R_1						
R_2						
R_3						
L_1						
L_2						
L_3						
Transition	1 → 4	3 → 5	6 → 2	2 → 3	4 → 6	5 → 1

Figure 3.13. Different configurations for rotation directions for transitions $1 \to 4 \to 6 \to 2 \to 3 \to 5 \to 1$.

in Fig. 3.13 implies that the configuration transition sequence implemented by the turning motion may be designed and conducted based on the analysis.

In the movement of a multi-segmental robot, the direction of the head segment plays a vital role in the direction of motion of the entire robot. Therefore, we refer to the direction of rotation of the head segment as the direction of this configuration transition.

According to the results given in Fig. 3.13, the configuration transitions 1 to 4, 3 to 5, and 5 to 1 rotate the robot body clockwise, and thus these are termed clockwise transitions. Conversely, the configuration transitions 2 to 3, 4 to 6, and 6 to 2 rotate the robot body counterclockwise, and thus these are termed counterclockwise transitions. Based on this analysis, we deduce the rotation principle for the supporting leg and the swinging leg. We also obtain the key factors that affect the rotation angle. Fig. 3.14 shows six motion configurations of the passive-spine six-legged robot that are analyzed.

These resulting features are utilized to design the turning gait. Based on the analysis of rotation principle of our configuration transition, a general model is proposed for the contribution of rotation, which is given as:

$$C_{total} = t_+ C_+ + t_- C_- \tag{3.28}$$

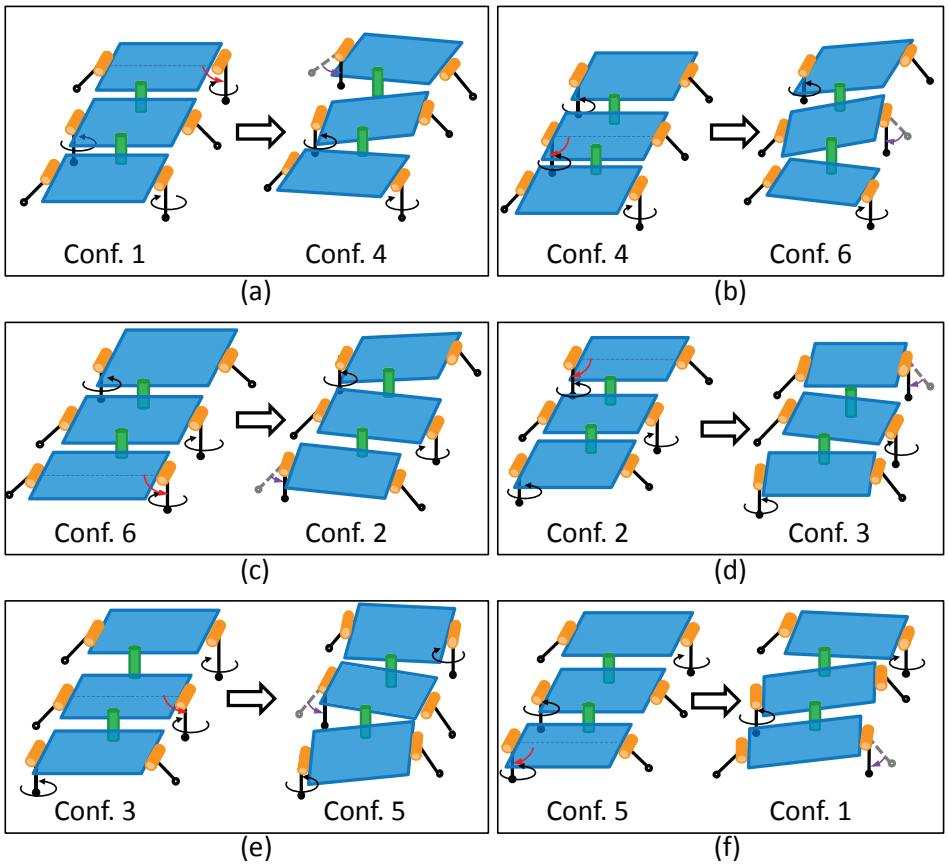

Figure 3.14. Six specific motion configurations showing the rotation direction of the body segments for transitions $1 \rightarrow 4 \rightarrow 6 \rightarrow 2 \rightarrow 3 \rightarrow 5 \rightarrow 1$.

where C_{total} represents the total contribution of the sequence of configurations to turn clockwise; C_+ and C_- represents the contribution of each configuration transition to turn clockwise and counterclockwise, respectively; and t_+ and t_- identifies the total time of transition with C_+ and C_+, respectively.

For example, in Fig. 3.15, in transitions $1 \to 4 \to 6 \to 2 \to 3 \to 5 \to 1$, according to the analysis results of the previous section, the contribution of each transition can be expressed as:

$$\begin{aligned} t_+C_+ &= \Delta t_{1\to4}C_{1\to4} + \Delta t_{3\to5}C_{3\to5} + \Delta t_{5\to1}C_{5\to1}, \\ t_-C_- &= \Delta t_{4\to6}C_{4\to6} + \Delta t_{6\to2}C_{6\to2} + \Delta t_{2\to3}C_{2\to3}, \end{aligned} \tag{3.29}$$

where $t_+ = \Delta t_{1\to4} + \Delta t_{3\to5} + \Delta t_{5\to1}$; $t_- = \Delta t_{4\to6} + \Delta t_{6\to2} + \Delta t_{2\to3}$; and the subscript of the Δt indicates the transition of the configuration state. The transition time points can be expressed as:

$$\begin{aligned} \Delta t_{1\to4} &= t_1 - t_0, \\ \Delta t_{3\to5} &= t_5 - t_4, \\ \Delta t_{5\to1} &= T - t_5, \\ \Delta t_{4\to6} &= t_2 - t_1, \\ \Delta t_{6\to2} &= t_3 - t_2, \\ \Delta t_{2\to3} &= t_4 - t_3. \end{aligned} \tag{3.30}$$

The transition time points are shown in Fig. 3.15, which indicates the length of the supporting phase and the swinging phase for each configuration transition clearly. Then, we can obtain the expression of contribution on each direction. Because $C_{1\to4}$ and $C_{2\to3}$, $C_{3\to5}$ and $C_{4\to6}$, and $C_{5\to1}$ and $C_{2\to3}$ have opposite contributions to turn clockwise, we will mainly consider the time coefficient on the total contribution. Then, we obtain:

$$C_{total} = \begin{cases} Clockwise \quad rotation & t_- \to 0 \\ Right \quad turning & t_+ > t_- \\ Forward \quad locomotion & t_+ = t_- \\ Left \quad turning & t_+ < t_- \\ Counter-clockwise \quad rotation & t_+ \to 0. \end{cases} \tag{3.31}$$

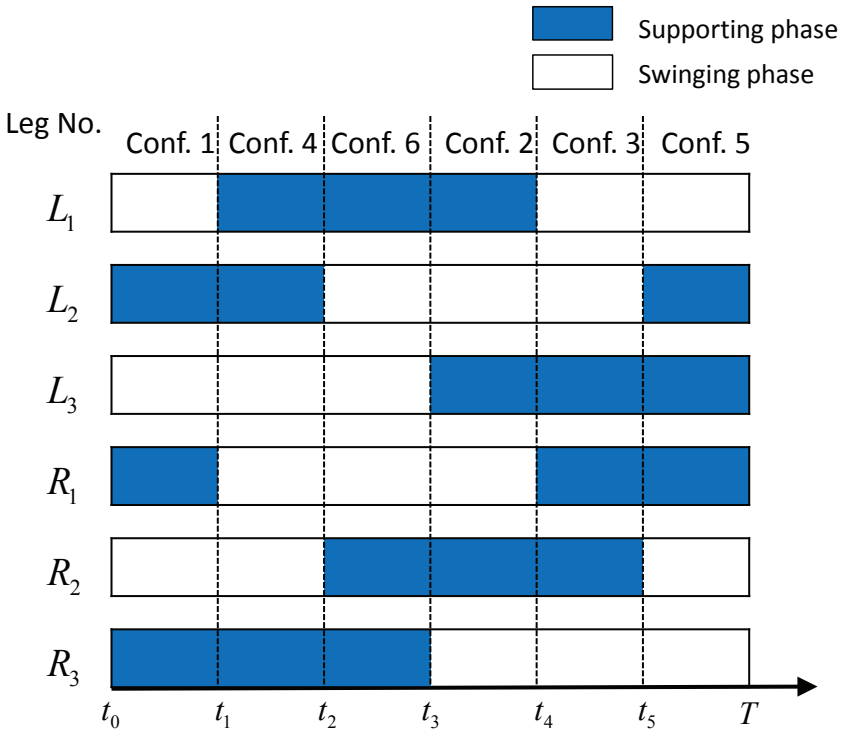

Figure 3.15. The supporting phase and the swinging phase for transitions $1 \to 4 \to 6 \to 2 \to 3 \to 5$ that generate a forward straight-line motion.

3.3 Summary

In this chapter, we have proposed a method to analyze the locomotion of the passive-spine legged robot with a simple design. Mobility of possible configurations has been analyzed to select the candidate configurations for generating different gait transitions. Based on the analysis of the kinematic model and the geometric model, the capability of straight-line locomotion and body-segment rotation which are generated by configuration transitions has been obtained. The gait patterns of the proposed robot will be discussed in Chapter 4 based on locomotion analysis.

Chapter 4

Gait Analysis of Passive-Spine Legged Robots

In order to realize movement diversity of multi-legged robot, the gait patterns of our proposed robot need to be analyzed and planned. We can also refer to the locomotion algorithms of other various kinds of multi-legged systems. For traditional multi-legged robots, which have one body segment and several legs, the turning gait can usually be planned by considering the foot trajectory. Miao and Howard presented a tripod turning gait for a six-legged robot. They focused on determining the appropriate trajectory of the supporting leg to make the robot body obtain the expected turning angle [5]. Gao et al. introduced a gait planning method of a hydraulic hexapod walking robot, in which foot trajectory and turning gait planning were analyzed based on kinematic analysis. The proposed gait planning method was verified in simulations [46]. Deng et al. proposed a new control method based on rolling gait and trajectory planning, which enabled hexapod robots to walk through complex environments [47]. The robot changed gaits to complete different tasks. However, the foot trajectory of conventional multi-legged robots is mostly controlled by the leg and body joints actively.

For multi-legged robots, not only for straight line motion, the study of turning and even omni-directional motions is requisite for detecting, rescuing, and other tasks in an actual

application environment [48, 49, 50, 51]. However, extant literature uses multiple active joints to achieve motion in all directions.

In conclusion, existing researches mainly focused on actively controlling the movement of the robot's legs to realize the desired locomotion direction, but our design constitutes a unique and simple leg-motion method, with the geometric features of the passive body segment joint, to drive the rotation of the body segment. Through the design of the sequence of gait patterns, changes are allowed in the position of the legs to achieve omni-directional movement of the robot. A versatile motion can be achieved with the proposed simple design, and this design can be modularly replicated for simple expansion, which is of great significance for motion and gait planning of legged robot platforms. The omni-directional locomotion algorithm for our robotic platform should be investigated.

4.1 Valuation of Sequences of Passive-Spine Gaits

Based on the mobility analysis in Chapter 3, the value of the configuration transition is calculated as:

$$V_t = \sum_{i=1}^{k} v_{ti}, \tag{4.1}$$

where V_t is the total value of a sequence of configuration transitions; and v_{ti} is the value of the configuration transition of the ith step. In this section, forward locomotion is generated from the transitions with a positive value. This value is easily determined from the signs of the transitions at each step. For example, the signs of the gait sequence of transitions $1 \to 4 \to 6 \to 2 \to 3 \to 5 \to 1$ are "$+ + + + ++$," implying a total value of "+6." The sequence of this gait is shown in Fig. 4.1 step by step. The posture of the robot at each configuration is plotted according to simulation results obtained in the next section.

The signs of the configuration transitions and their total values are listed in Table 3.1.

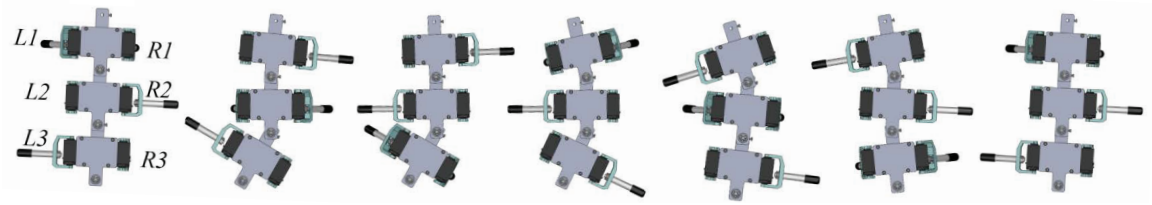

Figure 4.1. Gait sequences $1 \rightarrow 4 \rightarrow 6 \rightarrow 2 \rightarrow 3 \rightarrow 5 \rightarrow 1$. The robot's posture is plotted according to simulation results presented in Chapter 4.

4.2 Straight Line Motion

4.2.1 Straight-path Gaits

In the 22 configuration transitions obtained in Chapter 3, we use the sign "+" and "−" to represent the trend of forward and backward, respectively. Therefore, the configuration transitions completely represented as positive signs are selected as the configuration sequence that may generate a forward gait. Conversely, the configuration transitions that are fully represented as negative signs are selected as the configuration sequence that may generate a backward gait, thereby achieving straight-line motion of the robot. Six typical configuration transitions are selected to be simulated.

4.2.2 Simulation Results

The proposed passive-spine six-legged robot and configuration transitions are simulated in the Open Dynamics Engine (ODE). The gravitational acceleration is $9.8\,[\mathrm{m/s^2}]$. The interaction between the legs and the ground is modeled by symmetric friction, and the friction coefficient $\mu = 1$. The six-legged robot model in the simulation environment is shown in Fig. 4.2, and leg-ground contact is modeled as a collision of rigid bodies. The forward motion of the six-legged robot traversing a flat surface in the simulation environment is shown in Fig. 4.3. This result is generated by configuration transition 1, with locomotion possibility "+ + + + ++." Forward movement of the six-legged robot is observed.

The backward motion of the six-legged robot traversing a flat surface in the simulation environment is shown in Fig. 4.4. Backward movement of the six-legged robot is observed.

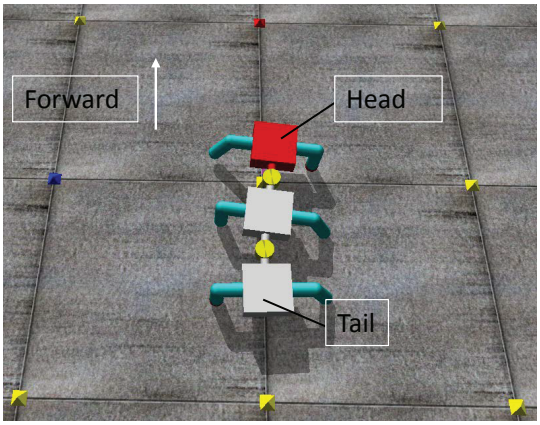

Figure 4.2. The six-legged robot in the simulation environment.

The movement of configuration transitions 3, 4, and 6 of the six-legged robot traversing a flat surface in the simulation environment is shown in Fig. 4.5.

In Fig. 4.6(a), the displacement in the direction of the x-axis of each body segment confirms that configuration transition 1 propels the robot forward. Gait transitions 9 and 16 also have positive locomotion potential, and similarly generate clear forward locomotion. In contrast, in Fig. 4.6(b), configuration transition 2, with negative locomotion possibility, generates backward locomotion. The results in Fig. 4.6(c) and Fig. 4.6(d) confirm that the motions generated by transitions "$+++---$" and "$---+++$" yield zero net movement, which drive the robot repeatedly to retrace its steps in a limited region.

The effects of these negative movements, such as repeating or retracing the trajectory, are enclosed by brown ellipses in the figures. The velocity of transition 9, containing a single retraction, is larger than that of transitions 1 or 2 in the simulation results. Thus, to investigate the effect of the performance of the locomotion, the configuration transition time and the duration of each configuration should be analyzed.

The transition time set in the simulations and experiments is listed in Fig. 4.7.

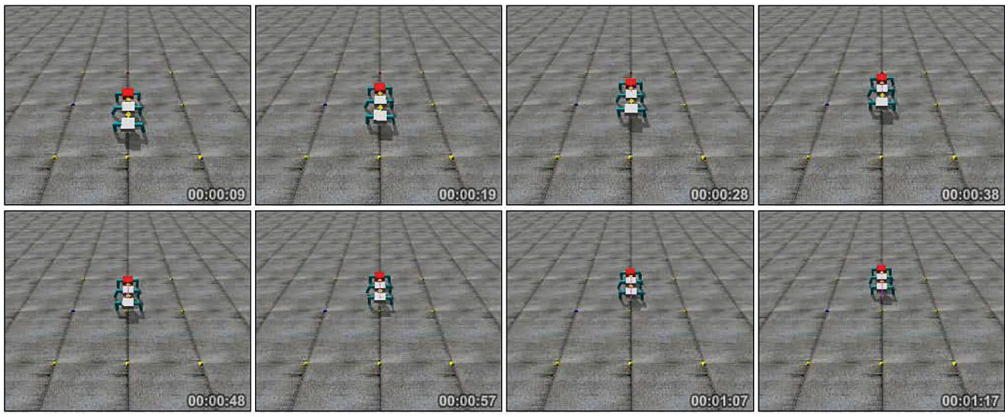

(a) Configuration transition 1

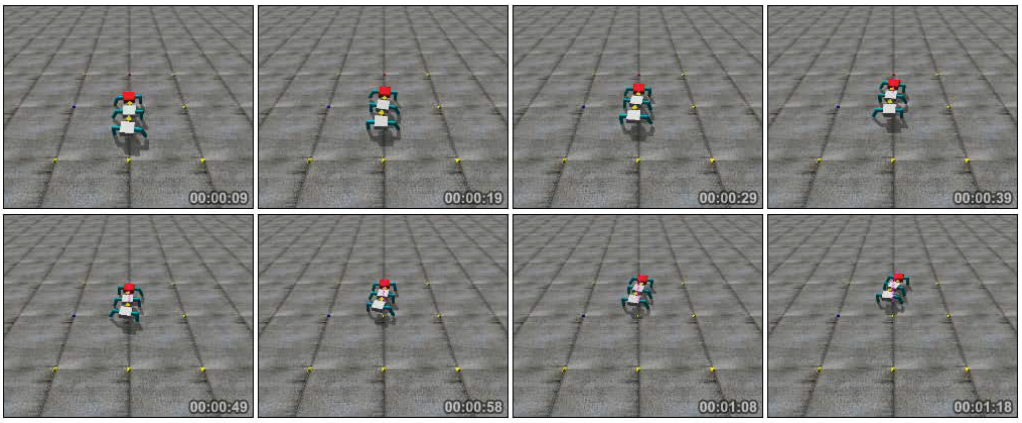

(b) Configuration transition 9

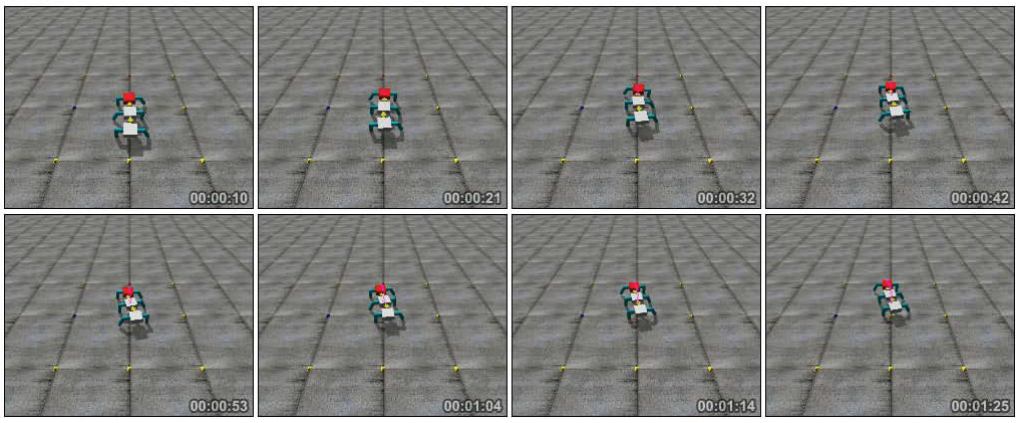

(c) Configuration transition 16

Figure 4.3. Forward motion generated by configuration transitions 1, 9, and 16.

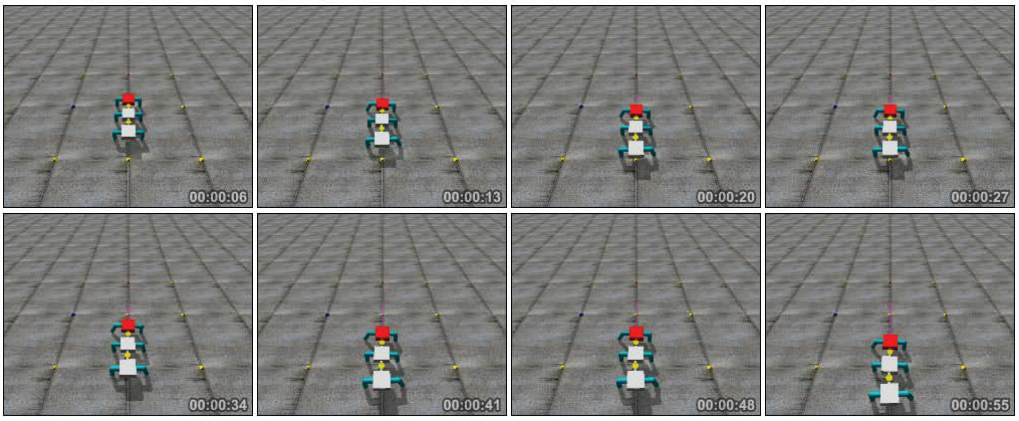

(a) Configuration transition 19

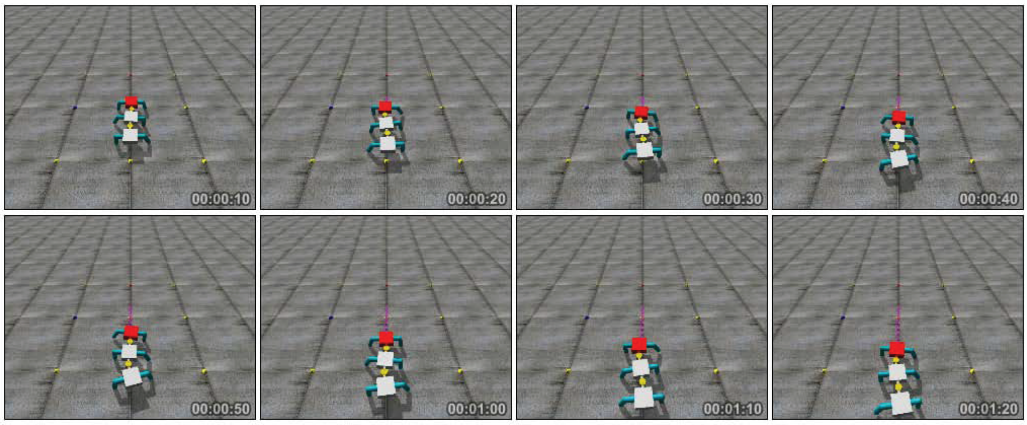

(b) Configuration transition 12

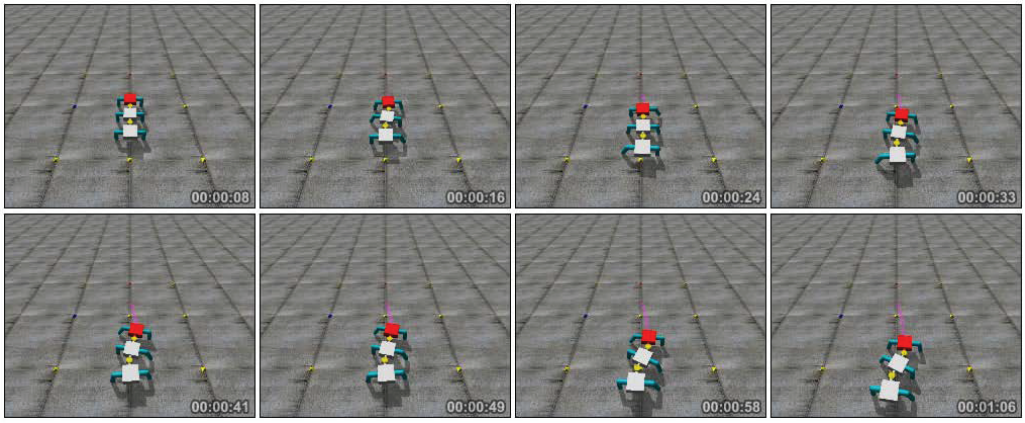

(c) Configuration transition 19

Figure 4.4. Backward motion generated by configuration transitions 2, 12, and 19.

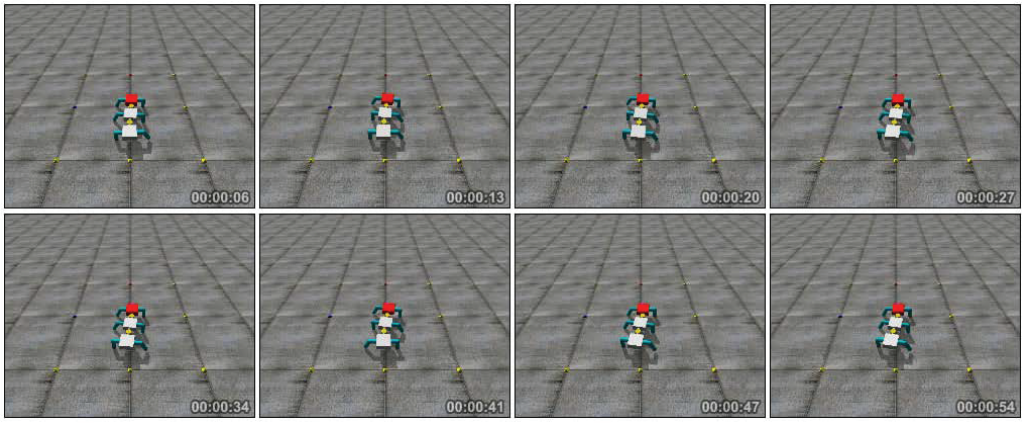

(a) Configuration transition 3

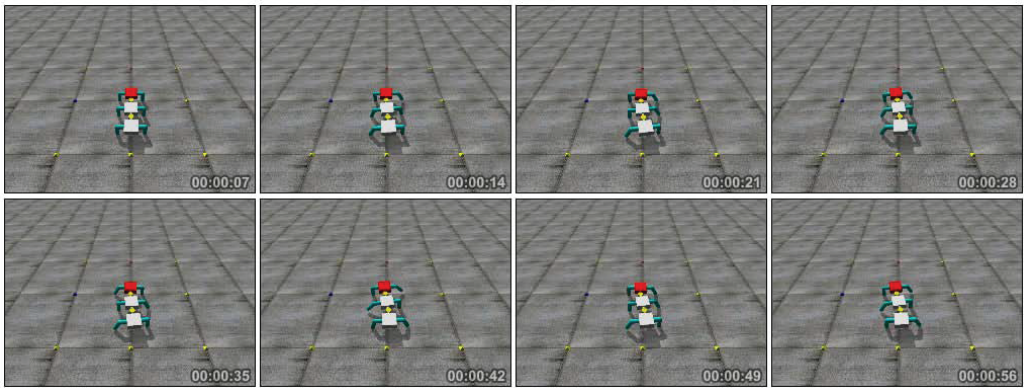

(b) Configuration transition 4

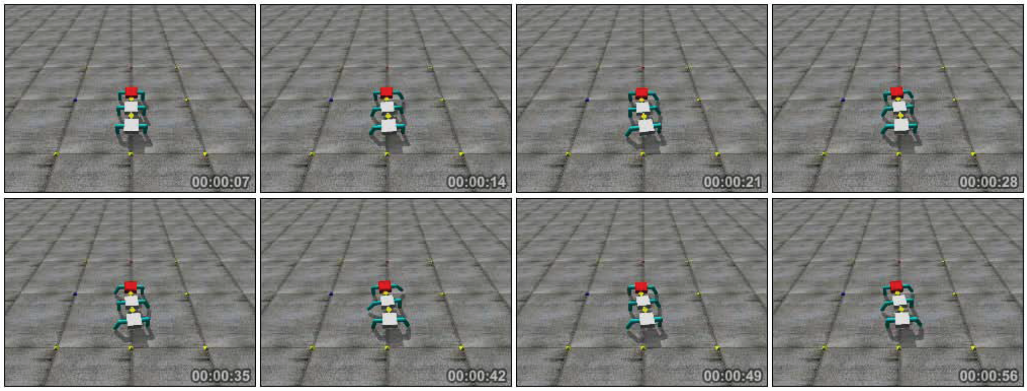

(c) Configuration transition 6

Figure 4.5. Backward motion generated by configuration transitions 3, 4, and 6.

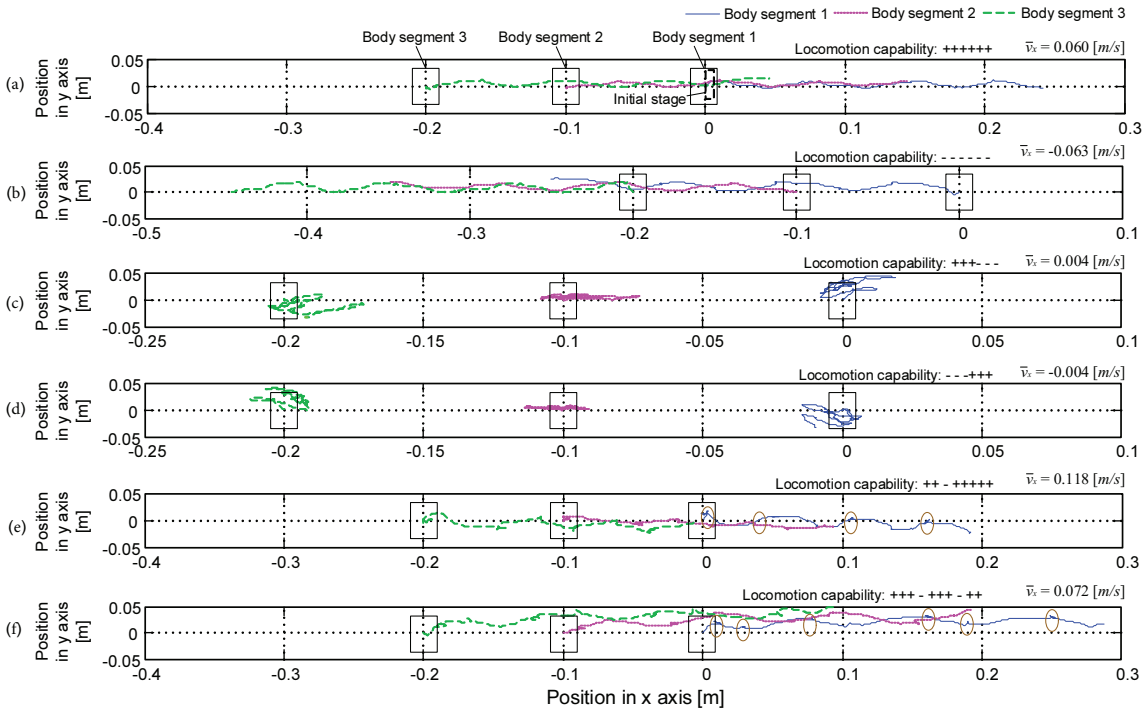

Figure 4.6. Simulation results of different configuration transitions. (a) Transition 1. (b) Transition 2. (c) Transition 3. (d) Transition 4. (e) Transition 9. (f) Transition 16. The black squares indicate body-segments-1, 2, and 3. The trajectories of the centers of mass (CoM) of body-segments-1, 2, and 3 are traced in blue, pink, and green color, respectively.

Transition time set of six-legged robot in different gait patterns

Locomotion direction	t_0	t_1	t_2	t_3	t_4	t_5	T [s]	Velocity [m/s]				Turning angle [rad]		Remark
								Simulation		Experiment		Simula-tion	Experi-ment	
								v_x	v_y	v_x	v_y			
Forward straight-line	0	T/6	2T/6	3T/6	4T/6	5T/6	2	0.1	0	0.05	0	-	-	Chapter 4.2.
Backward straight-line	0	T/6	2T/6	3T/6	4T/6	5T/6	2	-0.1	0	-0.05	0	-	-	Chapter 4.2.
Left turning to forward	0	3T/15	5T/15	7T/15	9T/15	12T/15	2	-	-	-	-	0.63	0.43	Chapter 4.3.
Right turning to forward	0	2T/15	5T/15	8T/15	11T/15	13T/15	2	-	-	-	-	0.63	0.40	Chapter 4.3.
Left turning to backward	0	2T/15	4T/15	6T/15	9T/15	12T/15	2	-	-	-	-	0.63	0.39	Chapter 4.3.
Left turning to forward	0	3T/15	6T/15	9T/15	11T/15	13T/15	2	-	-	-	-	0.63	0.39	Chapter 4.3.
Clockwise rotation	0	13T/45	15T/45	17T/45	30T/45	43T/45	2	-	-	-	-	-	-	Chapter 4.4.
Sideways motion	0	T/4	2T/4	3T/4	-	-	2	0	0.08	0	0.05	-	-	Chapter 4.5.

Figure 4.7. Transition time in different gait patterns.

4.3 Turning Motion

4.3.1 Turning Gaits

By using the geometric characteristics and the rotation principle obtained in Chapter 3, we generate the robot turning motion by changing the duration of the supporting phase or swinging phase in each configuration transition.

For example, in transitions $1 \rightarrow 4 \rightarrow 6 \rightarrow 2 \rightarrow 3 \rightarrow 5 \rightarrow 1$, the duration of the clockwise transitions 1 to 4, 3 to 5, and 5 to 1 may be extended as 1.2 times the original supporting phase before completing the transition. Here, when the duration of the supporting phase in the clockwise transition in Fig. 3.15 is extended, it becomes a new transition [called configuration transition A in Fig. 4.8(a)], and the supporting leg on the ground has more time to rotate the body segments of the robot, so the robot turns clockwise. Likewise, when the duration of the swinging phase of the clockwise transition in Fig. 4.8(b) is shortened, the same function contributes to the clockwise rotation of the robot and increases the rotation angle.

In addition, if the duration of the supporting phase in the clockwise transition is shortened and becomes a new transition [called configuration transition B in Fig. 4.8(b)], the supporting leg on the ground will have more time to rotate the body segments, and then the robot will turn counterclockwise to the left. For transitions $1 \rightarrow 5 \rightarrow 3 \rightarrow 2 \rightarrow 6 \rightarrow 4 \rightarrow 1$ in Fig. 4.9, the rotation direction results can be analyzed in the same way. Fig. 4.10(a) and (b) show that the left and right backward motion is generated by configuration transitions C and D, respectively. Chapter 5 demonstrates these four types of transitions experimentally.

4.3.2 Simulation Results

In order to verify that the geometric model is valid, the configuration transition from RLR to LLR is tested in the simulation environment firstly. Under the same condition of

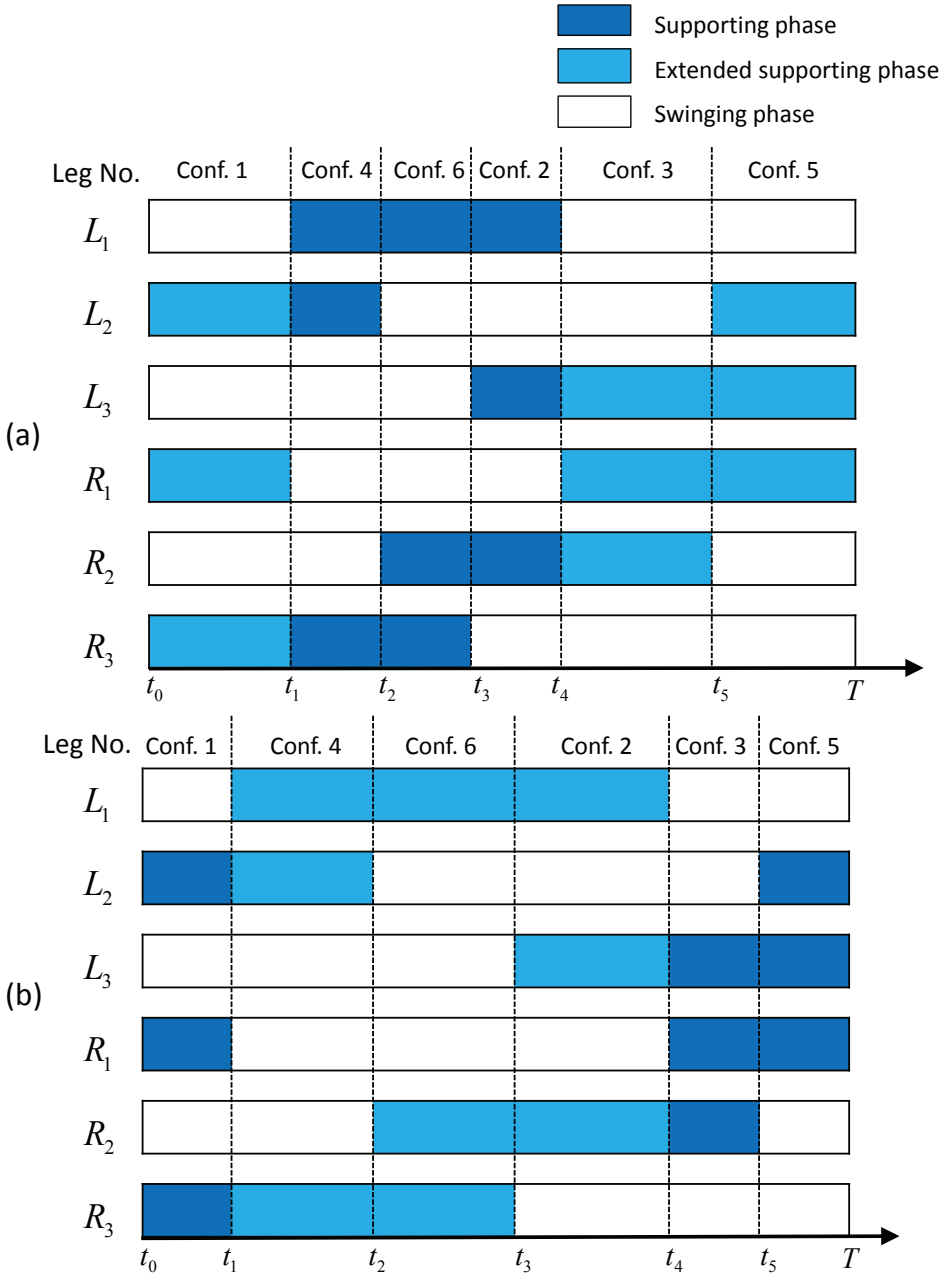

Figure 4.8. The supporting phase and the swinging phase for transitions $1 \rightarrow 4 \rightarrow 6 \rightarrow 2 \rightarrow 3 \rightarrow 5$. (a) Configuration transition A. Extending the duration of the supporting phases for situations that could generate a clockwise rotation. (b) Configuration transition B. Shortening the duration of the supporting phases of situations that could generate a counterclockwise rotation.

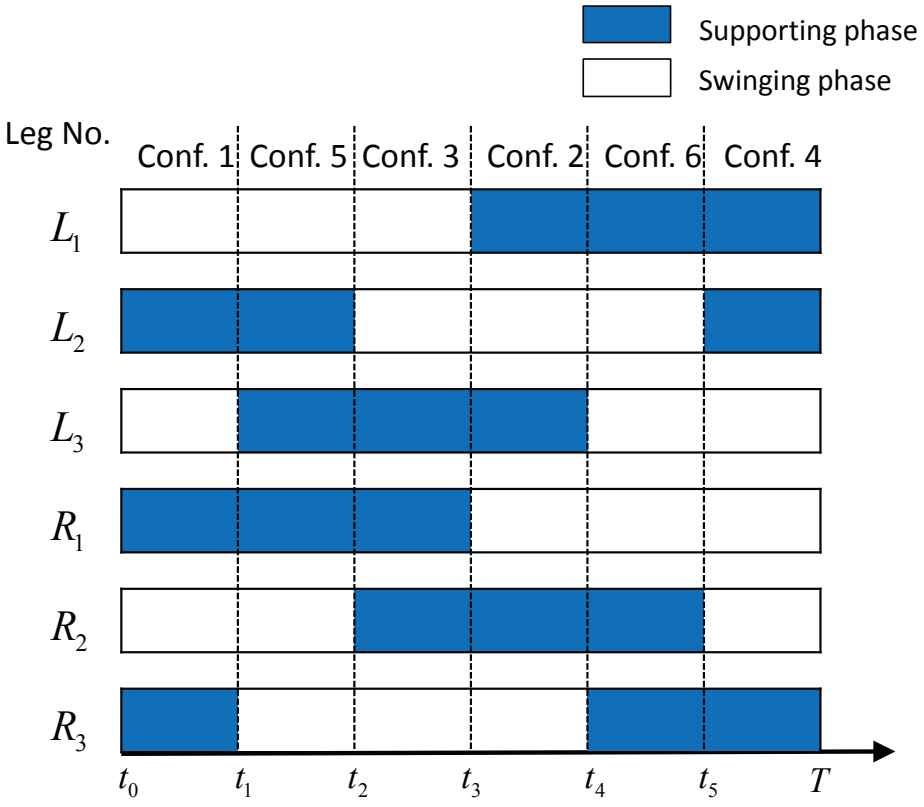

Figure 4.9. The supporting and swinging phases for transitions $1 \to 5 \to 3 \to 2 \to 6 \to 4$ that generate a backward straight-line motion.

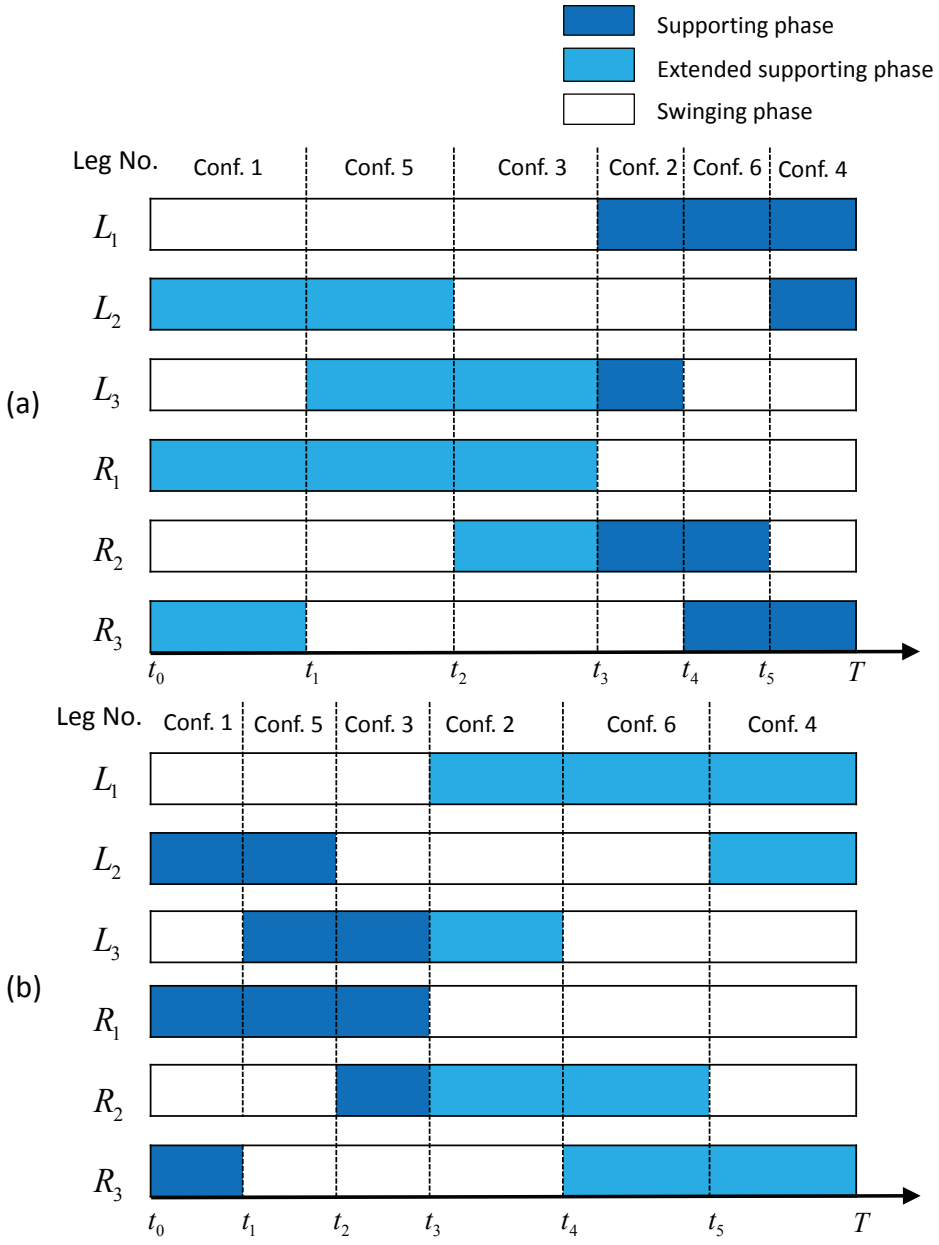

Figure 4.10. The supporting and swinging phases for transitions $1 \rightarrow 5 \rightarrow 3 \rightarrow 2 \rightarrow 6 \rightarrow 4$. (a)Configuration transition C. Extending the duration of the supporting phases for situations that could generate a clockwise rotation. (b) Configuration transition D. Shortening the duration of the supporting phases for situations that could generate a counterclockwise rotation.

joint angle with theoretical model analysis, i.e., deflection angle θ_{R1} has been changed as the function $\theta_{R1} = 0.3 \sin \pi t$.

In the simulation, the comparison of the simulation value and the theoretical value that is obtained from the geometric relationship between the supporting legs and the body segment joints are given [Fig. 4.11].

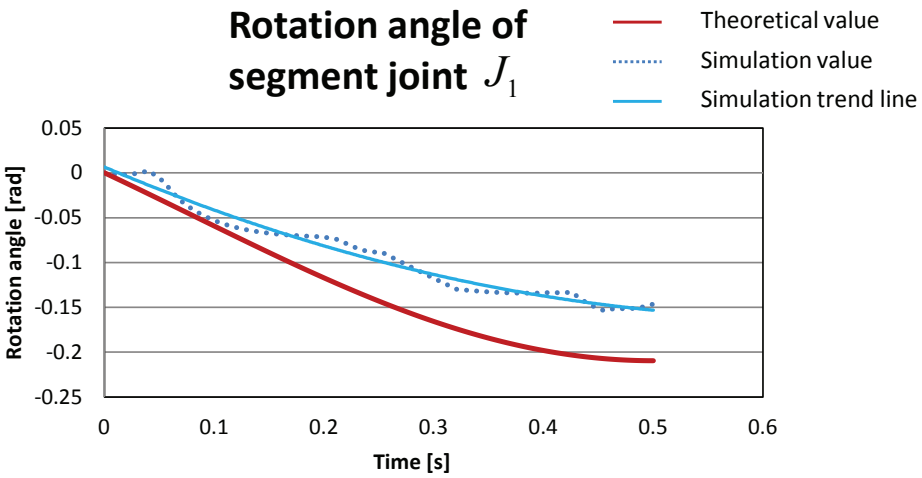

Figure 4.11. Comparison of theoretical and simulation value of rotation angle ϕ_{R1} during the transition RL to LL when deflection angle θ changes within 0.5 [s].

The red solid line represents the theoretical value of the body segment joint rotation angle obtained from the geometric model, the blue dotted line represents the corresponding simulation value in the ODE simulation environment, and the blue solid line represents the trend line of the simulation data. As the trend of the direction of the theoretical and simulation values is consistent in Fig. 4.11, we can conclude that the model can play a guiding role in determining the rotation direction of the supporting legs, as well as the turning gaits of the whole robot.

For the errors between the theoretical value and the simulation value, most of the reason for the errors is that the friction between the foot and the ground brings a loss of energy which cannot be reduced. In addition, passive segment joints also consume part of the energy during the process of transmission. Here, the consistency of the trend means that

the correctness of the rotation direction of the supporting leg based on the geometric model and the turning gait principle of the robot will be preliminarily verified.

The turning motion of the six-legged robot traversing a flat surface in the simulation environment is shown in Fig. 4.12 and Fig. 4.13.

In Fig. 4.14, the brown square indicates the CoM of the first body segment. The simulation results generate trajectories of these four configuration transitions which are consistent with the theoretical analysis.

4.4 Rotating Motion

4.4.1 Rotating Gait

For the transition which generates the turning motion, the rotating motion will be obtained by conducting Equation (3.30), and increasing the speed of each configuration transition can shorten the transition duration regularly. For example, in Fig. 4.15, for configuration transition A, if the duration of counterclockwise transitions 2 to 3, 4 to 6, and 6 to 2 are shortened and tend to zero, the contribution to counterclockwise of these transitions will equal zero approximately, and the robot will be expected to make a clockwise rotation. In contrast, if the duration of clockwise transitions is shortened, and 1 to 4, 3 to 5, and 5 to 1 tend to zero, the robot will be expected to perform a counterclockwise rotation.

4.4.2 Simulation Results

The rotating motion of the six-legged robot in the simulation environment is shown in Fig. 4.16. In Fig. 4.17, the red and grey squares indicate three body segments, the red square indicates the head of the robot, the yellow circles indicate the passive body segment joints, the blue curve is the trajectory of the rotating motion, and the green dotted arrow represents the direction of rotation. The simulation result shows that the robot can perform the rotating motion about the last body segment. Although there are a few places that are

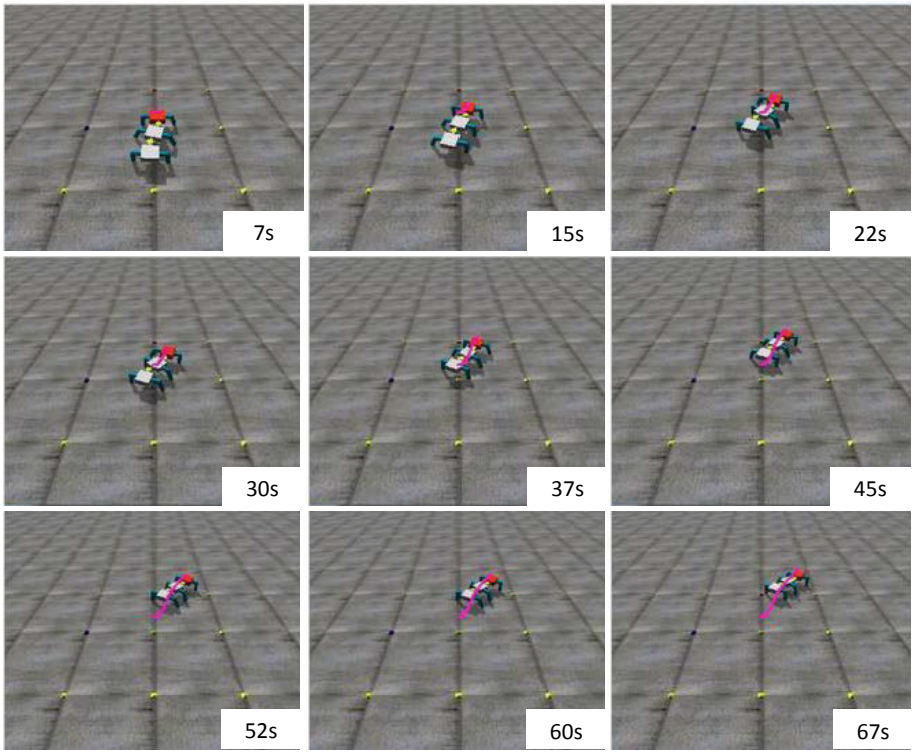

(a) Configuration transition A.

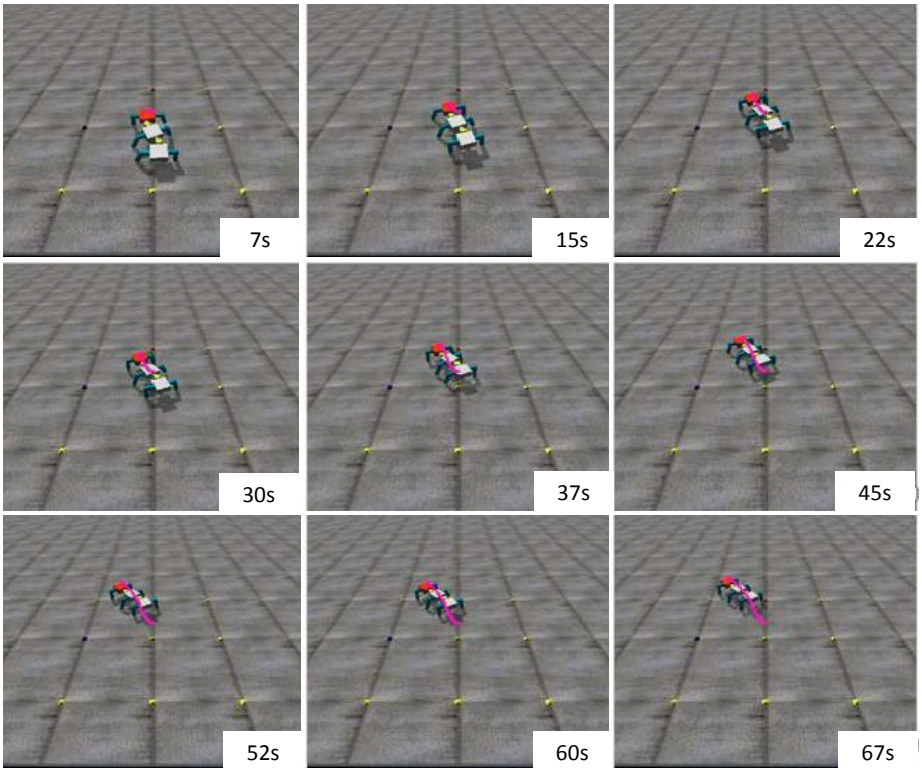

(b) Configuration transition B.

Figure 4.12. Turning motion generated by configuration transitions A and B.

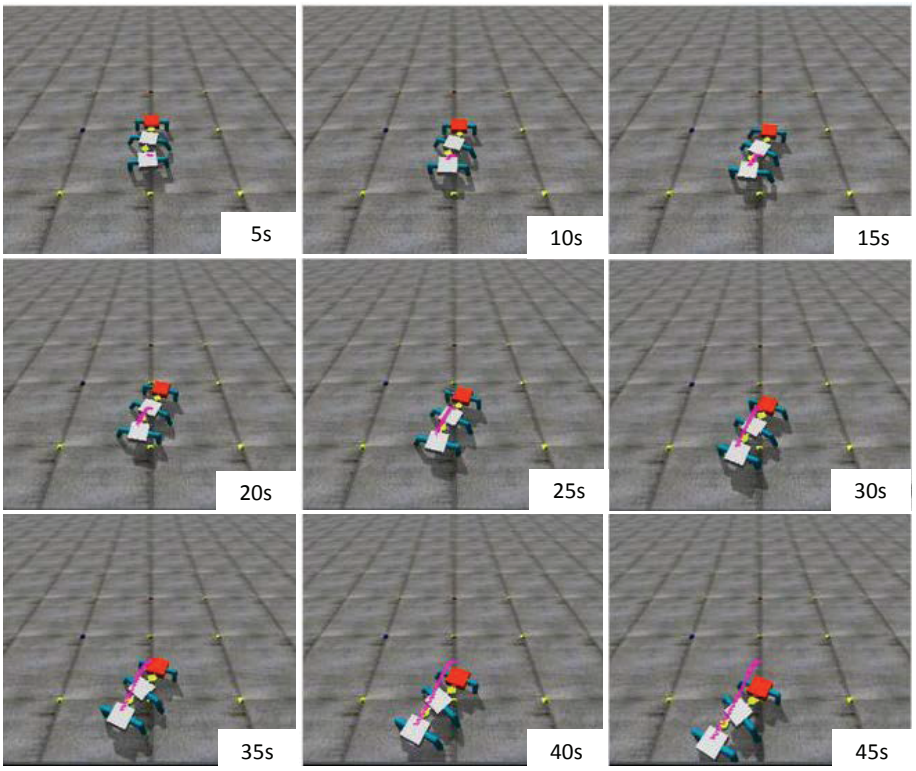

(a) Configuration transition C.

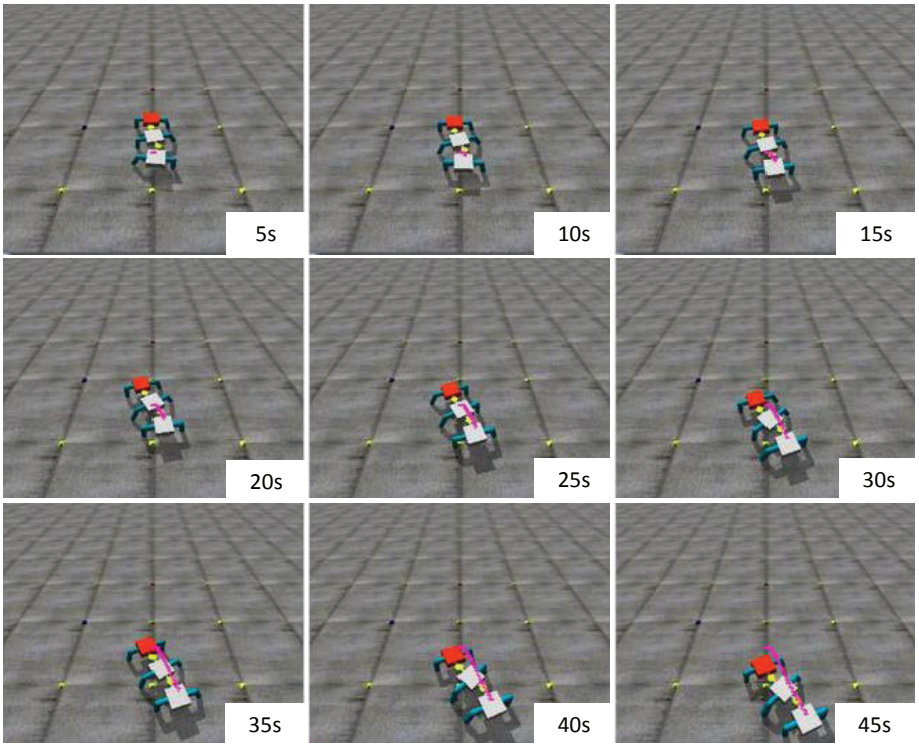

(b) Configuration transition D.

Figure 4.13. Turning motion generated by configuration transitions C and D.

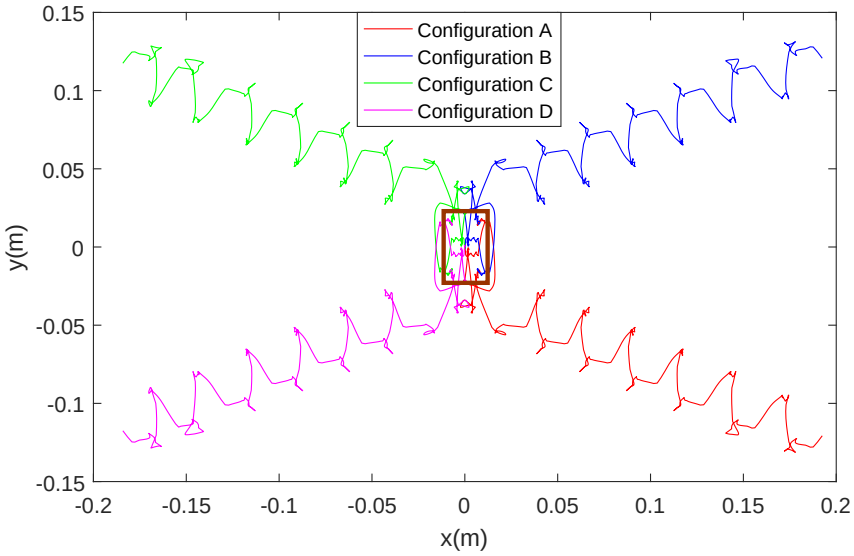

Figure 4.14. Different motion directions of transitions A, B, C, and D in the simulation environment.

not smooth, the direction of locomotion is consistent with the rotation principle and the general rotating method in Chapter 3.

4.5 Sideways Motion

4.5.1 Sideways Gait Analysis

The above analysis allows the robot to realize forward, backward, turning, and rotating motions. Based on the previous mobility analysis [52], configurations $7-10$ which have a suspended intermediate body segment can rotate about the supporting legs. The suspended body segment with two passive segment joints allows the body segments the rotational DOF around the z-axis. We can use this feature of the suspended body to cooperate with the lateral abduction of the leg to perform sideways locomotion. We take the configuration transitions $10 \rightarrow 9 \rightarrow 8 \rightarrow 7$ to generate sideways motion. The sideways motion of the six-legged robot in the simulation environment is shown in Fig. 4.18.

The transition sequence and the order of the legs' lifting of the body segments are shown in Fig. 4.19.

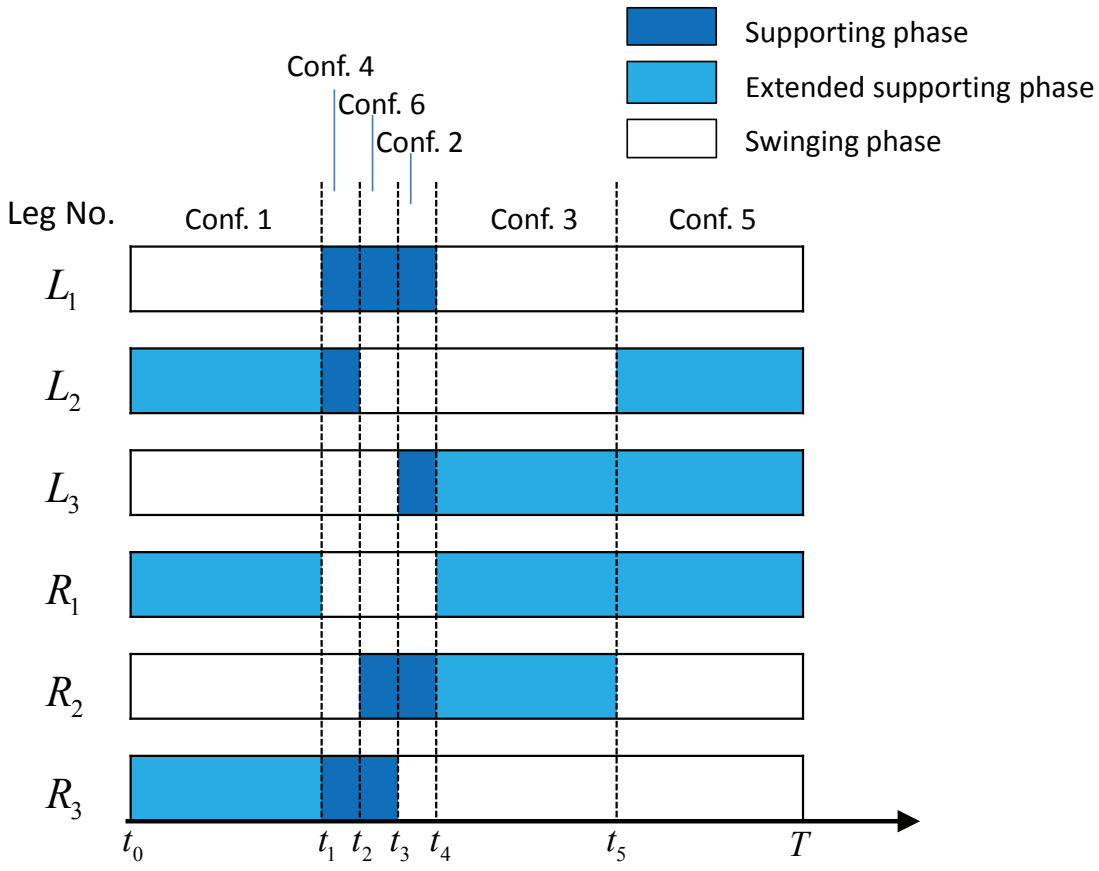

Figure 4.15. The supporting and swinging phases for transitions $1 \rightarrow 4 \rightarrow 6 \rightarrow 2 \rightarrow 3 \rightarrow 5$. Shortening the duration of the transitions which have a high contribution to counterclockwise to generate a clockwise rotation.

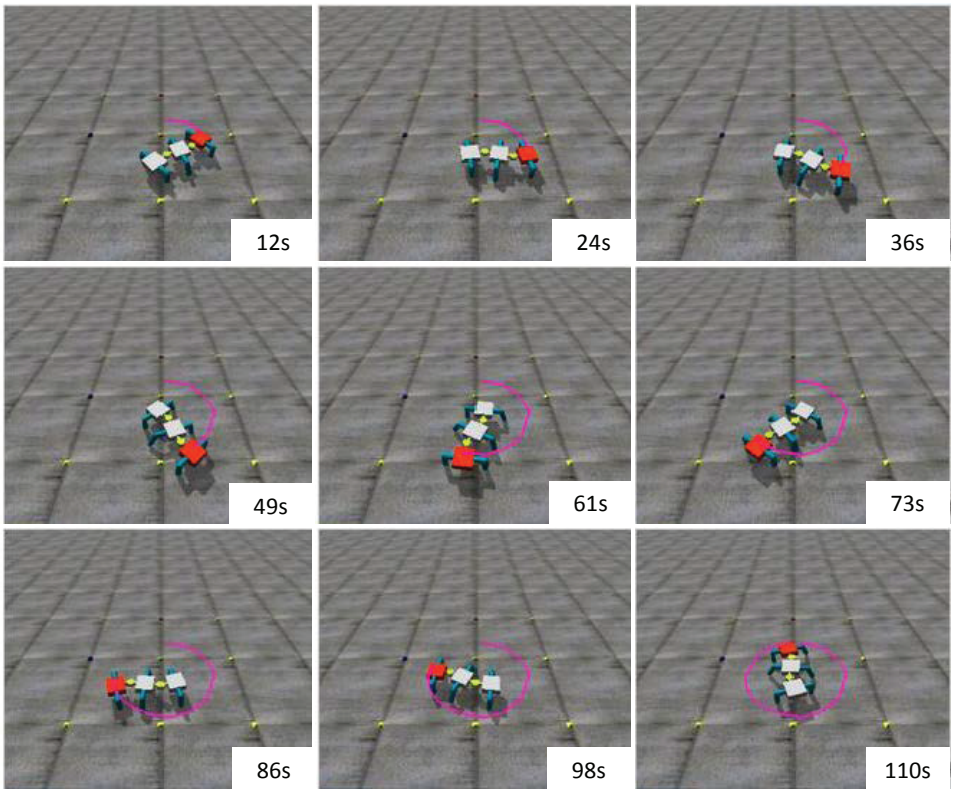

Figure 4.16. Rotating motion of the six-legged robot in the simulation environment.

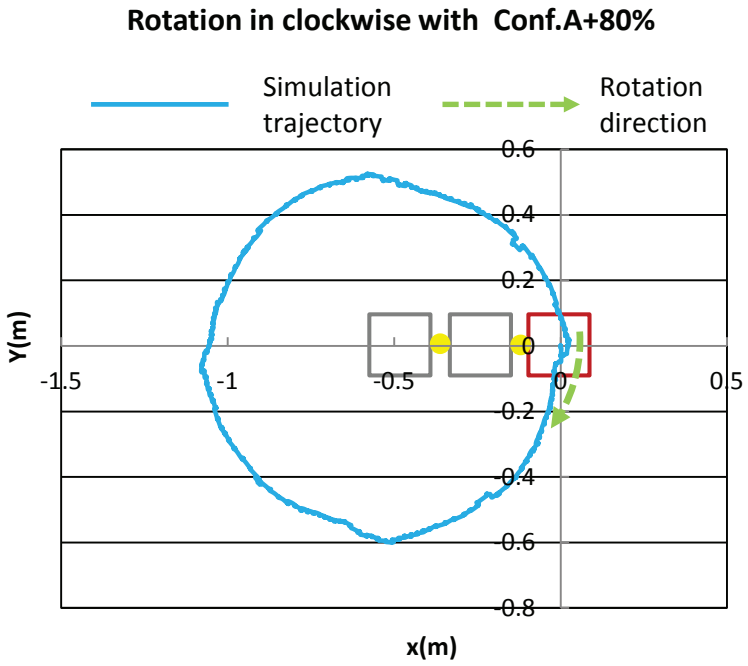

Figure 4.17. Trajectory of rotating motion in the simulation environment.

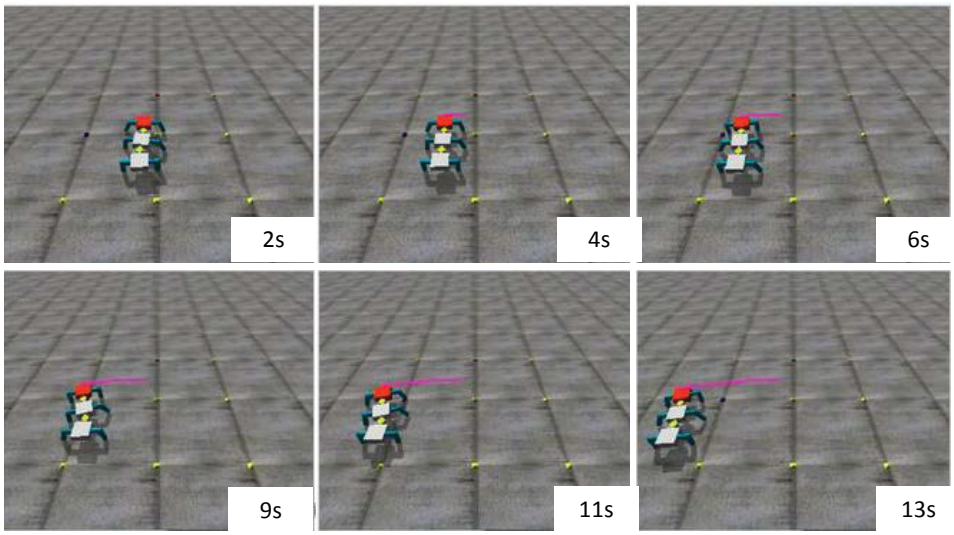

Figure 4.18. Sideways motion of the six-legged robot in the simulation environment.

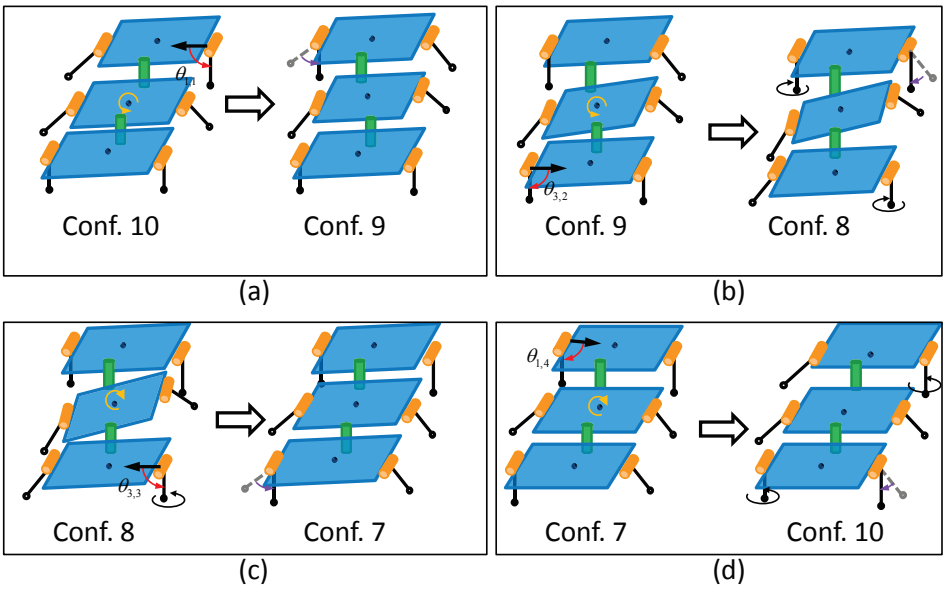

Figure 4.19. Four specific configurations showing the locomotion direction of the body segments for transitions $10 \rightarrow 9 \rightarrow 8 \rightarrow 7$ on the horizontal xy plane. The orange curve arrow indicates the rotation trend of the suspended body segment during the configuration transitions. (a) The step of configuration transition $10 \rightarrow 9$. (b) The step of configuration transition $9 \rightarrow 8$. (c) The step of configuration transition $8 \rightarrow 7$. (d) The step of configuration transition $7 \rightarrow 10$.

Next, the geometric model is utilized to analyze the specific configuration transitions of the sideways gait. In Fig. 4.20, the geometric relationship of the body segments can be expressed. The points $\mathbf{P_{j,i}^{supp}} = [x_{j,i}^{supp}, y_{j,i}^{supp}]^T$, and $\mathbf{P_{j,i}^{b}} = [x_{j,i}^{b}, y_{j,i}^{b}]^T$ are the positions of the supporting leg and CoM, respectively, of body segment j at the ith step; $\phi_{j,i}$ represents the rotation angle of the body segment about the supporting leg; and $\theta_{j,i}$ represents the deflection angle of the jth supporting leg at the ith step.

The CoM of the jth body segment in the direction of the y-axis is given by

$$y_{j,i}^{b} = y_{j,i-1}^{supp} + f_i(l_2 - l_1 \cos\theta_{j,i}) \sin\phi_{j,i} \tag{4.2}$$

where f_i is a constant equal to $+1$ and -1 when the right and left legs contact the ground, respectively. In order to judge the sideways motion of the whole robot, we need to examine the displacement of each body segment at each step. Since the body-segment-2 is the suspended body segment which will follow the other two segments during the locomotion, here we only take the displacement of the body-segments-1 and 3 of the robot as the object of study to analyze the sideways gait.

For the body-segment-1, on the first step $10 \rightarrow 9$, when leg R_1 is about to abduct, the friction force between the foot and ground pushes the body segment to move in the positive direction of the y-axis, and the expression can be given as:

$$y_{1,1}^{b} = y_{1,0}^{supp} + (l_2 - l_1 \cos\theta_{1,1}) \sin\phi_{1,1} \tag{4.3}$$

where $y_{1,0}^{supp} = -l_2$, $0 < \phi_{1,1} < \pi$, and $\pi/2 < \theta_{1,1} < \pi$, it means $\sin\phi_{1,1} > 0$, and $\cos\theta_{1,1} < 0$, therefore, $y_{1,1}^{b} > 0$.

Then, in the second step,

$$y_{1,2}^{b} = y_{1,1}^{supp} - (l_2 - l_1 \cos\theta_{1,2}) \sin\phi_{1,2} \tag{4.4}$$

where $\phi_{1,2} < \phi_{1,1}$, and $3\pi/2 < \phi_{1,1}, \phi_{1,2} < 2\pi$, it can be inferred that $\sin\phi_{1,2} > \sin\phi_{1,1}$, and

$$y_{1,1}^{supp} = y_{1,1}^{b} + l_2 \tag{4.5}$$

therefore, $y^b_{1,2} > y^b_{1,1}$.

This means that body-segment-1 moves in the positive direction of the y-axis in the first two steps. For the third and fourth step, because the two legs of body-segment-1 are always supporting on the ground, the displacement can be obtained as $y^b_{1,3} = y^b_{1,4} = y^b_{1,2} > 0$.

From the above analysis, it can be determined that the body-segment-1 changes displacement through four steps of motion, and the body segment moves in the positive direction of the y-axis. For the body-segment-3, the analysis method is similar to that of the first body segment. There is no displacement in the first and second step due to the supporting phase of the two legs of the segment. The third and fourth steps are similar to the first two steps of body segment 1. The body-segment-3 can move in the positive direction of the y-axis. Consequently, the locomotion direction of the sideways gait is obtained. The robot can move to the left by using the sideways gait with configuration transitions $10 \rightarrow 9 \rightarrow 8 \rightarrow 7$.

4.5.2 Sideways Gait

As shown in Fig. 4.21, the two legs of the intermediate body segment are always suspended, and the legs of the first and third body segments are sequentially swung in order to generate a sideways motion.

The generation of sideways gait proves the existence of passive joints, which can not only compensate for the limitation of fewer DOF on a single leg in the mobility of the whole robot, but can also be cooperated by the legs' active joints and the passive body joints to allow the same motion ability of the traditional legged robot.

4.5.3 Simulation Results

The six-legged robot adopts configuration transitions $10 \rightarrow 9 \rightarrow 8 \rightarrow 7$ to generate the sideways gait. In Fig. 4.22, the purple line is the trajectory of the sideways motion, and

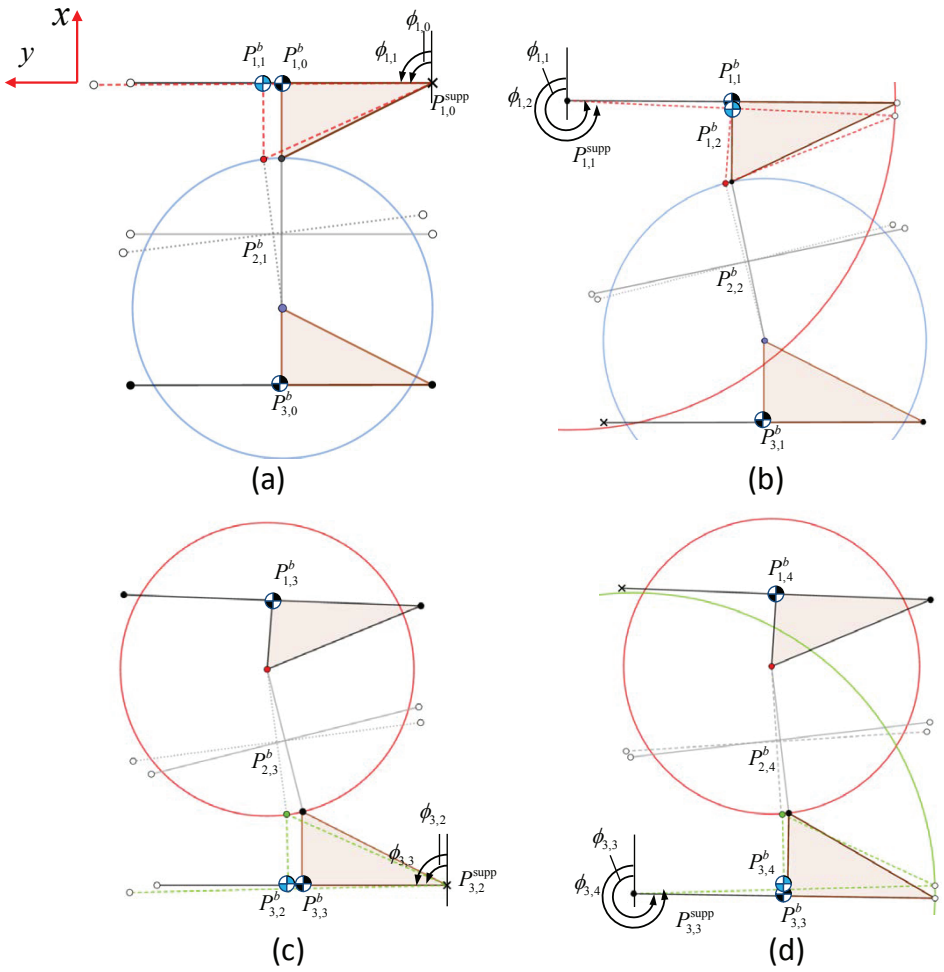

Figure 4.20. The posture changing with configuration transitions $10 \rightarrow 9 \rightarrow 8 \rightarrow 7$ on the horizontal xy plane. (a) The step of configuration transition $10 \rightarrow 9$. (b) The step of configuration transition $9 \rightarrow 8$. (c) The step of configuration transition $8 \rightarrow 7$. (d) The step of configuration transition $7 \rightarrow 10$.

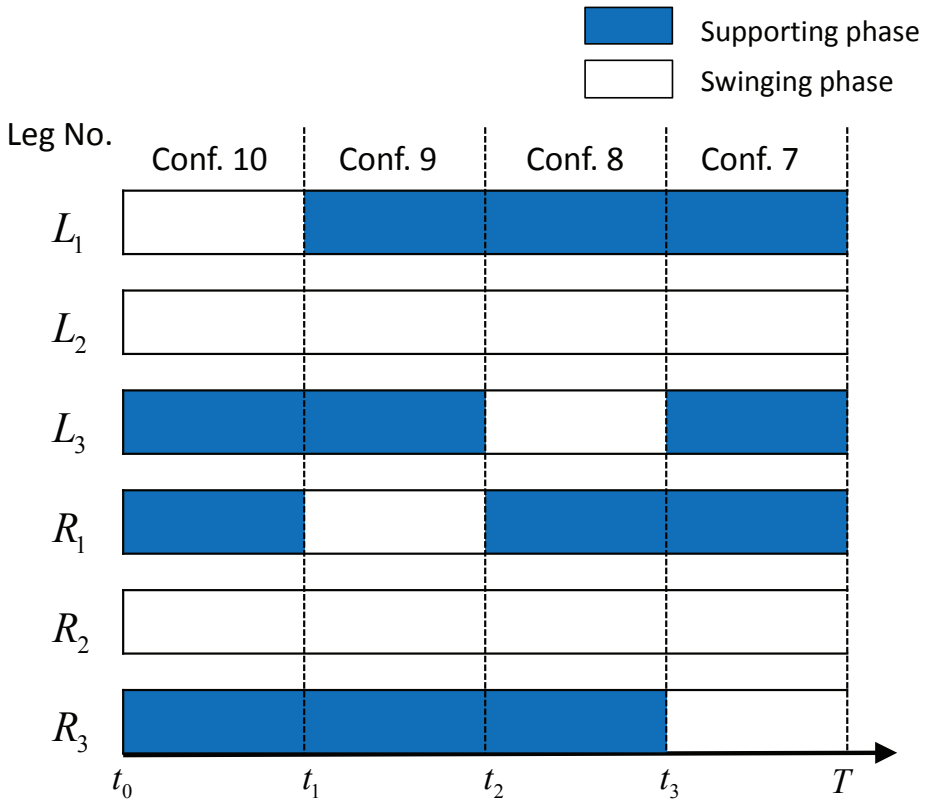

Figure 4.21. The supporting and swinging phases for transitions $10 \rightarrow 9 \rightarrow 8 \rightarrow 7$ that generate a sideways motion to the left.

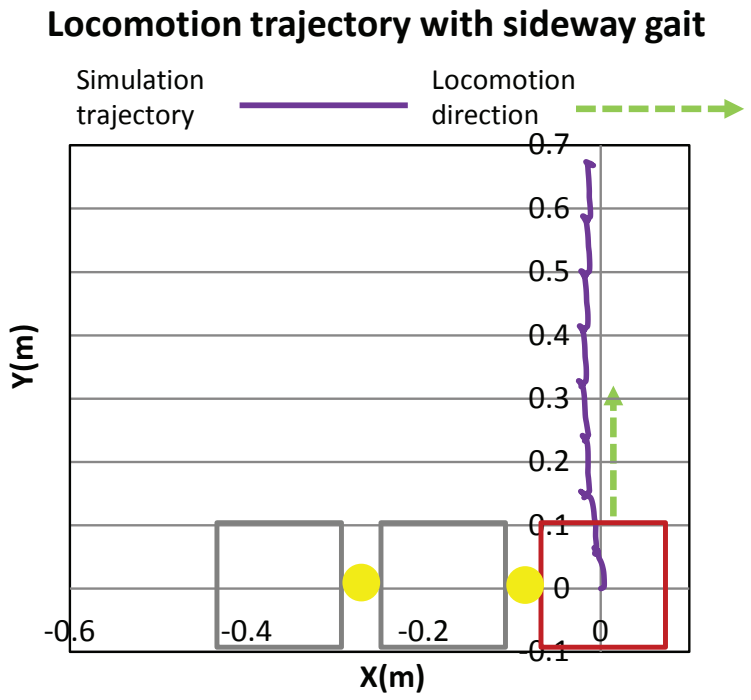

Figure 4.22. Trajectory of sideways motion in the simulation environment.

the green dotted arrow represents the direction of locomotion. In the simulation, the speed is 0.08 [m/s] in the direction of the y-axis.

4.6 Summary

In this chapter, we have analyzed omni-directional gait of the proposed six-legged robot. The sequence and the configuration transition time are given firstly to plan the straight-line motion, turning motion, rotating motion, and sideways motion. Omni-directional motion has been simulated in the simulation environment. Finally, the simulation results and the analysis results are consistent. The motion methodology in the six-legged robot has been verified in the simulation. In the next chapter, the methodology has been extended to the $2n$-legged robot to realize undulatory locomotion of the multi-legged robot.

Chapter 5

Undulatory Gait Planning Method of $2n$-Legged Robot

The robot proposed in this thesis is based on the movement mechanism of centipedes in nature. It consists of multiple body segments and moves in a certain order to achieve continuous motion of the whole robot.

In this chapter, we introduce the concept of Finite State Machine (FSM) theory into the gait planning method to realize movement of the $2n$-legged robot firstly. We then model the system of gait configuration transitions to generate undulatory gait patterns for multi-legged robots. The purposes of this chapter are: 1) to model the gait issue of this kind of multi-legged robot; 2) to design the gait pattern for the multi-legged robot; 3) to confirm the mobility of the robot by computer simulations and experiments; and 4) to lay the foundation for gait planning and intelligent operation control of similar robots.

5.1 Finite State Machine Theory in Gait Planning

Gait planning determines leg states, such as supporting or swinging phases. Different configuration states are composed of various of leg states on each segment. Brooks introduced the FSM theory into the robotics system [53, 54]. Some researchers designed the

FSM to manage transitions among different gait patterns [55, 56]. In this chapter, the gait patterns are planned by an FSM. FSM is a mathematical model which can change from one state to another state in response to some external inputs.

The conditions for applying the FSM are as follows:

1. The modeled system has a limited number of states;
2. The behavior in a certain state is the only corresponding result;
3. The system always stays in a certain state at any time;
4. The conditions of system state transitions are limited;
5. Transition is the system's reaction to the event.

Therefore, it is suitable for gait planning of the multi-legged robot. According to the previous analysis results [52], since this design requires at least three body segments to meet the mobility requirements, a six-legged robot can be viewed as a Unit State Module (USM) to analyze the states of the $2n$-legged robot. In other words, for any $2n$-legged robot, the distribution of the legs of any adjacent three body segments should satisfy the following condition:

$$C(i-1, i, i+1) \in A, \tag{5.1}$$

where C is the distribution of legs of any three adjacent body segments; and A represents candidate movable configurations (configurations 1-6 in Fig. 3.2) of the USM which are obtained in Chapter 3.

Based on the concepts about FSM above and the characteristics of passive-spine $2n$-legged robots, some definitions are made as follows:

Definition 1: A $2n$-legged robot consisting of n body segments whose motion gait is a quintuple set that contains five variables, which is defined as: $M = (\Sigma, S, s_0, \delta, F)$, where Σ represents a set of the finite gait states of the robot; S represents an input during the motion process; $s_0 \in S$ indicates the initial state of the robot; $F \in S$ represents the set of

final state; δ is the state transition function, $\delta : S \times \Sigma \to S$, for $\forall(s, a) \in S \times \Sigma$, and $\delta(s, a)$ indicates that the robot state is s when the input value is a.

Definition 2: The set of two different states of the n individual body segments of the robot is an n-dimensional set of binary arrays. The set can be expressed as $a = (x_1, x_2, x_3, \ldots, x_n)$, which can be given as:

$$x_i = \begin{cases} 0 & \text{when the } ith \text{ left leg is the supporting leg;} \\ 1 & \text{when the } ith \text{ right leg is the supporting leg.} \end{cases} \tag{5.2}$$

Definition 3: The undulatory locomotion sequence of the USM (Fig. 5.1) can be viewed as the laws of the state transitions of undulatory locomotion, which are referred to the previous analysis results of the six-legged robot [14]. The orange font in Fig. 5.1 represents the state of the USM. These states are used as key intervals in the state of the $2n$-legged robot to obtain the state transitions. The duration of each state and the distribution of the supporting legs are shown in Fig. 5.1. Time t represents the moment of transition between different states, which can be expressed as:

$$t_i = \frac{iT}{2n}, \tag{5.3}$$

where t_i represents the transition time between the $i-1$th and the ith states; T represents the cycle time; and for the six-legged robot, $n = 3$. In the next section, we will use this state table of the USM and the geometrical relationship of the configurations to obtain the states of the $2n$-legged robot.

5.2 Undulatory Gaits of 2n-Legged Robot Based on FSM

5.2.1 Undulatory Gaits

According to the geometric constraints of the configuration, for the $2n$-legged robot, the following situations should be noted for determining the states of the robot:

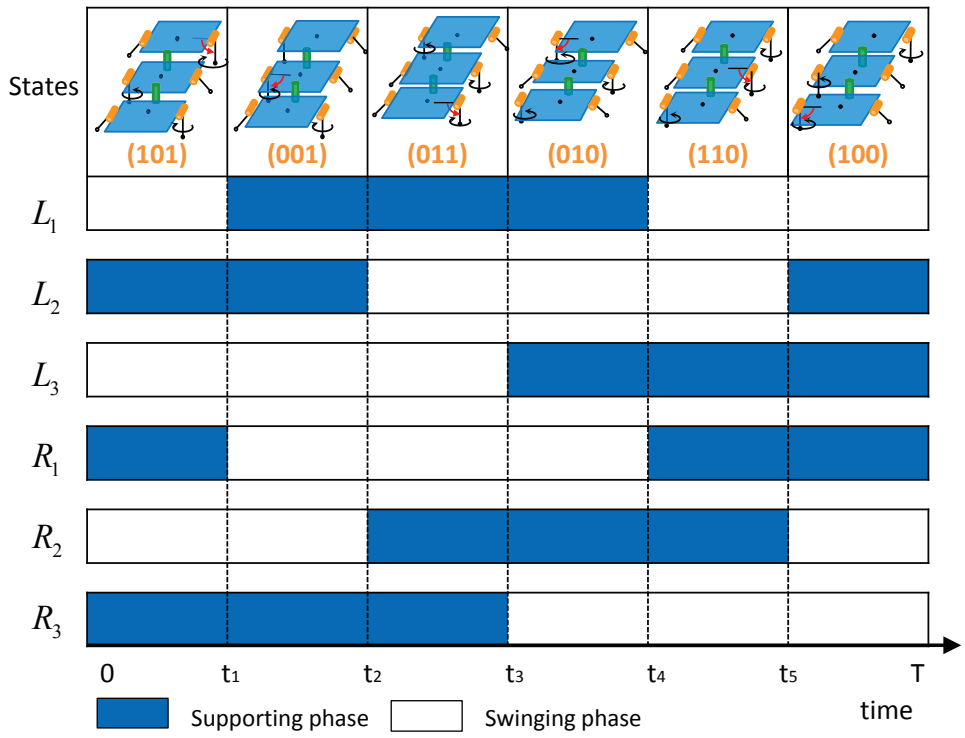

Figure 5.1. Transition state table of a USM. The sequence represents an undulatory gait that can generate forward locomotion, and the orange font represents the state of the USM. The empty rectangle represents the swinging period of the leg, and the blue rectangle represents the supporting period of the leg. $t_1 - t_5$ represents the transition time between adjacent states.

1. Due to the weight distribution of the robot, the supporting legs of the 1^{st}, the 2^{nd}, ..., the $(n-1)$th, the nth body segments can not be distributed on the same side; otherwise, the robot cannot stand. This means that the states $(1,1,1,\ldots,1,1)$ and $(0,0,0,\ldots,0,0)$ will not exist.

2. For the same reason, the states that contains the interval, such as $(1,0,0,0,\ldots)$, $(0,1,1,1,\ldots)$, $(\ldots,1,1,1,0)$, and $(\ldots,0,0,0,1,)$, due to the weight distribution will bring an unstable state to the robot. These states will not be considered.

3. According to the geometric relationship between the body segments and the supporting legs of the multi-legged robot, it is required that the same-side supporting legs of the adjacent body segments cannot continuously appear; otherwise, the geometric constraints will limit the movement of the robot. In other words, if the supporting legs of $(i-1)$th, the ith body segments are on the same side, the supporting legs of $(i+1)$th, $(i+2)$th body segments cannot simultaneously be on the opposite side, which means that the interval field of the states $(\ldots,1,1,0,0,\ldots)$ and $(\ldots,0,0,1,1,\ldots)$ will not exist.

Then, we can obtain n current configurations for 2n-legged robots in Fig. 5.2. In this state transition table, the combination of current state and input shows the next state. The orange font represents the key intervals in the state of the $2n$-legged robot which is obtained from the six-legged robot. Here, the input is the time of state transition, which can be confirmed by Equation (5.3). We can then achieve the state transition diagram for generating undulatory motion in any state of $2n$-legged robot in Fig. 5.4. In the $2n$-legged robot, when the transition of the first USM is finished, the key intervals transfer into the next USM to perform state transitions. For example, the state transition sequence of a 10-legged robot is shown in Fig. 5.3, and the third state (01101) is the switching point of the two USMs.

When the $2n$-legged robots transit in a certain order, the body segment changes its rotation direction as the supporting legs change, and then the forward locomotion is generated by the undulatory gaits.

State transition table of 2n-legged robot for forward locomotion

Current state / Input	State 1 (1010…01)	State 2 (0010…01)	State 3 (0110…01)	State 4 (0100…01)	… …	State (n-1) (1010…10)	State n (1010…00)
Input 1	(0010…01)						
Input 2		(0110…01)					
Input 3			(0100…01)				
Input i				… …			
Input (n-2)					(1010…10)		
Input (n-1)						(1010…00)	
Input n							(1010…01)

Figure 5.2. State transition table of the $2n$-legged robot for forward locomotion. The orange font represents the key intervals in the state.

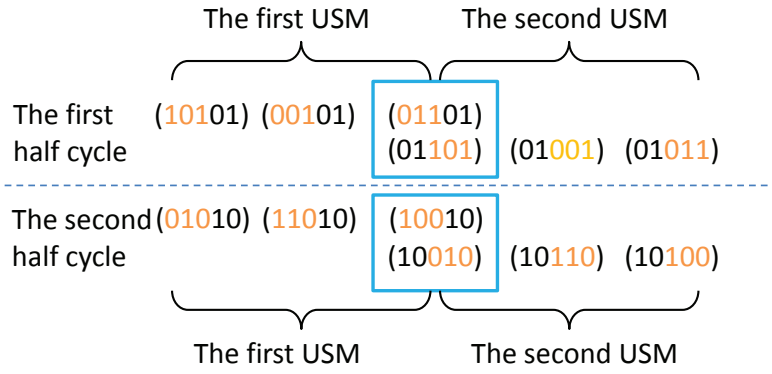

Figure 5.3. State transition table of the 10-legged robot. The orange font represents the key intervals in the state. The state in the blue rectangle is the switching point of the two USMs.

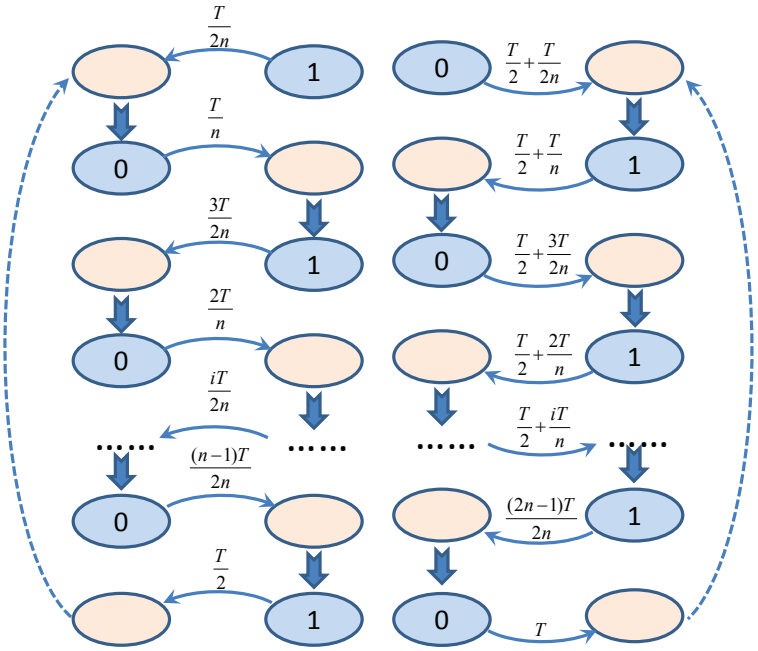

Figure 5.4. State transition diagram for generating undulatory motion in any state of the $2n$-legged robot. The blue ellipse and the orange ellipse represent the supporting state of the leg and the swinging state of the leg, respectively. The blue solid arrows and the blue dotted arrows represent the transition of the support state and the state transits from one side to the other side at the end of the half cycle, respectively. The blue thick arrow indicates the order of the body segment transition. Time above the arrow indicates the transition time.

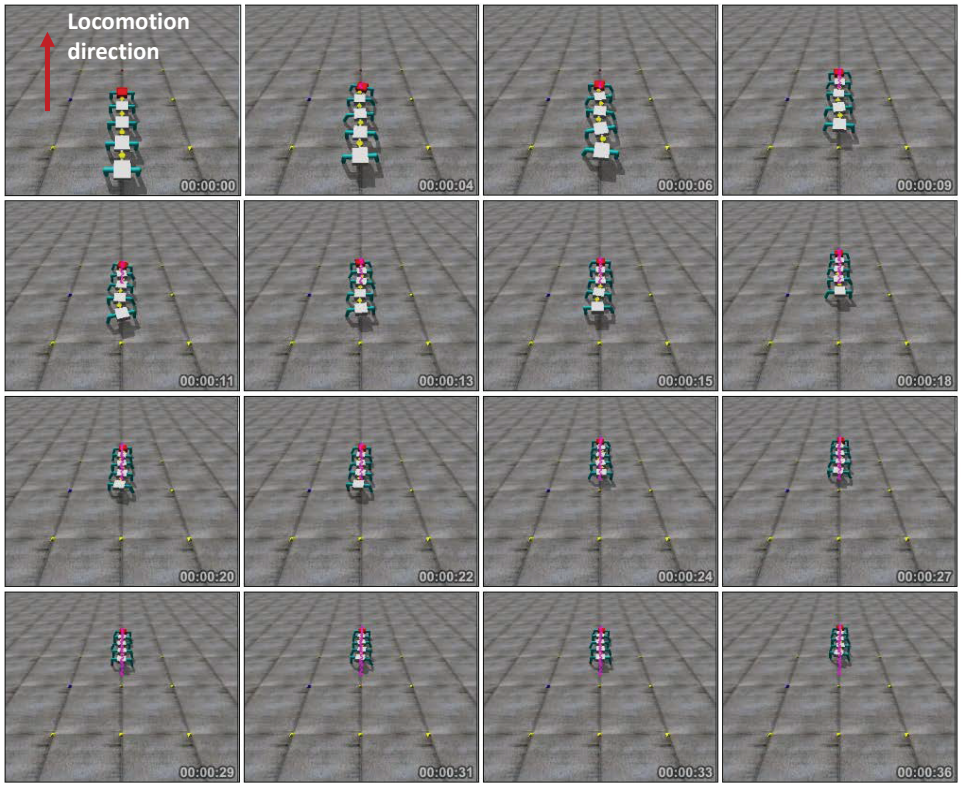

Figure 5.5. Simulation results. Frames of the movement of the 10-legged robot in the simulation environment.

5.2.2 Simulation Results

Fig. 5.5 shows the performances of the passive-spine 10-legged robot. The arrow indicates the direction of locomotion. In the simulation, the forward movements are obtained successfully. The results verified that the proposed gait planning method is available for $2n$-legged robots.

Fig. 5.6 presents the planar locomotion trajectory of the CoM of the first body segment of the 10-legged robot. The top blue curve indicates the generated undulation motion. The displacement in the x-direction reveals that the expected movement is realized in the simulation environment. In the simulation, the speed is approximately $0.25\,[\mathrm{m/s}]$ in the direction of the x-axis. A period is selected in the chart below, and the duration and contribution of each state are given correspondingly, which provides a basis for subsequent optimization of the duty cycle of each state.

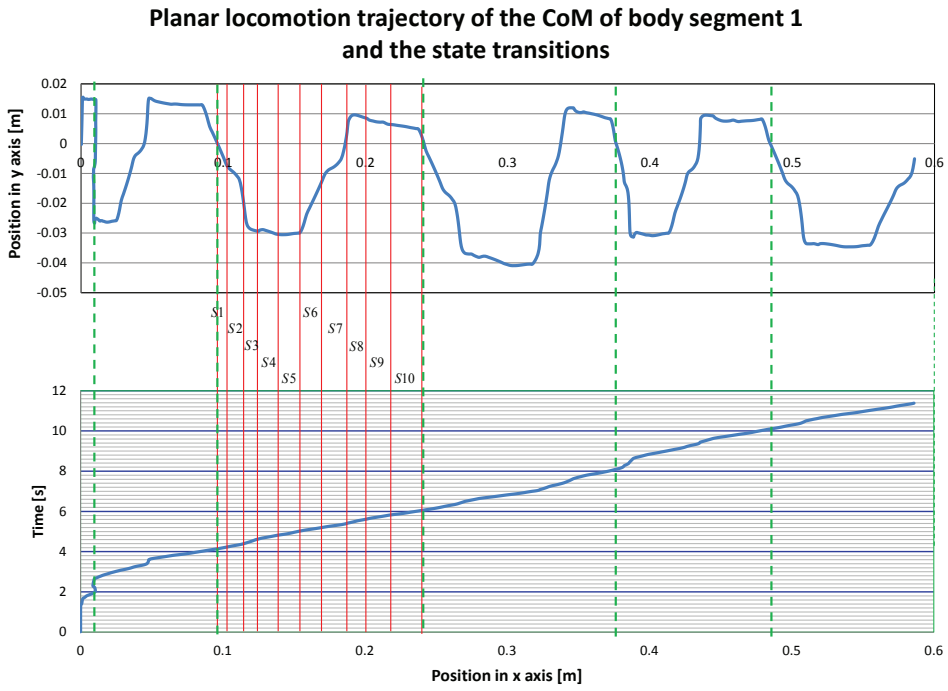

Figure 5.6. The planar position and the contribution of each state of the undulatory gait in the simulation environment. $S1$-$S10$ are marked in the figure to indicate the state 1-state 10 and the contribution of each state in the state transitions.

5.3 Turning Motion of $2n$-Legged Robot

5.3.1 Turning Gait

According to the gait planning analysis in Chapter 4, the turning gait planning method can be used in passive-spine $2n$-legged robots. The contribution of each state transition to the right or left turning in the movement can be obtained. The transition time is designed for achieving the turning motion.

For the 10-legged robot, based on the analysis results in Chapter 4, it can be known that the transitions between state $1 \rightarrow 2$, $7 \rightarrow 8$, $8 \rightarrow 9$, $9 \rightarrow 10$, and $10 \rightarrow 1$ provide a positive contribution to right turning; the transitions between state $2 \rightarrow 3$, $3 \rightarrow 4$, $4 \rightarrow 5$, $5 \rightarrow 6$, and $6 \rightarrow 7$ provide a positive contribution to left turning. Then, we can generate the robot turning motion by changing the transition time of the 10-legged robot, as shown in Fig. 5.7. We termed the gait sequence which performs left and right turning motions as Configuration transition E and F, respectively.

Transition time set in different gait patterns of ten-legged robot

State	S1	S2	S3	S4	S5	S6	S7	S8	S9	S10	
Transition time	0	t_1	t_2	t_3	t_4	t_5	t_6	t_7	t_8	t_9	T [s]
Forward straight-line	0	T/30	2T/30	3T/30	4T/30	5T/30	6T/30	7T/30	8T/30	9T/30	2
Right turning to forward	0	2T/30	6T/30	10T/30	14T/30	18T/30	22T/30	24T/30	26T/30	28T/30	2
Left turning to forward	0	4T/30	6T/30	8T/30	10T/30	12T/30	14T/30	18T/30	22T/30	26T/30	2

Figure 5.7. Transition time set of the 10-legged robot in different gait patterns.

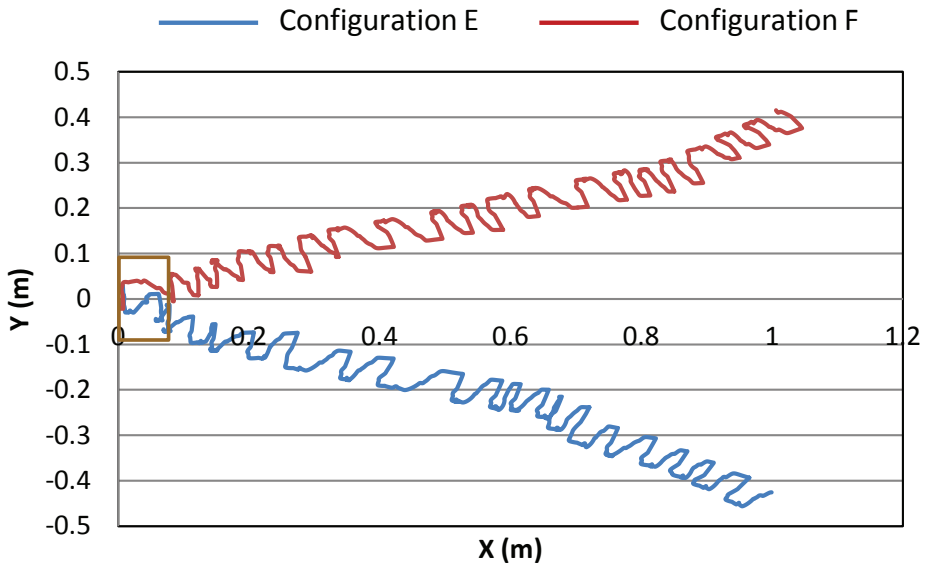

Figure 5.8. Different motion directions of transitions E and F in the simulation environment.

5.3.2 Simulation Results

In Fig. 5.8, the brown square indicates the CoM of the first body segment. The simulation results generate trajectories of these two configuration transitions which are consistent with the above analysis.

The performance of the turning gait of the 10-legged robot is shown in Fig. 5.9. In the simulation, the turning angle is approximately 0.38 [rad].

Performance of ten-legged robot
in different gait patterns

Locomotion direction	Velocity [m/s]				Turning angle [rad]	Remark
	Simulation		Experiment		Simulation	
	v_x	v_y	v_x	v_y		
Forward straight-line	0.05	0	0.03	0	-	Chapter 5.2.
Left turning to forward	-	-	-	-	0.38	Chapter 5.3.
Right turning to forward	-	-	-	-	0.37	Chapter 5.3.

Figure 5.9. Performance of the turning gait of the 10-legged robot in the simulation environment.

5.4 Summary

In this chapter, the FSM theory is introduced into the modular multi-legged robot gait planning method. Through the simulation of the gait design of the 10-legged robot, the proposed method for the gait planning of multi-segment and multi-legged robots is verified.

The $2n$-legged robot with passive-spines developed by the motion mechanism of the imitation organism constitutes the research object. This result suggests that a centipede robot inspired by the body morphology of centipedes can obtain both straight-line motion and turning motion by using undulatory gaits with lateral movement of legs and passive body segments, and does not require individual actuators installed between body segments to directly control segment rotation. Therefore, this chapter not only proves the correctness of the method of gait planning for multi-legged robots, but also provides insight into biology and demonstrates that the lateral movement of the legs can promote the body's undulatory gaits. This study lays the foundation for gait planning methods of similar robots in the future. The experiment results of the analysis of the 10-legged robot are discussed in Chapter 6.

Chapter 6

Experimental Verifications

6.1 Experiment Setup

In this chapter, straight-line motion, turning motion, rotating motion, and sideways motion are tested by the six-legged robot; the methodology of mobility and gait generation for the $2n$-legged robot are tested on the 10-legged robot. Table 2.1 shows the specifications of the six-legged robot prototype. The robot has the same body segment connected by passive body-segment joints.

6.2 Straight-line Motion

For the six-legged robot, the analysis in Chapter 3 yielded 22 configuration transitions and their locomotion capabilities. All of the 22 configuration transitions were experimentally tested on the six-legged robot, and each experiment was repeated five times on the ground. The locomotion direction was verified by measuring the horizontal displacement afterwards with a ruler. In Fig. 6.1, the locomotion direction was observed and recorded. The average velocity were obtained for each configuration transition. The experiment results and locomotion direction are summarized in Table 3.1.

The locomotion possibility was found to be consistent with the analysis results presented

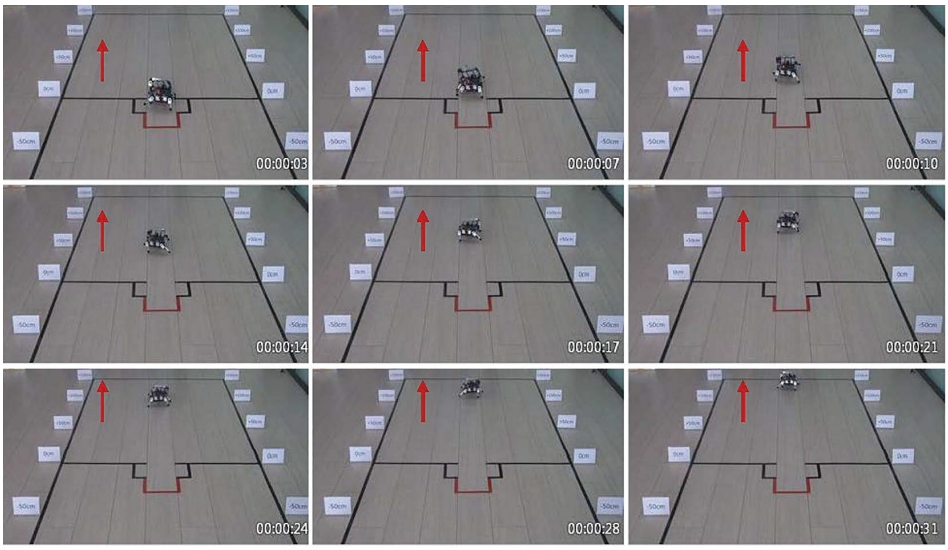

Figure 6.1. Frames of movement of the 10-legged robot in the experiment. The red arrow indicates the locomotion direction.

in Table 3.1. Therefore, the locomotion possibility of the proposed robot design which is analyzed in Chapter 3 has been demonstrated on an actual prototype robot.

The velocity of each configuration transition was also experimentally evaluated. Configuration transitions 1, 9 and 16, with the same locomotion possibility, exhibited different velocities. Although configuration transition 16 contains a negative symbol, which makes a negative contribution to its locomotion, its velocity is larger than that in configuration transition 1. However, the average simulated and experimental speeds are inconsistent, most likely for the following reasons: 1) leg slippage occurred in the experiments, while slippage was absent in the simulation because the friction between the legs and ground was set sufficiently high; and 2) the swinging speed of the legs and the configuration transition times at each step differed between simulations and experiments, with consequent differences in rotation angle of the passive body segment joints.

Moreover, the configuration transitions for forward or backward motion of the robot are tested on an uneven surface where a 5-mm thick aluminum plate is placed. In the experiment, the robot can be observed to pass over the plate successfully, which proves that the robot design and the gait patterns have the potential to overcome uneven terrain.

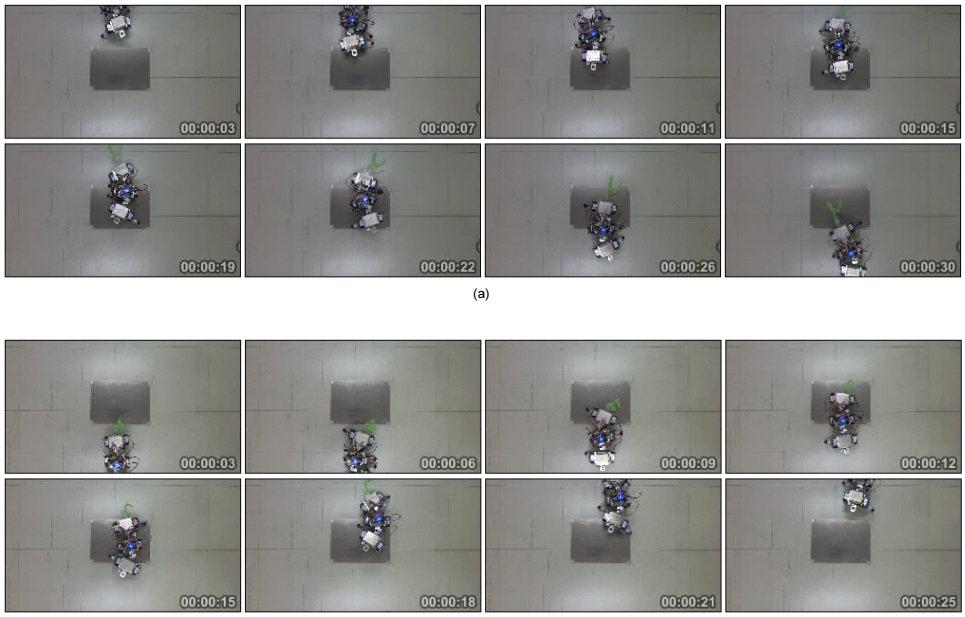

Figure 6.2. Frames of movement of the six-legged robot tested on an uneven terrain. (a) The robot moves forward successfully by transition 1. (b) The robot moves backward successfully by transition 2.

.

Frames of motion experiments of configurations 1 and 2 are shown in Fig. 6.2 (a) and (b), respectively. In the current stage, experiments on the prototype passive-spine robot have illustrated the potential of walking on uneven terrain. For more complex terrains, the movement of the robot will be studied and tested in the future.

6.3 Turning Motion

The analysis in Chapters 3 and 4 yields the four configuration transitions A, B, C, and D, all of which were experimentally tested on the six-legged prototype robot. Each experiment was repeated five times. In Fig. 6.3, the red squares mark the initial position of the robot. The direction of locomotion was recorded. The results and locomotion are shown in Fig. 6.3, in which the movement may be deduced from the change in the position between the frames. The configurations that were analyzed in Chapters 3 and 4 were experimentally tested on the six-legged robot. In Fig. 6.3, the large black square is set as the field of the

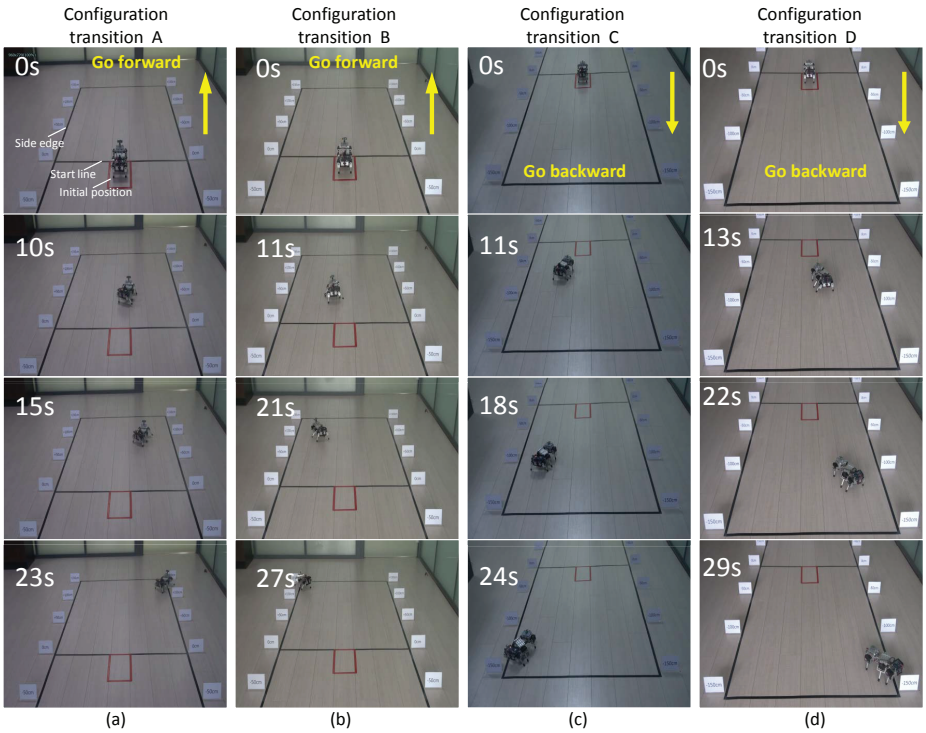

Figure 6.3. Stop-motion photographs of the six-legged robot undergoing configuration transitions. (a) A, (b) B, (c) C, and (d) D.

experiment with $1.2\,[\mathrm{m}] \times 3.0\,[\mathrm{m}]$, and the red squares mark the initial position of the robot. Locomotion videos for the different configuration transitions were recorded. The results and locomotion are shown in Fig. 6.3, in which the movement may be deduced from the change in the position between the frames.

Fig. 6.3(a) shows the frames for configuration transition A, in which the robot moves forward and to the right. Configuration transition B gives the forward motion and rotation to the left [Fig. 6.3 (b)]. In Fig. 6.3(c) and (d), it is shown that the robot can move backward to the left and right in configuration transitions C and D, respectively.

The turning directions are consistent with the results of the analysis presented in Chapter 4. The results demonstrate the turning gaits of the proposed robot design analyzed in Chapter 4. Although some differences in the speed of different configurations exist, our focus in the present research is on the ability to generate turning gaits. On this basis, the characteristics of motion will be investigated in the following.

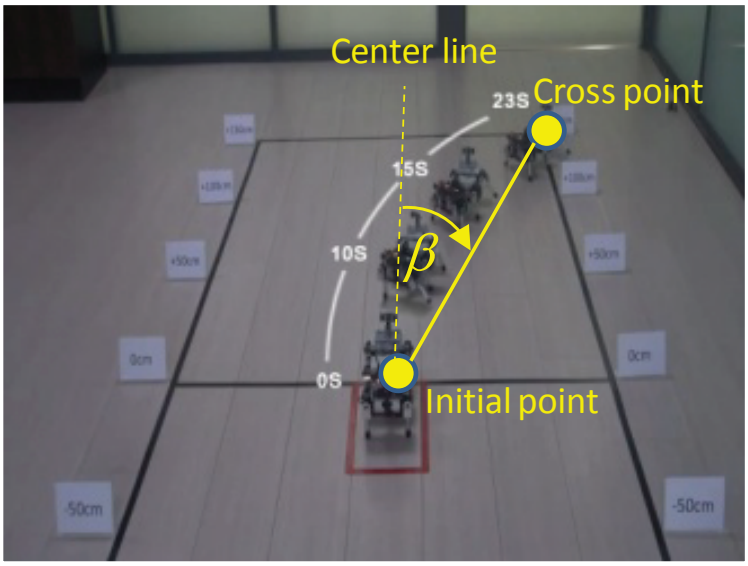

Figure 6.4. Definition of the turning angle.

In order to further elucidate the moving trends of different configuration transitions, a series of experiments on different speeds of configuration transitions A, B, C, and D are implemented by each configuration. Here, configuration transitions A, B, C, and D are viewed as standard configuration transitions. The turning angle β is defined as the angle from the center line to the line that is connected with the initial point and the cross point of the trajectory of the robot and the side edge of the experiment field in Fig. 6.4. Each set of experiments comprises five sets of data, with the $T = 2.1\,[\mathrm{s}]$, $T = 2\,[\mathrm{s}]$, $T = 1.9\,[\mathrm{s}]$, $T = 1.8\,[\mathrm{s}]$, and $T = 1.6\,[\mathrm{s}]$ of the standard configuration transition. Firstly, the trajectories of these experiments were recorded, and the directions of the movement under each group of configuration transitions are consistent with the results of the standard configuration transition. The direction of locomotion was then tracked by stop-motion photographs in Fig. 6.5. It is worth noting that the stop-motion photographs in the same experiment video were taken to combine into one picture to ensure that the position of the robot is not modified. Then, the trajectory of each configuration transition can be observed. The approximate turning directions of different speeds of the four standard configuration transitions are presented in Fig. 6.5. Finally, the turning trends are summarized in Fig. 6.6. The directions of the series of the standard configuration transitions are consistent with the

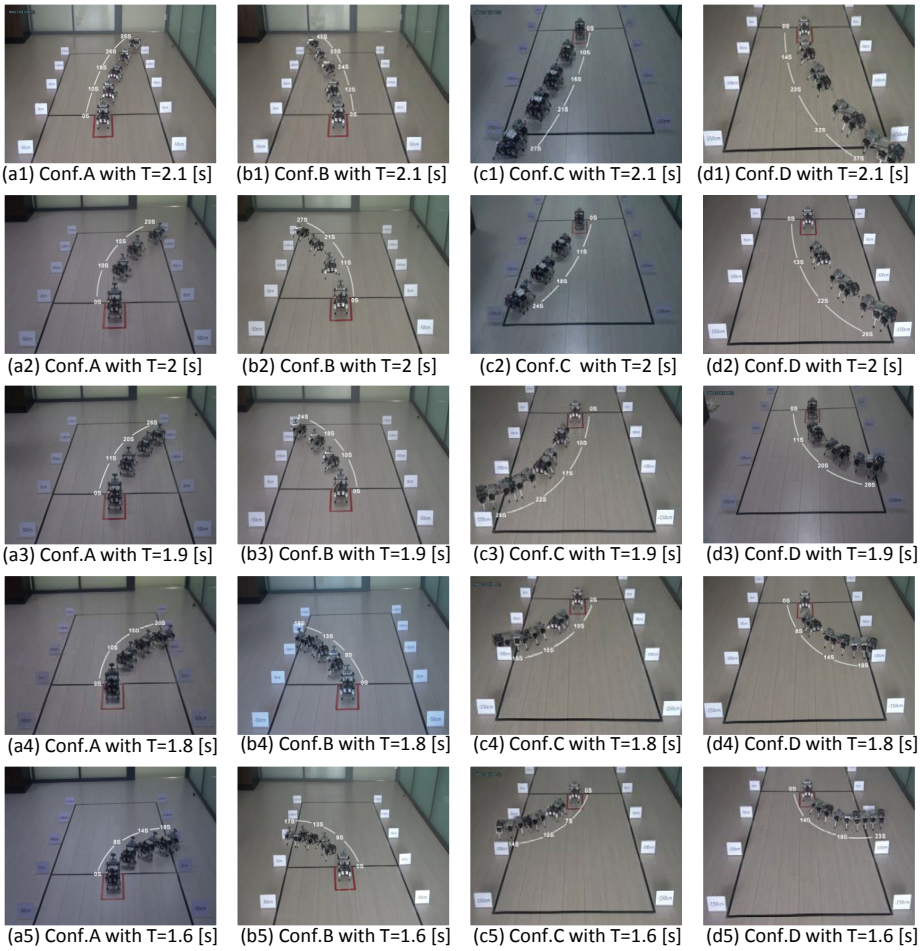

Figure 6.5. Position tracking for turning gaits of standard configuration transitions A, B, C, and D with different speeds. (a1) Configuration A with $T = 2.1\,[\mathrm{s}]$, (a2) Configuration A with $T = 2\,[\mathrm{s}]$, (a3) Configuration A with $T = 1.9\,[\mathrm{s}]$, (a4) Configuration A with $T = 1.8\,[\mathrm{s}]$, (a5) Configuration A with $T = 1.6\,[\mathrm{s}]$, (b1) Configuration B with $T = 2.1\,[\mathrm{s}]$, (b2) Configuration B with $T = 2\,[\mathrm{s}]$, (b3) Configuration B with $T = 1.9\,[\mathrm{s}]$, (b4) Configuration B with $T = 1.8\,[\mathrm{s}]$, (b5) Configuration B with $T = 1.6\,[\mathrm{s}]$, (c1) Configuration C with $T = 2.1\,[\mathrm{s}]$, (c2) Configuration C with $T = 2\,[\mathrm{s}]$, (c3) Configuration C with $T = 1.9\,[\mathrm{s}]$, (c4) Configuration C with $T = 1.8\,[\mathrm{s}]$, (c5) Configuration C with $T = 1.6\,[\mathrm{s}]$, (d1) Configuration D with $T = 2.1\,[\mathrm{s}]$, (d2) Configuration D with $T = 2\,[\mathrm{s}]$, (d3) Configuration D with $T = 1.9\,[\mathrm{s}]$, (d4) Configuration D with $T = 1.8\,[\mathrm{s}]$, and (d5) Configuration D with $T = 1.6\,[\mathrm{s}]$.

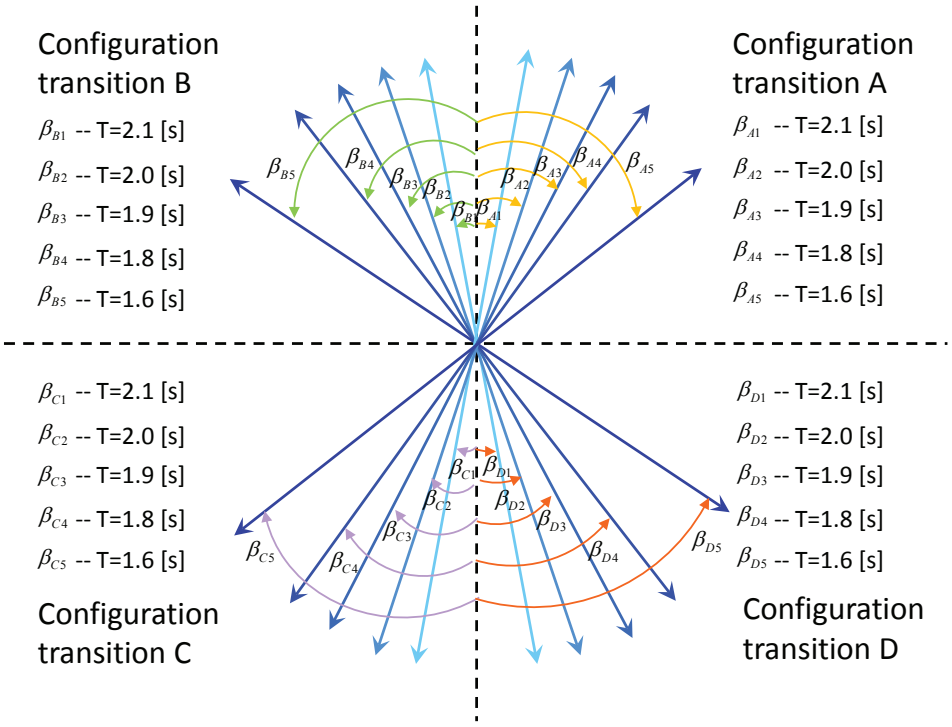

Figure 6.6. Turning directions of different speeds of configuration transitions A, B, C, and D.

results of the standard configuration transition. For example, the directions of the different speeds of configuration transition A are the same as configuration transition A to move forward and turn to the right. Overall, higher speeds tend to result in larger turning angles.

6.4 Rotating Motion

In Fig. 6.7, the red curve arrows are used to mark the movement of the center of the first body segment. It can be observed that the robot can approximately make a rotating motion around the last body segment. The experiment result is consistent with the simulation results.

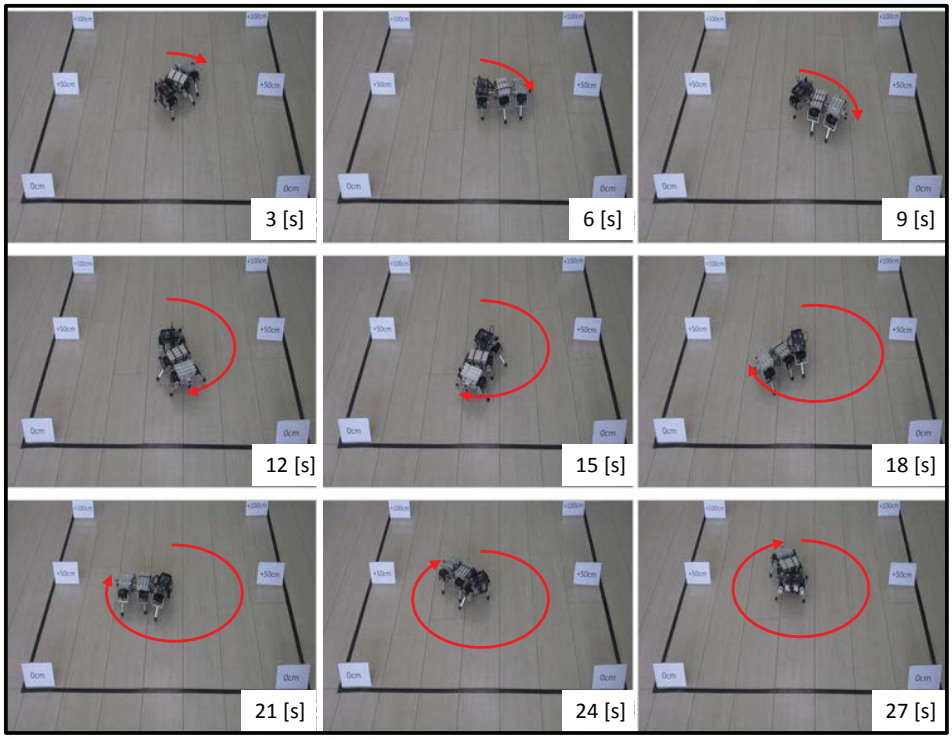

Figure 6.7. Rotating motion of the six-legged robot.

6.5 Sideways Motion

In Fig. 6.8, the red arrows indicate the locomotion direction. The speed of the sideways motion is approximately 0.05 [m/s] in the direction of the y-axis. The experimental results show that the success of the sideways gait is consistent with the analysis and simulation results. The errors between the simulation and experiment results were probably due to differences between the simulation and experiment environments. In the simulation, it is possible to decouple the hardware limitations with the control algorithms. Fig. 6.8 (a)-(d) and (e)-(h) show the stop-motion photographs in front view and side view, respectively. It can be observed that the robot can perform sideways motion successfully. The analysis, simulations, and experiments in this paper proved that the robot possesses the ability to turn with our proposed method.

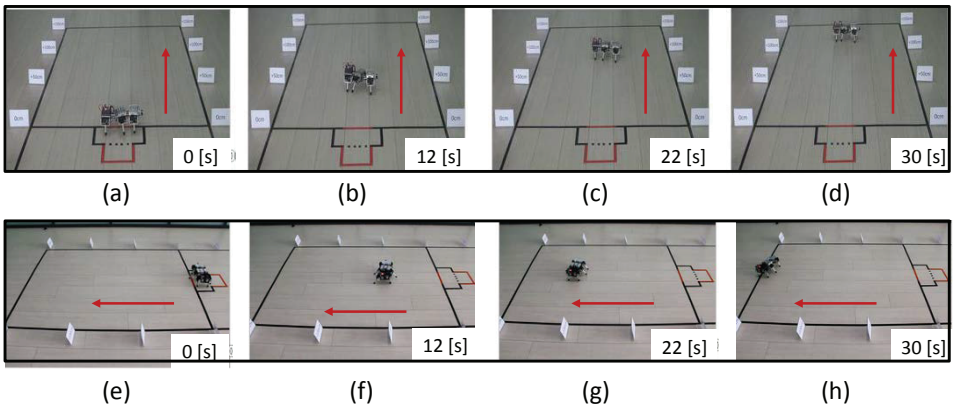

Figure 6.8. Sideways motion of the six-legged robot.

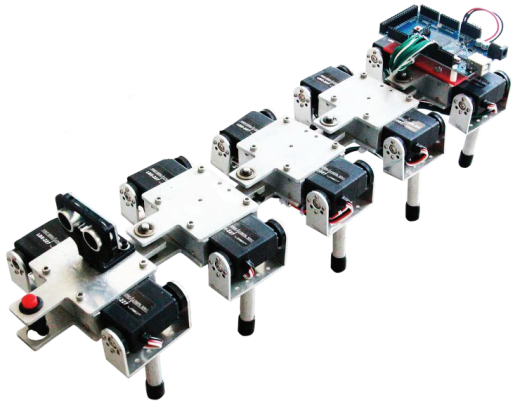

Figure 6.9. Prototype of the 10-legged robot.

6.6 Undulatory Motion

The obtained configuration transitions were experimentally tested on a 10-legged prototype robot (Fig. 6.9), and each experiment was repeated five times on the ground. The locomotion direction was observed and recorded in Fig. 6.10.

The locomotion direction was found to be consistent with the analysis results presented in Chapter 5. A general method for obtaining the configuration transitions for $2n$-legged robots has been examined in this paper.

The following discussion can be obtained by the simulations and experiments: 1. Based on the movement principle of centipedes, the multi-legged robot uses the passive joints

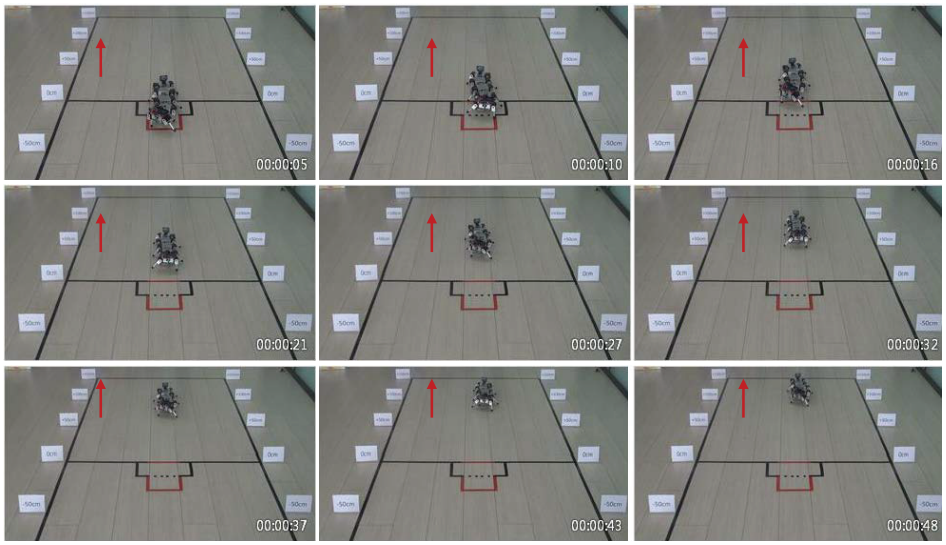

Figure 6.10. Frames of the movement of the 10-legged robot in the experiment. The red arrow indicates the locomotion direction.

between the body segments to realize the motion through the rotation of the supporting leg around each body segment, which is of guiding significance for the realization of the motion of similar robots. 2. The FSM theory is used to analyze the motion gaits of the robot, which proves that the method is feasible. 3. When the number of body segments increases, the method is simple to implement and provides a motion control research method for similar robots.

6.7 Summary

Through the experiments of omnidirectional gaits, we can know that the minimum turning radius of the robot approaches zero, and the robot can rotate around the last body segment of the robot. We can also conclude that higher speeds tend to result in larger turning angles and smaller turning radiuses by using the same configuration transition during turning gaits. For turning motions, the turning angles of configurations $A - D$ are 0.43 [rad], 0.40 [rad], 0.39 [rad], and 0.39 [rad], respectively. For sideways motion, the highest speed currently achievable is approximately 0.05 [m/s]. For straight-line motion, the highest speed currently achievable is approximately 0.25 [m/s]. Although there are small

errors in the simulation and experimental errors, the motion trends are consistent, which demonstrates the omni-directional mobility of the robot, and the proposed design and gait planning methods.

Chapter 7

Conclusion and Future Work

7.1 Conclusion

In this thesis, a new method for legged locomotion of passive-spine multi-legged robots with a minimal number of actuated joints has been presented. The $2n$-legged robot that has only $2n$ active actuators by introducing passive body segment joints can realize omni-directional locomotion successfully. First, the candidate configurations have been selected by a mobility analysis of the multi-legged robot. Next, the potential principle of locomotion has been obtained based on the movement characteristic. The gait patterns that have been designed for achieving planar locomotion have been tested on a six-legged robot.

Then, we have demonstrated that the omni-directional locomotion of the passive-spine multi-legged robot has been realized with very few active degrees of freedom and a simple structure. The proposed locomotion method and gait planning method enable a passive-spine legged robot to perform omni-directional motions. Geometric analysis of the system configurations has been performed to map the relationship between the leg movements and the body rotating motions. The robot omni-directional motions have been achieved by modifying the duration of each transition configuration. Effectiveness of this method has been validated via tests in the simulation and on the physical platform. A general method

of the $2n$-legged robot with more joints and configuration transitions has been obtained for undulatory motion.

Finally, the method for the robot design and the omni-directional gait patterns have been verified through simulations and experiments. The proposed mechanism design methodology ensures high walking performance of the robot with fewer actuated joints than in previously proposed multi-legged robots.

7.2 Future Work

In our future work, the control system of the proposed robot will be investigated. Currently, the robot can travel on flat or simple uneven surfaces; travel across rougher terrain constitutes a subsequent work. This study lays the foundation for gait planning methods of similar robots in the future.

Mobility analysis and gait analysis results, as well as the design methodology of the proposed passive-spine robot, can be easily expanded to multi-legged robots with more segments. Experimental studies of the robustness of passive-spine legged robots are required and should significantly impact the future design of this type of robot as a platform for research into legged locomotion on both large and small scales.

We have proven that omni-directional locomotion could be realized using a multi-legged platform with fewer actuators. Analysis of the results and design methods of omni-directional gaits of the proposed passive-spine robot can readily be extended to multi-legged robots with more segments. The planning method can be utilized to achieve omni-directional motion for similar cases of legged robots without active turning DOF. Experimental studies of the robustness of legged robots are requisite, and should significantly impact future design and behavior compensation for damage to the robot. Although this paper is a preliminary study, it constitutes an important foundation for our future research. In subsequent research, turning gaits on uneven terrains will be analyzed and tested. A

general method for obtaining transitions between different gaits for multi-legged robots will also be examined in future work.

Bibliography

[1] K. Arikawa and S. Hirose, "Mechanical design of walking machines," *Philosophical Transactions of the Royal Society of London A: Mathematical, Physical and Engineering Sciences*, vol. 365, no. 1850, pp. 171–183, 2007.

[2] A. Torige, S. Yagi, H. Makino, T. Yagami, and N. Ishizawa, "Centipede type walking robot (cwr-2)," in *Intelligent Robots and Systems, 1997. IROS'97., Proceedings of the 1997 IEEE/RSJ International Conference on*, vol. 1. IEEE, 1997, pp. 402–407.

[3] M. Sfakiotakis and D. P. Tsakiris, "Pedundulatory robotic locomotion: Centipede and polychaete modes in unstructured substrates," in *Robotics and Biomimetics, 2008. ROBIO 2008. IEEE International Conference on.* IEEE, 2009, pp. 651–658.

[4] J. T. Machado and M. F. Silva, "An overview of legged robots," in *International symposium on mathematical methods in engineering.* MME Press Ankara, Turkey, 2006.

[5] S. Miao and D. Howard, "Optimal tripod turning gait generation for hexapod walking machines," *Robotica*, vol. 18, no. 6, pp. 639–649, 2000.

[6] L. T. Phan, Y. H. Lee, Y. H. Lee, H. Lee, H. Kang, and H. R. Choi, "Study on quadruped bounding with a passive compliant spine," in *Intelligent Robots and Systems (IROS), 2017 IEEE/RSJ International Conference on.* IEEE, 2017, pp. 2409–2414.

[7] S. Nishikori, S. Hokamoto, and T. Kubota, "Kinematic discussion and development of a multi-legged planetary exploration rover with an isotropic leg arrangement," *Advanced Robotics*, vol. 25, no. 6-7, pp. 789–804, 2011.

[8] K. Yoneda and Y. Ota, "Non-bio-mimetic walkers," *The International Journal of Robotics Research*, vol. 22, no. 3-4, pp. 241–249, 2003.

[9] Y. Zhao, X. Chai, F. Gao, and C. Qi, "Obstacle avoidance and motion planning scheme for a hexapod robot octopus-iii," *Robotics and Autonomous Systems*, vol. 103, pp. 199–212, 2018.

[10] O. Bulichev, A. Klimchik, and N. Mavridis, "Optimization of centipede robot body designs through evolutionary algorithms and multiple rough terrains simulation," in *Robotics and Biomimetics (ROBIO), 2017 IEEE International Conference on.* IEEE, 2017, pp. 290–295.

[11] H. Zhang, Y. Liu, J. Zhao, J. Chen, and J. Yan, "Development of a bionic hexapod robot for walking on unstructured terrain," *Journal of Bionic Engineering*, vol. 11, no. 2, pp. 176–187, 2014.

[12] J. Estremera, J. A. Cobano, and P. G. De Santos, "Continuous free-crab gaits for hexapod robots on a natural terrain with forbidden zones: An application to humanitarian demining," *Robotics and Autonomous Systems*, vol. 58, no. 5, pp. 700–711, 2010.

[13] J.-M. Yang, Y.-K. Park, and J.-G. Kim, "Fault-tolerant gait planning of multi-legged robots," in *Mobile Robotics, Moving Intelligence*. InTech, 2006.

[14] S. Hirose, "A study of design and control of a quadruped walking vehicle," *The International Journal of Robotics Research*, vol. 3, no. 2, pp. 113–133, 1984.

[15] K. Radkhah, S. Kurowski, and O. Von Stryk, "Design considerations for a biologically inspired compliant four-legged robot," in *Robotics and Biomimetics (ROBIO), 2009 IEEE International Conference on*. IEEE, 2009, pp. 598–603.

[16] T. Karakurt, A. Durdu, and N. Yilmaz, "Design of six legged spider robot and evolving walking algorithms," *International Journal of Machine Learning and Computing*, vol. 5, no. 2, pp. 96–100, 2015.

[17] J. Zhang, Z. Jin, and Y. Zhao, "Dynamics analysis of leg mechanism of six-legged firefighting robot," *Journal of Mechanical Science and Technology*, vol. 32, no. 1, pp. 351–361, 2018.

[18] B. Klaassen, R. Linnemann, D. Spenneberg, and F. Kirchner, "Biomimetic walking robot scorpion: Control and modeling," *Robotics and autonomous systems*, vol. 41, no. 2-3, pp. 69–76, 2002.

[19] P. Manoonpong, F. Pasemann, and H. Roth, "Modular reactive neurocontrol for biologically inspired walking machines," *The International Journal of Robotics Research*, vol. 26, no. 3, pp. 301–331, 2007.

[20] J. A. Galvez, J. Estremera, and P. G. De Santos, "A new legged-robot configuration for research in force distribution," *Mechatronics*, vol. 13, no. 8-9, pp. 907–932, 2003.

[21] J. Li, J. Wang, S. X. Yang, K. Zhou, and H. Tang, "Gait planning and stability control of a quadruped robot," *Computational intelligence and neuroscience*, vol. 2016, 2016.

[22] A. Cully, J. Clune, D. Tarapore, and J.-B. Mouret, "Robots that can adapt like animals," *Nature*, vol. 521, no. 7553, p. 503, 2015.

[23] M. Kaneko, M. Abe, and S. Tachi, "Basic considerations of the degrees of freedom of multi-legged locomotion machines," *Advanced robotics*, vol. 1, no. 2, pp. 101–116, 1986.

[24] A. Preumont, P. Alexandre, I. Doroftei, and F. Goffin, "A conceptual walking vehicle for planetary exploration," *Mechatronics*, vol. 7, no. 3, pp. 287–296, 1997.

[25] S. Inagaki, T. Niwa, and T. Suzuki, "Follow-the-contact-point gait control of centipede-like multi-legged robot to navigate and walk on uneven terrain," in *Intelligent Robots and Systems (IROS), 2010 IEEE/RSJ International Conference on*. IEEE, 2010, pp. 5341–5346.

[26] B. Jimenez and A. Ikspeert, "Centipede robot locomotion," *Master's thesis, Ecole Polytechnique Federale de Lausanne, Lausanne, Switzerland*, 2007.

[27] L. Matthey, L. Righetti, and A. J. Ijspeert, "Experimental study of limit cycle and chaotic controllers for the locomotion of centipede robots," in *Intelligent Robots and Systems, 2008. IROS 2008. IEEE/RSJ International Conference on.* IEEE, 2008, pp. 1860–1865.

[28] U. Saranli, M. Buehler, and D. E. Koditschek, "Rhex: A simple and highly mobile hexapod robot," *The International Journal of Robotics Research*, vol. 20, no. 7, pp. 616–631, 2001.

[29] Y.-C. Chou, K.-J. Huang, W.-S. Yu, and P.-C. Lin, "Model-based development of leaping in a hexapod robot," *IEEE Transactions on Robotics*, vol. 31, no. 1, pp. 40–54, 2015.

[30] D. Grzelczyk, B. Stańczyk, and J. Awrejcewicz, "Prototype, control system architecture and controlling of the hexapod legs with nonlinear stick-slip vibrations," *Mechatronics*, vol. 37, pp. 63–78, 2016.

[31] J.-u. Choi, B. L. Rutter, D. A. Kingsley, R. E. Ritzmann, and R. D. Quinn, "A robot with cockroach inspired actuation and control," in *Advanced Intelligent Mechatronics. Proceedings, 2005 IEEE/ASME International Conference on.* IEEE, 2005, pp. 1569–1574.

[32] A. Roennau, T. Kerscher, and R. Dillmann, "Design and kinematics of a biologically-inspired leg for a six-legged walking machine," in *Biomedical Robotics and Biomechatronics (BioRob), 2010 3rd IEEE RAS and EMBS International Conference on.* IEEE, 2010, pp. 626–631.

[33] C. Liang, M. Ceccarelli, and G. Carbone, "A novel biologically inspired tripod walking robot," *environments*, vol. 1, p. 2, 2009.

[34] T. Kinugasa, K. Osuka, R. Hayashi, N. Miyamoto, and K. Yoshida, "Development of a small and lightweight myriapod robot using passive dynamics," *Artificial Life and Robotics*, vol. 22, no. 4, pp. 429–434, 2017.

[35] S. Aoi, T. Tanaka, S. Fujiki, T. Funato, K. Senda, and K. Tsuchiya, "Advantage of straight walk instability in turning maneuver of multilegged locomotion: a robotics approach," *Scientific reports*, vol. 6, p. 30199, 2016.

[36] D. Koh, J. Yang, and S. Kim, "Centipede robot for uneven terrain exploration: Design and experiment of the flexible biomimetic robot mechanism," in *Biomedical Robotics and Biomechatronics (BioRob), 2010 3rd IEEE RAS and EMBS International Conference on.* IEEE, 2010, pp. 877–881.

[37] A. J. Ijspeert, "A connectionist central pattern generator for the aquatic and terrestrial gaits of a simulated salamander," *Biological cybernetics*, vol. 84, no. 5, pp. 331–348, 2001.

[38] B. Anderson, J. Shultz, and B. Jayne, "Axial kinematics and muscle activity during terrestrial locomotion of the centipede scolopendra heros," *Journal of experimental biology*, vol. 198, no. 5, pp. 1185–1195, 1995.

[39] K. L. Hoffman and R. J. Wood, "Myriapod-like ambulation of a segmented microrobot," *Autonomous Robots*, vol. 31, no. 1, p. 103, 2011.

[40] K. W. Wait and M. Goldfarb, "A pneumatically actuated quadrupedal walking robot," *IEEE/ASME Transactions on Mechatronics*, vol. 19, no. 1, pp. 339–347, 2014.

[41] Y. Go, X. Yin, and A. Bowling, "Navigability of multi-legged robots," *IEEE ASME TRANSACTIONS ON MECHATRONICS*, vol. 11, no. 1, p. 1, 2006.

[42] A. Fukuhara, Y. Koizumi, S. Suzuki, T. Kano, and A. Ishiguro, "Minimal model for body–limb coordination in quadruped high-speed running," in *International Conference on Simulation of Adaptive Behavior*. Springer, 2018, pp. 56–65.

[43] Z. Huang and Q. Ge, "A simple method for mobility analysis using reciprocal screws," in *ASME 2006 International Design Engineering Technical Conferences and Computers and Information in Engineering Conference*. American Society of Mechanical Engineers, 2006, pp. 1229–1237.

[44] J. S. Dai, Z. Huang, and H. Lipkin, "Mobility of overconstrained parallel mechanisms," *Journal of Mechanical Design*, vol. 128, no. 1, pp. 220–229, 2006.

[45] R. Diestel, "Graph theory. 1997," *Grad. Texts in Math*, 1997.

[46] H. Gao, M. Jin, Y. Liu, L. Ding, H. Yu, and Z. Deng, "Turning gait planning and simulation validation of a hydraulic hexapod robot," in *Fluid Power and Mechatronics (FPM), 2015 International Conference on*. IEEE, 2015, pp. 842–847.

[47] H. Deng, G. Xin, G. Zhong, and M. Mistry, "Gait and trajectory rolling planning and control of hexapod robots for disaster rescue applications," *Robotics and Autonomous Systems*, vol. 95, pp. 13–24, 2017.

[48] J. Dupeyroux, G. Passault, F. Ruffier, S. Viollet, and J. Serres, "Hexabot: a small 3d-printed six-legged walking robot designed for desert ant-like navigation tasks," in *IFAC Word Congress 2017*, 2017.

[49] Y. Mae, T. Inoue, K. Kamiyama, M. Kojima, M. Horade, and T. Arai, "Direct teleoperation system of multi-limbed robot for moving on complicated environments," in *2017 IEEE International Conference on Robotics and Biomimetics (ROBIO)*. IEEE, 2017, pp. 1171–1174.

[50] T. Fukuda, Y. Adachi, H. Hoshino, I. Matsunaga, and F. Arai, "An omni-directional six-legged walking robot," *Advanced robotics*, vol. 9, no. 2, pp. 177–191, 1994.

[51] K. Kamikawa, T. Arai, K. Inoue, and Y. Mae, "Omni-directional gait of multi-legged rescue robot," in *IEEE International Conference on Robotics and Automation, 2004. Proceedings. ICRA'04. 2004*, vol. 3. IEEE, 2004, pp. 2171–2176.

[52] Y. Tang, S. Ma, Y. Sun, and D. Ge, "Planar legged walking of a passive-spine hexapod robot," *Advanced Robotics*, vol. 29, no. 23, pp. 1510–1525, 2015.

[53] R. A. Brooks, "New approaches to robotics," *Science*, vol. 253, no. 5025, pp. 1227–1232, 1991.

[54] ——, "Intelligence without representation," *Artificial intelligence*, vol. 47, no. 1-3, pp. 139–159, 1991.

[55] H.-W. Park, A. Ramezani, and J. Grizzle, "A finite-state machine for accommodating unexpected large ground-height variations in bipedal robot walking," *IEEE Transactions on Robotics*, vol. 29, no. 2, pp. 331–345, 2012.

[56] A. M. Howard and L. T. Parker, "A hierarchical strategy for learning of robot walking strategies in natural terrain environments," in *2007 IEEE International Conference on Systems, Man and Cybernetics*. IEEE, 2007, pp. 2336–2341.

[57] J. K. Davidson, K. H. Hunt, and K. H. Hunt, *Robots and screw theory: applications of kinematics and statics to robotics*. Oxford University Press on Demand, 2004.

Appendix A

Mobility Calculation Based on Screw Theory

A unit screw $\$$ is defined by a pair of vectors [57]:

$$\$ = (\mathbf{s}; \mathbf{s_o}) = (\mathbf{s}; \mathbf{r} \times \mathbf{s} + h\mathbf{s},) \tag{A.1}$$

where $\mathbf{s}$ is a unit vector specifying the direction of the screw axis; $\mathbf{s_o}$ is the moment vector of the line about origin O; $\mathbf{r}$ is the position vector of any point on the screw axis in terms of a reference coordinate system; and h describes the pitch.

If a screw $\$^r = (\mathbf{s_r}; \mathbf{s_{or}})$, and a set of screws, $\$_1, \$_2, \$_3, ..., \$_n$, can satisfy the condition:

$$\$_j \circ \$^r = \mathbf{s}_j \cdot \mathbf{s_{or}} + \mathbf{s_r} \cdot \mathbf{s}_{oj} = 0, (j = 1, 2, 3, ..., n) \tag{A.2}$$

where $\$^r = (\mathbf{s_r}; \mathbf{s_{or}})$, "$\circ$" represents the reciprocal product; and $\$_j$ represents the j th screw of the screw set, $\$^r$ is called the reciprocal screw of screw set $\$_j$. A screw is called a twist if it indicates an instantaneous motion of a rigid body. A screw is called a wrench if it indicates a force and a coaxial couple acting on a rigid body. A couple or a translation can be expressed by $(0; \mathbf{s})$, and a force or a rotation can be expressed by $(\mathbf{s}; \mathbf{r} \times \mathbf{s})$. In this paper, the mobility means the number of redundant DOFs, and the screw means the direction of the DOFs.

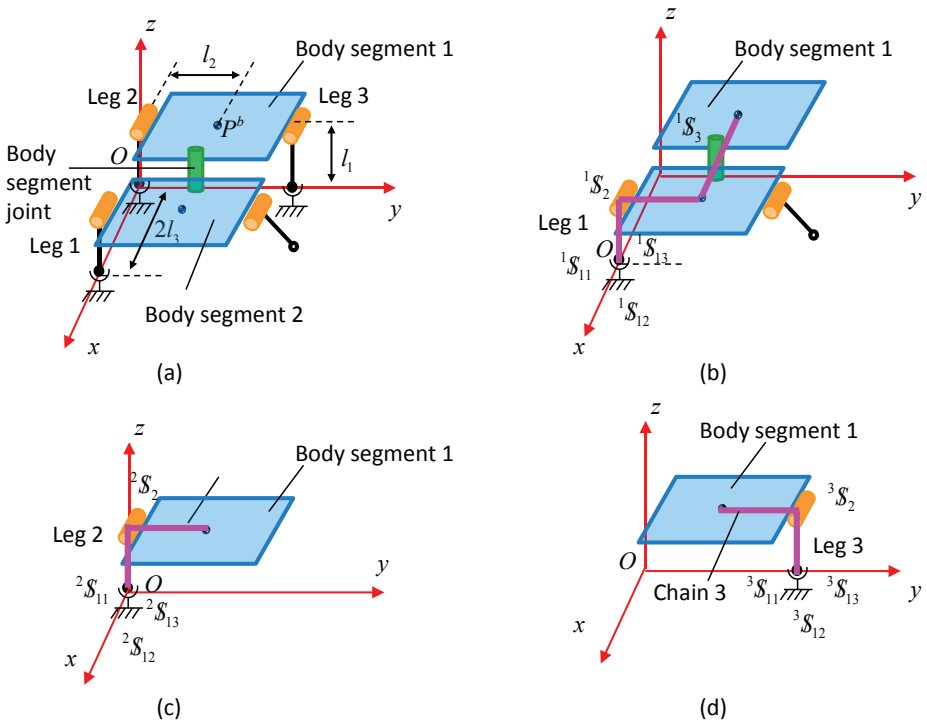

Figure A.1. (a)Configuration $2L$. l_1 specifies the height of the leg of the robot, while l_2 is the distance between the axis of the body segment joint and the x-axis. The distance between leg 1 and leg 2 in the direction of the x-axis is $2l_3$. For instance, considering body-segment-1 of a four-legged robot, (b) chain 1, which is formed by leg 1 and the body segment joint, (c) and (d) legs 2 and 3 form chains 2 and 3, respectively.

When all joints in a mechanism are associated with unit screws, their common constraint is the reciprocal of each screw. For example, in Fig. A.1, taking body-segment-1 of the four-legged robot as the subject, leg 1 and the body segment joint form chain 1 of the mechanism, and legs 2 and 3 form chains 2 and 3, respectively.

In this case, chain 1 comprises a single contact point, which is considered as a spherical joint and two revolute joints $\$_2$ and $\$_3$. Thus, the motion screw of chain 1 is expressed as:

$$
\begin{aligned}
^1\$_{11} &= (1\ 0\ 0;\ 0\ 0\ 0),\\
^1\$_{12} &= (0\ 1\ 0;\ 0\ 0\ 2l_3),\\
^1\$_{13} &= (0\ 0\ 1;\ 0\ 2l_3\ 0),\\
^1\$_2 &= (1\ 0\ 0;\ 0\ l_1\ 0),\\
^1\$_3 &= (0\ 0\ 1;\ l_2\ l_3\ 0).
\end{aligned}
\tag{A.3}
$$

The first three screws denote rotations about the x-axis, and the axis which is parallel to the y-axis and the z-axis, respectively. The last two screws denote rotations about the axis which is parallel to the x-axis and the z-axis, respectively. The motion screw of chain 2 is given by:

$$\begin{aligned} {}^2\$_{11} &= (1\ 0\ 0;\ 0\ 0\ 0), \\ {}^2\$_{12} &= (0\ 1\ 0;\ 0\ 0\ 0), \\ {}^2\$_{13} &= (0\ 0\ 1;\ 0\ 0\ 0), \\ {}^2\$_{2} &= (1\ 0\ 0;\ 0\ l_1\ 0). \end{aligned} \tag{A.4}$$

The first three screws denote rotations about the x-axis, y-axis, and z-axis, respectively. The last screw denotes rotations about the axis which is parallel to the x-axis. The motion screw of chain 3 is given by:

$$\begin{aligned} {}^3\$_{11} &= (1\ 0\ 0;\ 0\ 0\ 2l_2), \\ {}^3\$_{12} &= (0\ 1\ 0;\ 0\ 0\ 0), \\ {}^3\$_{13} &= (0\ 0\ 1;\ 2l_2\ 0\ 0), \\ {}^3\$_{2} &= (1\ 0\ 0;\ 0\ l_1\ 2l_2). \end{aligned} \tag{A.5}$$

The first two screws denote rotations about the axis which is parallel to the x-axis and the y-axis, respectively. The last two screws denote rotations about the axis which is parallel to the z-axis and the x-axis, respectively. The constraint of chain 1 is the reciprocal screw of chain 1, and is given by:

$${}^1\$_1^r = (0\ 0\ 1;\ 0\ -2l_3\ 0), \tag{A.6}$$

which restricts the translations along the z-axis. The reciprocal screw of chain 2 is given by:

$$\begin{aligned} {}^2\$_1^r &= (1\ 0\ 0;\ 0\ 0\ 0), \\ {}^2\$_2^r &= (0\ 0\ 1;\ 0\ 0\ 0), \end{aligned} \tag{A.7}$$

which restricts the translations along the x-axis and the z-axis. The reciprocal screw of chain 3 is given by:

$$\begin{aligned} {}^3\$_1^r &= (1\ 0\ 0;\ 0\ 0\ -2l_2), \\ {}^3\$_2^r &= (0\ 0\ 1;\ -2l_2\ 0\ 0), \end{aligned} \tag{A.8}$$

which restricts the translations along the x-axis and the z-axis. According to the analysis results above, the number of common constraints λ is 0. From Equation (3.4), we conclude that the number of redundant constraints ν is 0, and thus the mobility of segment 1 can be calculated from Equation (3.2), yielding $M_1 = 6(6-7-1)+13+0 = 1$. The mobility of body-segment-2, calculated in the same manner, is also 1.

By calculating the screws reciprocal to Equations (A.6), (A.7) and (A.8), the motion screw $\$_m$ of body segment can be obtained as:

$$\$_m = (0\ 0\ 0;\ 0\ 1\ 0). \tag{A.9}$$

which shows that the feasible motion of the body segment is translation along the y-axis.

With the same method, for body-segment-1 of the configuration LRL, the mobility $M_1 = 2$ with the motion screw $\$_m$ that indicates the allowable relative motions between different chains of the mechanism, is given by:

$$\begin{aligned} \$_{m1} &= (1/l_1\ 0\ 0;\ 0\ 1\ 0), \\ \$_{m2} &= (0\ 0\ 1;\ 2l_2\ 0\ 0). \end{aligned} \tag{A.10}$$

which shows that the feasible motions of the body segment include a translation along the y-axis, and a rotation about the axis that is parallel to the z-axis.

The mobilities $M_2 = 2$ and $M_3 = 2$ of body-segment-2 and 3, respectively, are similarly obtained. The mobility of a robot with this configuration is 2. The body segment of the alternative six-legged robot with $M_r = 2$ in Fig. 2.3 can rotate about a vertical axis parallel to the z-axis.

The mobility of the other configurations can be obtained by the same method. Due to space limitations, the terms of mobility calculation of the candidate configurations which are mainly discussed in this paper are listed in Table A.1.

Table A.1. Mobility calculation of candidate configurations

Classification	Analyze subject	d	n	g	f	v	ξ	λ	M_i	M_r
	segment 1								$M_1 = 2$	
LRL, RLR	segment 2	6	7	8	14	0	0	0	$M_2 = 2$	2
	segment 3								$M_3 = 2$	
	segment 1								$M_1 = 2$	
LLR, LRR, RRL, RLL	segment 2	6	7	8	14	0	0	0	$M_2 = 2$	2
	segment 3								$M_3 = 2$	
	segment 1	6	7	8	14	0	1	0	$M_1 = 1$	
$20L, 20R$	segment 2	6	7	8	14	0	0	0	$M_2 = 2$	2
	segment 3	6	7	8	14	0	0	0	$M_3 = 2$	
	segment 1	6	7	8	14	0	0	0	$M_1 = 2$	
$L02, R02$	segment 2	6	7	8	14	0	0	0	$M_2 = 2$	2
	segment 3	6	7	8	14	0	1	0	$M_3 = 1$	

Published Papers During Doctoral Course

Journal Papers:

1. **Yongchen Tang**, Yi Sun, Shugen Ma and Dingxin Ge, Planar Legged Walking of a Passive-spine Hexapod Robot, ***Advanced Robotics***, vol.29, pp. 1510–1525, 2015.

2. **Yongchen Tang**, Guoteng Zhang, Dingxin Ge, and Shugen Ma, Omni-directional gait of a passive-spine hexapod, ***Robotics and Autonomous Systems***, 2019. [Accepted]

International Conference Papers:

1. **Yongchen Tang**, Yi Sun, Shugen Ma and Dingxin Ge, Multi-legged Robot with Less Actuators by Applying Passive Body Segment Joint, In *Proc. of the 2012 IEEE Int. Conf. on Intelligent Robots and Systems (**IROS'12**)*, Vilamoura, Portugal, pp. 1828–1833, Oct., 2012.